Modeling of Acoustic Wave Propagation in Turbulent Flow

by

Xuening Lu

Advisor: Dr. Vijay Chatoorgoon

A thesis

presented to the University of Manitoba

in fulfillment of the

thesis requirement for the degree of

Master of Science

in

Mechanical & Manufacturing Engineering

Winnipeg, Manitoba, Canada, 2005

THE UNIVERSITY OF MANITOBA

FACULTY OF GRADUATE STUDIES

*****

COPYRIGHT PERMISSION

"Modeling of Acoustic Wave Propagation in Turbulent Flow"

BY

Xuening Lu

A Thesis/Practicum submitted to the Faculty of Graduate Studies of The University of Manitoba in partial fulfillment of the requirement of the degree

Of

MASTER OF SCIENCE

Abstract

The objective of this thesis is to develop an analytical 1-D linear turbulence model to analyze acoustic wave propagation in the fluid-filled pipes. This work, which comprises an analytical study only, is built upon the concept of turbulence boundary layer behaviour under the imposed frequency disturbances. A two-region linear time-invariant turbulence eddy viscosity model for rough-walled pipe is employed. A transfer function is then obtained for the high mean Reynolds number turbulent flows. In addition, a formula to calculate the volumetric drag coefficient of the turbulent pipe flow has also been developed.

The experiments of the outlet feeder of the STERN Loop at a temperature of 60.6 degrees are applied to verify the proposed model with other five models. The simulation results show that the resonant amplitude predictions using the current two-region linear turbulence model agree well with the experimental data. Accordingly, the present turbulence model provides a methodology for the computation of the turbulence volumetric drag used in the ABAQUS acoustic analysis. The development of the formula eliminates the uncertainty in choosing the values of the volumetric drag used in the ABAQUS, or the transfer matrix method for analyzing the nuclear reactor acoustics.

Acknowledgements

Completing a M.Sc program of study in general and a master's dissertation in particular, in a society other than my society of origin, and in a language other than my mother tongue was not something I could have done without a high degree of motivation and enormous support. Various people and agencies have helped me make it possible.

I would first like to thank the members of my dissertation committee, Dr. R. W. Derksen and Dr. K. Snelgrove, for the careful reading of my thesis and useful comments. In addition, I am grateful to the staffs of department of Document Delivery, E. Dafoe Library, University of Manitoba, for helping me collect the references throughout the course of this research.

Above all, however, I would like to express my special gratitude to my advisor, Dr. Vijay Chatoorgoon, who was a great source of inspiration for me, with his hardworking, caring personality and academic knowledge.

I wish to thank my beloved parents for their sacrifices, encouragement, and for always being supportive to my decisions.

Finally, I reserve my warmest gratitude for the support, kindness and patience of my dearest wife, Danli.

Table of Contents

Chapter 3

Literature Review

Chapter 4

1-D Linear Acoustic Model for Turbulence

List of Figures

List of Tables

Nomenclature

The notation used is given in the following order: Roman, Greek, superscripts, subscripts, symbols and abbreviations.

Roman notation

A	pipe cross-sectional area
$A,\ B,\ C_j,\ D_j$	integration constants
$B(z),\ K(z)$	Kelvin's functions of the first-kind and second-kind
$B'(z),\ K'(z)$	derivatives of Kelvin's functions of the first-kind and second-kind
b	the rate of change of ν_T from ν at the wall to the value of $0.07\left(Ru_{st}^{*}\right)$ at the core / outer-layer interface
C_0	theoretical isentropic sound speed of a small disturbance in an infinite fluid ($C_0 = \sqrt{K_f/\rho}$ $(or:\ \sqrt{(\partial p/\partial\rho)_{S_0}})$
C	theoretical isentropic sonic velocity for thick-walled conduit ($C = C_0\left\{1+\left(K_f/E\right)\left\{2(1+\upsilon)\left[\frac{\left(R_{out}{}^2+R^2\right)-2\upsilon R^2}{R_{out}{}^2-R^2}\right]\right\}\right\}^{-1/2}$
C_{eff}	effective sonic velocity ($C_{eff} = \sqrt{\frac{K_{eff}}{\rho}}$)
D	pipe internal diameter
E	Young's modulus of elasticity of conduit walls
f	friction factor

$f(x,s)$ any function that can be decided by any non-zero particular forcing function of $d\hat{p}'(x,s)/dx$ $\left(f(x,s)=\frac{1}{\rho_0 s}\frac{d\hat{p}'(x,s)}{dx}\right)$

I_0, K_0, I_1, K_1 modified Bessel functions of first and second kinds of order zero and order one, respectively

i complex variable ($i \equiv \sqrt{-1}$)

K_f fluid bulk modulus of elasticity

K_{eff} effective bulk modulus of elasticity

$\left(K_{eff}=\left\{1+\left(K_f/E\right)\left\{2(1+\upsilon)\left[\left(R_{out}{}^2+R^2\right)-2\upsilon R^2\right]/\left(R_{out}{}^2-R^2\right)\right\}\right\}^{-1}\right)$

L pipe length

l Prandtl mixing length

m_0 magnitude perturbation in the eddy viscosity

N constant chosen to properly match the wall shear to the far-field flow

p pressure

$\hat{p}_1'$, $\hat{p}_2'$, $\hat{u}_1'$, $\hat{u}_2'$ pressure / axial velocity perturbations at the pipe inlet and outlet

R_{out} pipe external radius

R pipe internal radius

r radial coordinate

Re_{st} Reynolds number based on the steady axial mean flow velocity $(\mathrm{Re}_{st}=\tilde{u}_{m,st}D/\nu)$

R_V Zhou's turbulence volumetric drag

R_v turbulence volumetric drag

R_{12}	correlation coefficient relates the product of $\overline{u'v'}$ to the square of fluctuation velocity-scale (*Appendix A*)
S	entropy
S_0	constant entropy (isentropic condition)
s	*LaPlacian* variable ($s = iw$)
T_p	time period
t	time
$U(x),\ P(x)$	any particular functions of x
U_f	fluid velocity
u	x component velocity
$\bar{u}_m(x,t)$	instantaneous axial flow mean velocity ($\bar{u}_m(x,t) = \tilde{u}_{m.st}(x) + \tilde{u}'_m(x,t)$)
u^*_{st}	steady friction velocity ($u^*_{st} = v\sqrt{\frac{f}{8}}\frac{\mathrm{Re}_{st}}{D}$)
$U,\ V'^2$	turbulence characteristic velocity-scales (*Appendix A*)
$\overline{u'v'}$	Reynolds shear stress
v	r component velocity
$V(x,r,s)$	transformation of variable ($V = \hat{u}'_J(x,r,s) + \frac{1}{\rho_0 s}\frac{d\hat{p}'(x,s)}{dx}$)
x	axial coordinate (Cartesian or polar cylindrical system)
y	distance from the pipe wall
$z_j(r)$	transformation of variables
$\tilde{Z}$	specific acoustic impedance ($\tilde{Z} = \hat{p}'/\hat{u}'$)
$\tilde{Z}_0$	specific acoustic impedance at $x = 0$
$\tilde{Z}_L$	specific acoustic impedance at $x = L$

Z_α Thurston's analogous specific acoustic impedance per unit length ($Z_\alpha = \psi/\theta$)

Greek notation

$\alpha,\ \alpha_j$ transformation of variables

$\alpha_{imag},\ \alpha_{real}$ imaginary and real parts of α

β transformation of variable ($\beta = \left(-\frac{\rho_0 C^2}{s}.\Gamma\right)$)

ρ fluid density

ρ_0 fluid steady mean density

$\overline{\rho}(x,t)$ fluid mean density ($\overline{\rho}(x,t) = \rho_0(x) + \tilde{\rho}'(x,t)$)

υ line Poisson's ratio

ϕ velocity vector ($\phi = (v,w,u)$)

φ phase angle perturbation in the eddy viscosity

ξ transformation variable ($\xi = \sqrt[1]{\frac{1}{s}.\left[\nu_w + bu^*_{st}(R-r)\right]}$)

ψ negative pressure gradient down the tube

θ average particle velocity over the tube cross-section

$\theta^*,\ \theta_1^*,\ \theta_2^*$ transformation of variables

$\theta^*_{real},\ \theta^*_{imag}$ real and imaginary parts of θ^*

λ resistance coefficient

μ fluid dynamic viscosity

$\Delta_1,\ \Delta_2$	transformation of variables
ν	fluid kinematic viscosity
$\nu_{edd}(r,t)$	turbulence kinematic eddy viscosity ($\nu_{edd}(r,t)=\nu_{edd\_st}(r)+\nu_{edd}^{"}(r,t)$)
$\nu_{edd\_st}(r)$	steady turbulence kinematic eddy viscosity
$\nu_{edd}^{"}(r,t)$	unsteady turbulence kinematic eddy viscosity
ν_T	time-mean part of the modified total kinematic viscosity ($\nu_T=\nu+\nu_{edd}$)
$\nu_T^{'}$	perturbation in the modified total kinematic viscosity
$\nu_{T,j}$	modified total kinematic viscosity of sub-region j
w	angular frequency
$\tau_{w,st}$	steady wall shear stress ($\tau_{w,st}=\rho_0\nu.\left.\frac{\partial\tilde{u}_{st}(x,r,t)}{\partial r}\right\|_{r=R}$)
ε	proportional coefficient relates pipe axial length scale to the radial length scale (*Appendix A*)
ε_{rou}	material roughness
ε_{rou}^{*}	roughness Reynolds number
$\Gamma(s)$	wave propagation constant
γ	Ohmi's wave propagation constant

Superscripts

$\bar{}$	ensemble-average mean value
$'$	turbulent fluctuating components
$\tilde{}$	steady components of the ensemble-average mean value

$\tilde{}'$	excess components of the ensemble-average mean value
$\hat{}$	LaPlace transform
$\hat{}'$	excess components of the ensemble-average mean value after LaPlace transformation with respect to time

Subscripts

i, j	arbitrary index
st	steady state components
m	cross-sectional mean value

Symbols

∇	gradient operator
$\nabla.$	divergence operator
$\nabla\times$	curl operator
$L[\ ]$	LaPlace transformation
$\|\ \|$	modulus

Abbreviations

1-D	one dimensional
Ch	channel (e.g. Ch29, Ch30 and Ch31)
Hz	hertz
IM	Impedance Method
MOC	Method of Characteristics
TMM	Transfer Matrix Method

Chapter 1
Introduction

Acoustic pressure resonance in liquid-transporting pipe systems affect performance and safety. Bad performance costs money; failure of piping systems can have disastrous effects, leading to injuries or fatalities. Accurate predictions of acoustic pressure amplitudes are a necessary requirement for any practical piping system subjected to acoustic excitations. For the past years, the understanding of acoustic damping in laminar flows is better developed up to 100 Hz, but in turbulent flows is still unfolding. As most industry applications encounter the high Reynolds number turbulent flow, new methodologies for determining the acoustic damping in turbulent flow have to be found.

1.1 Background of Problem

Acoustics is the science that studies the emission, transmission, and reception of sound waves. It touches on disciplines as disparate as psychology and meteorology, and includes many subdisciplines such as architecture acoustics, bioacoustics, underwater acoustics, and environmental acoustics. Acoustic wave propagation in tubes has been studied for more than 200 years, starting with the research on the propagation of waves in arteries by Leonard Euler in 1775. It is related to many practical applications, such as pressure wave propagation in blood vessels, dynamic response of pressure transmission lines, missile propellant pumping, acoustic delay lines, hydroelectric power generation,

water-hammer and other fields involving the transmission of power through fluid.

A recent accident, and also a severe one, is the problem of fuel bundle damage and pressure tube fretting in the Darlington Nuclear Generation Station (e.g. Chatoorgoon *et al.* (1993)), which was identified to be caused by acoustic resonance in the CANDU (Canada Deuterium Uranium) heat-transport systems. To be able to solve or prevent the problem, it is important to understand the mechanisms that are responsible for the propagation and dissipation of acoustic energy in the piping. The study of these mechanisms is the starting point in the development of practical methods for analyzing the piping acoustic resonance.

This thesis presents some new contributions to theoretical methods to analyze the acoustic pressure resonance of turbulence in water-filled tubes under sinusoidal perturbation.

1.2 Objectives

The scope of this research is investigating theoretical methods used for analyzing acoustic wave propagation in turbulent pipe flow. The objectives of the study are:

(a) To understand and document the current state-of-art of work on acoustic resonance in laminar and turbulent flows by performing a literature review.

(b) To compare existing turbulence models, and, if possible, develop a better 1-D linear turbulence model for acoustic analyses.

(c) To develop a formula of the turbulent volumetric drag term (acoustic damping), that can be expressed in terms of flow and geometric parameters.

1.3 Outline of This Thesis

The thesis is arranged as follows. The first chapter is a brief review of the background of acoustic wave propagation and introduces the scope of current research. The second chapter presents the fundamental theoretical principles about acoustic wave propagating in pipes. The parameters affecting the acoustic wave propagation, including sonic velocity and wall elasticity, are discussed. The third chapter reviews state-of-art acoustic models for laminar and turbulent flows. The fourth chapter presents a 1-D linear acoustic model of turbulence by employing the modified two-region time-independent eddy viscosity distributions. A formula for the calculation of turbulence volumetric drag is developed. The fifth chapter investigates six turbulent acoustic models using quasi-steady perturbation, zero perturbation (or time invariant) and uniform dynamic perturbation (or time variant) eddy viscosity distributions. Some analytical solutions compared with the experimental data by using different turbulence models are given. The sixth chapter discusses the conclusions and makes recommendations for future work.

Chapter 2
Acoustic Wave Propagation Fundamentals

This chapter presents the main acoustic theoretical fundamentals needed to understand the work. The derivation of the acoustic wave equations for turbulent flows with non-uniform cross-sectional area is considered. Detailed derivations can be found in Samuel (1981), Lighthill (1978), Chaudhry (1987) and Wylie & Streeter (1993). The discussion here is limited to the one-dimensional standing wave.

2.1 Viscous Wave Governing Equations

Acoustic wave propagation in tubes can be assumed one-dimensional or "longitudinal", in the sense that the wavelength λ_f is much larger than the pipe diameter D. Lighthill (1978) indicated that the propagation of sound waves of any frequency is this longitudinal mode, whereas propagation of other modes (e.g. plane wave mode) is only possible at frequencies exceeding a certain critical value (for which the wavelength is comparable with a pipe diameter). The following derivation of the equations for acoustic waves is based upon that presented by Chaudhry (1987).

2.1.1 One-dimensional equation of continuity

The 1-D continuity equation is:

$$\frac{1}{\rho}\frac{D\rho}{Dt}+\frac{1}{A}\frac{DA}{Dt}+\frac{\partial U_f}{\partial x}=0 \tag{2.1}$$

where: ρ is the fluid density, U_f is the fluid velocity, A is the conduit cross-sectional area, and $\frac{D}{Dt}=\frac{\partial}{\partial t}+U_f\frac{\partial}{\partial x}$ is the material differential operator.

Eq. (2.1) includes the effect of pipe wall elasticity through the cross-sectional area term, which varies with axial direction x and time t.

2.1.2 One-dimensional equation of momentum

The 1-D momentum equation is:

$$\frac{\partial U_f}{\partial t}+U_f\frac{\partial U_f}{\partial x}+\frac{1}{\rho}\frac{\partial p}{\partial x}-\frac{4\mu}{3\rho}\frac{\partial^2 U_f}{\partial x^2}=0 \tag{2.2}$$

where: μ is the flow dynamic viscosity.

2.1.3 Equation of state

For fluids or gases, the equation of state relates to pressure and can be expressed as a function of density and entropy:

$$\frac{Dp}{Dt}=\left(\frac{\partial p}{\partial \rho}\right)_S\frac{D\rho}{Dt}+\left(\frac{\partial p}{\partial S}\right)_\rho\frac{DS}{Dt}, \tag{2.3}$$

where: S is the entropy and p is the pressure. In this thesis, the thermal effects are

negligible and the isentropic condition ($S \equiv S_0$, where S_0 is a constant) is held throughout. The state relation therefore can be expressed as:

$$\frac{Dp}{Dt} = \left(\frac{\partial p}{\partial \rho}\right)_{S_0} \frac{D\rho}{Dt} \quad or \quad \frac{D\rho}{\rho} = \frac{Dp}{K_f} \tag{2.4}$$

where: K_f is the fluid bulk modulus of elasticity (invariant with time), and $(\partial p/\partial \rho)_{S_0} = K_f/\rho$.

2.2 Analytical Methods

To solve the acoustic wave equation, there are two fundamentally different theoretical approaches: time-domain and frequency-domain. The time-domain analysis usually focuses on the non-linear applications and is better suited for transients. The frequency-domain analysis is applied to the linearized equations and the convection terms are usually neglected.

The most common approach for the time domain analysis of classic waterhammer is the Method of Characteristics (MOC). Principles of MOC and other methods including finite difference or finite element are discussed in Chaudhry (1987) and Wylie & Streeter (1993). The advantages of these numerical methods are: (1) they solve the general non-linear partial differential equations, which may yield more accurate predictions of the axial velocity profile than the linear solution; (2) they can be easily extended to more complex hydraulic systems or multi-dimensional applications, etc. On the contrary, the

primary drawback is that it requires larger CPU times comparing with the linear method.

In the frequency domain two linear methods are commonly used for acoustic analysis: Transfer Matrix Method (TMM) and Impedance Method (IM). However, the two methods are structured differently. The IM has the advantage of characterizing the system dynamics without specifying a particular excitation. The TMM, on the other hand, uses state vectors of pressure and flow velocity at sections in the system that are related to state vectors at other locations by transfer matrices, which encompass the transfer functions. Advantages of this method include: (1) it is suitable for both hand and digital computations; (2) it is suitable for analyzing systems whose oscillations are considered to be more than two variables (e.g., pressure, velocity, density, temperature).

In the present thesis, a combination of impedance approach and transfer matrix approach is chosen to model the acoustic resonance in turbulent flow. It is based on the two-port or four-terminal networks respectively.

2.3 Parameters Affecting Acoustic Wave Propagation

2.3.1 Sonic velocity

The mechanical properties of the pipe wall material and the rigidity of the pipe supports may significantly influence the sound speed. The accuracy of solution depends on a good estimate of the sonic velocity. Theoretically, the isentropic sound speed of a small

disturbance in an infinite fluid is defined as $C_0 = \sqrt{K_f/\rho}$ $(or: \sqrt{(\partial p/\partial \rho)_{S_0}})$. This is computed by the equation of state. The actual velocity of sound is related to the isentropic compressibility of the pure substance and the conduit walls. Therefore, one can define the modified sound speed by solving the mass conservation equation and state relation using the hoop stress formula. The detailed derivation can be found in Chaudhry (1987) and Wylie & Streeter (1993). A popular theoretical formula from Chaudhry (1987) including Poisson's ratio for thick-walled conduit is of the form:

$$C = C_0 \left\{ 1 + \left(K_f/E\right) \left\{ 2\left(1+\upsilon\right) \left[\frac{\left(R_{out}{}^2 + R^2\right) - 2\upsilon R^2}{R_{out}{}^2 - R^2} \right] \right\} \right\}^{-1/2} \tag{2.5}$$

in which E is Young's modulus of elasticity of conduit walls, υ is line Poisson's ratio, R_{out} and R are external and internal radii of conduit respectively. For liquid and pipe wall behaving linearly, the effective bulk modulus of elasticity, K_{eff}, and the effective sonic velocity, C_{eff}, are given by:

$$K_{eff} = \left\{ 1 + \left(K_f/E\right) \left\{ 2\left(1+\upsilon\right) \left[\frac{\left(R_{out}{}^2 + R^2\right) - 2\upsilon R^2}{R_{out}{}^2 - R^2} \right] \right\} \right\}^{-1} \quad and \quad C_{eff} = \sqrt{\frac{K_{eff}}{\rho}} \tag{2.6}$$

Recently, Sou *et al.* (1990), Munjal and Thawani (1997) and Prek (2004) addressed the issue of complex valued and frequency-dependent sonic velocity for wave propagation in fluid-filled viscoelastic pipes. Large pipe size and viscoelasticity of pipe wall material could result in a frequency-dependent wave speed.

The influence of viscoelastic properties of the pipe-wall material on wave propagation is modelled through a frequency-dependent wavespeed and a separate frequency-dependent damping factor. By incorporating the complex creep compliance of the wall material into the unsteady momentum and continuity equations (2.1) & (2.2), Sou *et al.* (1990) derived the complex valued and frequency-dependent wavespeed for a pressure wave propagating in a viscoelastic pipe. Using the complex wavespeed, the standard Impedance Method (IM) or Transfer Matrix Method (TMM) was directly used to analyze resonating conditions in a viscoelastic piping system. Munjal and Thawani (1997) proposed and derived a more comprehensive model in the similar way. It accounts for both the elastic reaction and inertial effects of the pipe wall on wave propagation. Lately, Prek (2004) studied the frequency-dependent sonic velocity experimentally and concluded that the elastic reaction of the wall to expansion of the cross section greatly exceeds the wall inertial reactions. He reported that the wall compliance significantly decreased the sound speed, while the structural damping caused wave attenuation.

2.3.2 Acoustic damping

Correct estimations of acoustic resonant amplitudes are vital for any acoustic computer code used in engineering analysis (e.g. for investigating a nuclear reactor channel susceptibility to damage). Therefore, a methodology for determining the acoustic damping must be sufficiently accurate and general to cover the wide range of geometry and flow conditions encountered in real engineering environment.

The energy losses of acoustic waves in the transportation medium may be divided into three basic types: viscous losses, heat conduction losses, and losses associated with internal molecular processes. In the present study, assumptions of the fluid being adiabatic, homogeneous, and isentropic are made; consequently the viscous losses are considered to be the major loss (e.g. Samuel (1981) and Lighthill (1978)) for acoustic waves in the fluids.

Ontario Hydro (now OPG) and AECL (e.g. Chatoorgoon *et al.* (1993), and Zhou & Chatoorgoon (1994)) have been using the ABAQUS code to analyze acoustic resonance in the piping systems of a nuclear reactor. A volumetric drag is used in the ABAQUS code as the damping parameter, which is usually determined from experimental data. The shortcoming is obvious if no experimental data is available a priori to obtain a representative volumetric drag. This empirical method therefore introduces a great deal of uncertainty when the experimental data do not apply precisely to the design under study. In addition, the dependency of the damping term on frequency for turbulent flow is not considered in ABAQUS.

Different theories have been developed to model the acoustic damping for laminar and turbulent flows. The earlier work of Chatoorgoon *et al.* (1995) indicated that for the non-zero mean velocity or unsteady turbulence, the predictions of the magnitudes and phasing of the resonant amplitude do not always compare well with the experimental data

except for the lower frequencies. They assumed that damping is a function of the wall shear stress. This in turn is a function of the Reynold's number, velocity wave acceleration and amplitude, and the steady mean-flow pressure drop. The phasing of the friction-factor may also important as the proper phasing can reduce wave amplitudes by as much as 40% (Brown *et al.* (1969)). Consequently, the time-dependent wall shear stress can be described by the time-varying two-dimensional Navier-Stokes equations. These simulate the two-dimensional nature of the boundary layer behaviour for sinusoidal pressure waves and better describe the reality.

Chapter 3
Literature Review

Acoustic wave propagation in the fluid-filled pipes has been studied extensively during the last decades. Different applications have led to a wide range of publications variously related in subject. To better understand the nuance of the various methodologies and the approaches being used in deriving engineering solutions, a review of the literature is reported here.

3.1 Review of Acoustic Damping Models

Accurate predictions of acoustic amplification and damping are essential for assessing the validity of any acoustic model. Damping is modelled through the wall shear stress terms in the momentum equation (Eq. 2.2). In steady flows, the profile of the boundary layer attached to the wall is time-independent, but in flows with high frequency (e.g. >20 Hz) acoustic waves, the boundary distorts rapidly with time. This means that the wall shear stress also becomes time-variant and caution must be exercised when applying steady-state friction formula. A number of unsteady friction models for transient pipe flow in the time-domain have been investigated by Bergant *et al.* (2001). In this thesis, the reviews of the previous work mainly focus on the following two groups:

1) The friction term is based on the cross-sectional distribution of the instantaneous flow velocity (e.g. Brown *et al.* (1969, 1981), Wood and Funk (1970), Ohmi *et al.* (1976, 1978, 1981, 1982, 1985), Vardy and Hwang (1991), Eichinger and Lein (1992), and Pezzinga (1999)),

2) The friction term is dependent on the instantaneous mean flow velocity and weights of past velocity changes (e.g. Ziekle (1968), Trikha (1975), Brown (1984), Suzuki *et al.* (1991), Vardy (1992), Vardy *et al.* (1993), Schohl (1993), Vardy and Brown (1995, 1996), and Shuy (1995)).

3.1.1 Damping models for laminar flow

Acoustic wave propagation in laminar flow has been well studied for low frequency up to 100 Hz over the past 40 years. Many authors, including D'Souza and Oldenburger (1964), Foster and Parker (1964) used the linearized Navier-Stokes equations transformed in the *LaPlacian* domain to derive the frequency response equations. By comparisons against experiments, they showed the damping increases with the frequency perturbations, and showed that correct amplitudes could be achieved by paying proper attention to the viscous shear-stress terms. However, the minimum predicted amplitudes using above linear transfer function models did not always compare well with the experimental measurements.

Zielke's paper (1968) is an important contribution to modeling frictional effects of water

hammer or acoustic waves in laminar flow. The friction term is dependent on the instantaneous mean flow velocity and weights of past velocity changes. The unsteady part of friction part is expressed in term of a convolution integral:

$$\tau_{wu} = \frac{2\rho\nu}{R}\int_0^t W(t-\varsigma)\frac{\partial U}{\partial t}(\varsigma)\,d\varsigma \qquad (3.1)$$

where: $W(t-\varsigma)$ is the weighting function and ς is the time used in the convolution integral. Various authors (Trikha (1975), Suzuki *et al.* (1991), Schohl (1993)) have developed useful simplifications to the time domain solutions of this convolution integral. It is also clear that the convolution integral gives a time variant damping coefficient. Zielke (1968) stated that the instantaneous fluid friction is highly dependent upon the rate of change of mean flow velocity, and implied this is the reason why higher harmonics attenuate faster than lower frequency components.

Rzentkowski *et al.* (1993) used the linear wave theory based on a transmission matrix method to derive the frequency-dependent matrix elements (e.g. the wave propagation constant and the characteristic impedance) for the zero-mean laminar flow. They obtained good predictions of the pressure amplitudes comparing with the experimental results (up to the 3-rd acoustic mode) for both 12.8-meter and 7.03-meter instrumental lines. The agreement on the resonant frequencies between the computational results and experimental data for a 12.8-meter tube is better than for the 7.03-meter tube above the 3-rd acoustic mode and the reason for this is not given.

3.1.2 Damping models for smooth-walled turbulent flow

Recently, acoustic wave propagating in the smooth-walled tubes has been explored for turbulent flows. Some existing 1-D turbulence models using multi-regional eddy viscosity distributions are reviewed in the following sections. The time-invariant and time-variant approximations to eddy viscosity distributions in pipes are defined based upon the experimental data obtained from Laufer (1954).

3.1.2.1 Existing time-independent eddy viscosity models

Brown *et al.* (1984) studied the frequency response of acoustic waves in circular tubes for unsteady turbulent flow. They applied the time-invariant eddy viscosity models by dividing the pipe cross section into two and three regions. Corresponding results for the acoustic behaviour of small amplitude disturbances superimposed on a gross turbulent flow over the frequency ranges of 50 Hz ~ 30000 Hz were presented.

The later work of Ohmi and Usui *et al.* (1976) proposed multi-regional time-independent eddy viscosity models of two-, three-, four-, and thirteen-region. Analytical solutions based on each model were developed to obtain the acoustic velocity and pressure profiles in oscillating turbulent flows in smooth-walled pipes. Comparisons of these analytical solutions indicated that the four region-model proposed by von Kármán (1939) reasonably described the characteristics of flow behaviour.

Zielke's (1968) weighting function model takes account of the influence of the local velocity history at any point along a pipe when deducing the instantaneous magnitude of the local skin friction. Vardy *et al.* (1993) extended Zielke's model (1968) to predict the skin friction of high Reynolds number smooth-walled turbulent flows. They first presented the flow in a manner suggested by Wood and Funk (1970), namely as a laminar annulus adjacent to the pipe wall and a central core of uniform velocity (this implies an infinite viscosity in the core). The governing equations were solved to derive a general function relating instantaneous wall shear stresses to historical values of the flow mean velocity. Vardy and Brown (1995, 1996) subsequently presented an improved form of the above model in which the eddy viscosity is assumed to vary linearly across the outer annulus shear layer, but constant in time. A family of weighting function curves was obtained numerically for several high Reynolds numbers.

3.1.2.2 Existing time-dependent eddy viscosity models

In the preceding sections, the assumed eddy viscosity distribution is regarded as "frozen" in time. Naturally, this may not be an exact representation of physical reality. Ohmi *et al.* (1978) computed the velocity distribution in a pulsating turbulent pipe flow by using a time-variant eddy viscosity distribution to describe the Reynolds stresses. The four-region eddy viscosity profile of von Kármán's (1939) was used. The time-dependent eddy viscosity was considered to arise mainly from the change of the instantaneous friction velocity u^* corresponding to the instantaneous axial velocity distribution $\bar{u}_m$

through the pipe cross-section. Numerical solutions were obtained in two cases of the time–variant u^* and of the time-independent one corresponding to the time-averaged velocity profile. They concluded that the pressure and velocity distributions calculated using the time-dependent eddy viscosity agreed well with those using the time-independent one.

Kita *et al.* (1980) also defined time-dependent eddy viscosity approximations and applied them as empirical relationships in five successive radial regions of pipes. Using the approximations, the governing flow equations were integrated numerically to obtain the velocity profiles and wall shear stresses in unsteady, oscillating turbulent flows. Comparing with the velocity profiles computed using Ohmi's model (1978), Kita's model (1980) was proved to be similar to that of Ohmi (1978).

As a complementary work, Ohmi *et al.* (1981) analyzed the unsteady velocity and pressure profiles for the pulsating turbulent pipe flows. Variations of the static pressure in the axial direction along the pipe, as well as the radial velocity profiles, were numerically computed by using either a time-dependent friction velocity or a time-independent one. The numerical results were verified with experiments.

Eichinger and Lein (1992) used a *k-epsilon* model to represent the unsteady turbulence structure. This has the advantage of enabling account to be taken of time dependence of

the eddy viscosity. They used their model together with the method of characteristics to obtain numerical solutions of radial velocity profiles of various unsteady flows in pipelines, and reported good agreement of amplitude and phase with experimental measurements of Holmboe and Rouleau (1967).

3.1.2.3 Experiments relating to time invariant eddy viscosity distribution

Attention now turns to the assumption that changes in the eddy viscosity distribution may be neglected during the transient flow process. This assumption may not be valid over large time scales because the perturbations in the eddy viscosity must adjust to the evolving conditions. There are supporting evidences for the above descriptions.

Brown (1981) investigated the attenuation and wave speed of small disturbances superimposed on turbulent mean flow for intermediate frequencies (i.e. 9 Hz ~ 90 Hz) of interest with two time-averaged Reynolds numbers (i.e. $\mathrm{Re}_{st} = 6000$ *and* $\mathrm{Re}_{st} = 10000$). He proposed three single region eddy viscosity profiles: (1) quasi-steady perturbations in the eddy viscosity profile applicable at low frequencies, (2) zero perturbations eddy viscosity model meaningful at high frequencies, (3) uniform dynamic perturbations eddy viscosity model with an assumption of being invariant for all radii applicable over a broad band frequency range. Experimental results were then interpreted in terms of these mean response fluctuations in the eddy viscosity due to the wave-induced perturbations in the velocity gradient. Brown indicated that:

(a) At frequencies greater than 90 Hz, the perturbations in eddy viscosity vanished, thus the consequent wave parameters were easily deduced.

(b) There was a phase lag between the perturbations in eddy viscosity and a step change in the velocity gradient for frequencies less than 29 Hz. The amplitude of eddy viscosity perturbations changed little compared with its quasi-steady value for lags up to roughly 100 degrees. The major consequence was a reduction in the wave attenuation.

(c) For frequencies in the range of 29 Hz ~ 90 Hz, the phase lag continued to grow following the perturbations in velocity gradient, but the amplitude of the perturbations in eddy viscosity diminished to a small fraction of its quasi-steady value before the phase lag reached 180 degrees.

He and Jackson (2000) reported experiments with ramp changes (increase and decrease) in velocity over various time periods. They identified three separate time scales and confirmed slug flow nature of the initial response in the core region. They also showed that the eddy viscosity in the outer region does not respond as rapidly as the local velocity gradients.

Vardy *et al.* (2003) recently indicated that: (1) there is a phase lag between the step change in flow mean velocity and the resulting change in the eddy viscosity, (2) the variation in the eddy viscosity changes insignificantly in the early stage after the step

change in mean velocity over the pipe cross section. Therefore, the assumption of non-uniform and constant in time in eddy viscosity may be plausible for unsteady turbulent flows.

3.1.3 Damping models for rough-walled turbulent flow

The above models were initially developed for smooth-walled flows. In contrast, Zhou (1995) developed a two-region model to predict the volumetric drag (damping) in rough-walled turbulent pipe flows. His two-region model was based on the time-independent eddy viscosity profile of Ohmi *et al.* (1976), but with different near-wall treatments. Zhou (1995) proposed a piece-wise eddy viscosity distribution where the total eddy viscosity was proportional to the dimensionless parameter $\frac{R\,u_{st}^{*}}{\nu}$ and fluid kinematic viscosity ν with a smaller coefficient in each sub-region. He stated that the characteristics of the near wall region depended on the pipe wall surface protrusions and the steady flow characteristics, which determines whether the near wall region is laminar or turbulent. Zhou stated that only if the thickness of the laminar sub-layer adjacent to the pipe wall is substantially larger than the wall surface protrusions, the near wall region could be considered laminar. For commercial steel, Zhou calculated some laminar sub-layer thickness and compared those values with the recommended wall-surface protrusion (or "cutoff") value of 0.5 millimetre, the results were significantly smaller than the threshold value.

Lately, Vardy and Brown (2004) developed a weighting-function model of unsteady skin friction in fully rough-walled flows in one-dimensional pipes. Their model assumed a two-region linear time invariant eddy viscosity distribution by matching the experiments of Laufer (1954). The viscosity at the core region was approximated equal to $0.065Ru_{st}^{*}$, and the viscosity at the wall was assumed greater than the laminar viscosity by an unknown amount. With these assumptions, the unsteady shear stress was found to depend on a weighted integral over the acceleration history. Considering a special case of uniform acceleration, Vardy *et al.* stated that: (1) the limiting value of the unsteady skin friction coefficient is independent of steady Reynolds number, but is strongly dependent on the relative roughness of the wall; (2) the time required to approach the limiting value decrease with increasing roughness and with increasing Reynolds number. However, the authors hoped that future experiments would give certain support to the rough-walled predictions represented above.

Chapter 4

1-D Linear Acoustic Model for Turbulence

4.1 Introduction

This chapter presents the one-dimensional linear acoustic model for rough-walled turbulent pipe flow. Starting from the pertinent compressible Navier-Stokes equation, the 1-D acoustic governing equations are obtained for turbulent flow. A two-region time-invariant eddy-viscosity distribution is obtained by matching the Laufer's (1954) experimental measurements. Thereafter, a linear transfer function is derived to predict pressures at the line ends based on the combination of transfer matrix method and impedance method. This analytical solution is then used to predict the acoustic pressure amplifications in a single pipeline system. Primary frequency-dependent acoustic parameters, such as wave propagation constant and specific acoustic impedance are developed, which are incorporated into the acoustic model. A concept of turbulence volumetric drag is introduced and developed herein as the acoustic damping parameter.

4.2 Assumptions

The assumptions used for the present model in this chapter are:

1) Thermal effects and external forces are negligible;
2) The pipe length is much larger than the pipe diameter (L >> D) and the 1-D approximation is made;

3) The disturbances imposed on the sound waves are small so that linearization is applicable; the convection effects are negligible;

4) The elasticity of the pipe is considered, which is believed to affect the isentropic sonic velocity propagating in the fluid;

5) The losses in the wave transportation medium associated with the internal molecular processes is negligible;

6) The Mach number of the steady flow component is small and a uniform density is assumed;

7) The pressure is uniform across the cross section of the pipe and becomes a function of x and t only;

8) The ensemble-average/short-time average of the flow is axisymmetric and sinusoidal, (i.e. the ensemble-average value has a steady component and a deviation component);

9) The excitation frequency is in the range of 50 ~ 500 Hz;

10) The turbulence eddy viscosity is time invariant and can be approximated by that for steady mean flow;

11) No-slip condition at the wall;

12) Continuity of velocity and shear stress on the interface between two adjacent sub-regions.

4.3 1-D Linear Acoustic Governing Equations

4.3.1 Turbulence mean-flow governing equations

The acoustic wave transmission of turbulence can be modeled by using the fundamental compressible Navier-Stokes equation. The basic Navier-Stokes equation for unsteady viscous compressible flow of is expressed as:

$$\frac{\partial(\rho\phi)}{\partial t} = -\nabla.(\rho\ \phi\phi) - \nabla p + \frac{4\mu}{3}\nabla(\nabla.\phi) - \mu\nabla\times(\nabla\times\phi) \tag{4.1}$$

In cylindrical coordinate system with x being along the pipe axial direction, ϕ is velocity vector of $\phi=(v,w,u)$, ρ is the fluid density, and μ is fluid dynamic viscosity. Where $\nabla\phi$, $\nabla.\phi$, *and* $\nabla\times\phi$ are gradient, divergence, and curl respectively.

Starting with the two dimensional compressible Navier-Stokes equations in a cylindrical coordinate system and excluding the radial equation of motion, the governing equations before averaging become:

Continuity equation:

$$\frac{\partial\rho}{\partial t} + \left(\frac{\partial(\rho u)}{\partial x} + \frac{\partial(\rho v)}{\partial r} + \frac{(\rho v)}{r}\right) = 0 \tag{4.2}$$

x - Momentum equation:

$$\frac{\partial(\rho u)}{\partial t} + \frac{\partial(\rho u.u)}{\partial x} + \frac{\partial(\rho u.v)}{\partial r} = -\frac{\partial p}{\partial x} + \mu\left(\frac{\partial^2 u}{\partial x^2} + \frac{\partial^2 u}{\partial r^2} + \frac{1}{r}\frac{\partial u}{\partial r}\right) + \frac{\mu}{3}\frac{\partial}{\partial x}\left(\frac{\partial u}{\partial x} + \frac{\partial v}{\partial r} + \frac{v}{r}\right) \tag{4.3}$$

Equation of state:

$$\frac{Dp}{Dt} = \left(\frac{\partial p}{\partial\rho}\right)_{S_0}\frac{D\rho}{Dt} = \left(\frac{K_{eff}}{\rho}\right)\frac{D\rho}{Dt} \tag{4.4}$$

The isentropic sound speed and the effective bulk modulus of elasticity are defined in Chapter 2. The meanings of parameters used in Eqs. (4.2) ~ (4.4) are referred to the *Nomenclature*.

The density fluctuating part is assumed negligible for low Mach-number flows, therefore $\rho = \overline{\rho}$ (fluid mean density). Decomposing other flow instantaneous variables into a mean and fluctuating part as:

$$p(x,t) = \overline{p}(x,t) + p'(x,t), \quad u(x,r,t) = \overline{u}(x,r,t) + u'(x,r,t), \quad v(x,r,t) = \overline{v}(x,r,t) + v'(x,r,t) \tag{4.5}$$

Where the prime "'" denotes the turbulent fluctuating components and the overscore "–" denotes the ensemble-average (i.e. short-time average) value. The timescale used to average the equations above must be short compared to the acoustic wave timescale but sufficiently long to filter out turbulence fluctuations. The Favre-averaging procedure results in the same form as the Reynolds-averaging procedure inasmuch as the fluid density variation is slight. An introductory description of the derivation of the turbulence mean equations, and various averaging methods, are given in Hinze (1975).

Substituting Eq. (4.5) into Eqs. (4.2) ~ (4.4) and Favre-averaging or Reynolds-averaging gives:

Continuity equation:

$$\frac{\partial \bar{\rho}}{\partial t}+\left(\frac{\partial\left(\overline{\rho u}\right)}{\partial x}+\frac{\partial\left(\overline{\rho v}\right)}{\partial r}+\frac{\left(\overline{\rho v}\right)}{r}\right)=0 \tag{4.6}$$

x - Momentum equation:

$$\frac{\partial\left(\overline{\rho u}\right)}{\partial t}+\frac{\partial\left(\overline{\rho . u^{2}}\right)}{\partial x}+\frac{\partial\left(\overline{\rho . u\ v}\right)}{\partial r}+\frac{\partial\left(\overline{\rho u'^{2}}\right)}{\partial x}+\frac{\partial\left(\overline{\rho}\ \overline{u'v'}\right)}{\partial r}=-\frac{\partial \bar{p}}{\partial x}+\mu\left(\frac{\partial^{2}\bar{u}}{\partial r^{2}}+\frac{1}{r}\frac{\partial \bar{u}}{\partial r}\right)+\frac{4\mu}{3}\frac{\partial^{2}\bar{u}}{\partial x^{2}}+\frac{\mu}{3}\frac{\partial}{\partial x}\left(\frac{\partial \bar{v}}{\partial r}+\frac{\bar{v}}{r}\right) \tag{4.7}$$

Equation of state:

$$\frac{D\bar{p}}{Dt}=\left(\frac{\partial \bar{p}}{\partial \bar{\rho}}\right)_{S_0}\frac{D\bar{\rho}}{Dt}=\left(\frac{K_{eff}}{\bar{\rho}}\right)\frac{D\bar{\rho}}{Dt} \tag{4.8}$$

The above equations can be further simplified by comparing magnitudes, as shown in *Appendix A*. The 1-D simplified turbulence mean-flow governing equations are:

Continuity equation:

$$\frac{D\bar{\rho}}{Dt}+\bar{\rho}\left(\frac{\partial \bar{u}}{\partial x}+\frac{\partial \bar{v}}{\partial r}+\frac{\bar{v}}{r}\right)=0 \tag{4.9}$$

x - Momentum equation:

$$\frac{\partial \bar{u}}{\partial t}=-\frac{1}{\bar{\rho}}\frac{\partial \bar{p}}{\partial x}+\frac{\mu}{\bar{\rho}}\left(\frac{\partial^{2}\bar{u}}{\partial r^{2}}+\frac{1}{r}\frac{\partial \bar{u}}{\partial r}\right)-\frac{\partial}{\partial r}\left(-\nu_{edd}\frac{\partial \bar{u}}{\partial r}\right) \tag{4.10}$$

The Reynolds shear stress $\overline{u'v'}$ in Eq. (4.7) is expressed in terms of the turbulence kinematic eddy viscosity ν_{edd}, as $\overline{u'v'}=-\nu_{edd}\frac{\partial \bar{u}}{\partial r}$.

4.3.2 Linearization

To analyze the one-dimensional acoustic wave behaviour in turbulent flow under sinusoidal perturbations, the above non-linear equations (4.8) ~ (4.10) are linearized before further analysis. Most sound waves disturb the state of steadiness in the fluid slightly, so the variables associated with sound, such as excess pressure, excess density and particle velocity may be assumed to be small magnitudes of first order. Inasmuch as the ensemble-averaged pressure and velocity can be divided into steady and excess / deviation components, also the density and ν_{edd} can be expressed as the sum of steady and perturbed parts:

$$\overline{p}(x,t)=\tilde{p}_{st}(x)+\tilde{p}'(x,t),\quad \overline{u}(x,r,t)=\tilde{u}_{st}(x,r)+\tilde{u}'(x,r,t),\quad \overline{v}(x,r,t)=\tilde{v}_{st}(x,r)+\tilde{v}'(x,r,t),$$
$$\nu_{edd}(r,t)=\nu_{edd\_st}(r)+\nu_{edd}''(r,t),\quad \textit{and}\quad \overline{\rho}(x,t)=\rho_0(x)+\tilde{\rho}'(x,t). \tag{4.11}$$

Where the prime denotes the perturbed quantities, $_{st}$ denotes the steady state components.

Correspondingly, the deviations from the steady state throughout the fluid are assumed as:

$$\left|\tilde{p}'\right|<<\tilde{p}_{st},\ \left|\tilde{u}'\right|<<\tilde{u}_{st},\ \left|\tilde{v}'\right|<<\tilde{v}_{st},\ \left|\tilde{\rho}'\right|<<\rho_0,\ \textit{and}\ \ \nu_{edd}''\ \textit{is negligible}\ . \tag{4.12}$$

At oscillation frequencies greater than 50 Hz, ν_{edd}'' is considered to be negligible because of the inertia of the turbulent (i.e. the difference between the turbulence production and dissipation does not act long enough in a half cycle to change the turbulence level significantly). These restrictions are then used to linearize Eqs. (4.9) and (4.10).

Finally, the complete linear acoustic wave equations, before cross sectional averaging, are:

Continuity Equation before cross-sectional averaging:

$$\frac{\partial \tilde{p}'}{\partial t} + \rho_0 \cdot \left[C^2\right]_{\bar{\rho}=\rho_0} \frac{\partial \tilde{u}'}{\partial x} + \rho_0 \cdot \left[C^2\right]_{\bar{\rho}=\rho_0} \left[\frac{\partial \tilde{v}'}{\partial r} + \frac{\tilde{v}'}{r}\right] = 0 \tag{4.13}$$

$$\text{where: } \left[C^2\right]_{\bar{\rho}=\rho_0} == \left[\frac{K_{eff}}{\bar{\rho}}\right]_{\bar{\rho}=\rho_0}$$

Momentum Equation before cross-sectional averaging:

$$\frac{\partial \tilde{u}'}{\partial t} = -\frac{1}{\rho_0}\frac{\partial \tilde{p}'}{\partial x} + \frac{1}{r}\frac{\partial}{\partial r}\left(r \nu_T \frac{\partial \tilde{u}'}{\partial r}\right) \tag{4.14}$$

where $\nu_T = \nu_w + \nu_{edd\_st}$ is the modified total turbulent kinematic viscosity with ν_{edd}'' is neglected (as Eq. (4.12)). ν_w is defined as the effective viscosity at the wall, and for smooth wall, ν_w is equivalent to the laminar viscosity ν. After integrating the flow variables from the pipe axis to the wall, the 1-D linear acoustic equations are obtained as follows (***m*** denotes the cross-sectional mean value):

1-D Continuity Equation:

$$\frac{\partial \tilde{p}'}{\partial t} + \rho_0 C^2 \frac{\partial \tilde{u}_m'}{\partial x} = 0 \quad where: \; C^2 = \left[\frac{K_{eff}}{\bar{\rho}}\right]_{\bar{\rho}=\rho_0} \tag{4.15}$$

1-D Momentum Equation:

$$\frac{\partial \tilde{u}_m'}{\partial t} = -\frac{1}{\rho_0}\frac{\partial \tilde{p}'}{\partial x} + \left\{\frac{2}{R^2}\int_0^R \frac{1}{r}\frac{\partial}{\partial r}\left(r \nu_T(r) . \frac{\partial \tilde{u}'}{\partial r}\right) r dr\right\} \tag{4.16}$$

Note that to derive the continuity equation, the integration relation of: $\underbrace{\frac{2}{R^2}\int_0^R\left(\frac{\partial\tilde{v}}{\partial r}+\frac{\tilde{v}}{r}\right)rdr}_{\text{cross-sectional average}} \equiv \underbrace{\left[\frac{2}{R^2}\left[\tilde{v}\,r\right]_0^R-\frac{2}{R^2}\int_0^R\left(\frac{\partial\tilde{v}}{\partial r}r\right)dr\right]}_{\frac{2}{R^2}\int_0^R\left(\frac{\tilde{v}}{r}\right)rdr\ \text{integration by parts}}+\frac{2}{R^2}\int_0^R\frac{\partial\tilde{v}}{\partial r}rdr=\frac{2}{R^2}\left[\tilde{v}\,r\right]_0^R\equiv 0$ is employed. An eddy viscosity distribution is then needed to close the acoustic wave equations. This is described in the following sections.

4.4 Proposed Eddy-viscosity Distribution

In steady turbulent flows, the viscosity is non-uniform in space, but constant in time. In unsteady turbulent flows, it is both non-uniform and non-constant. This behaviour greatly complicates the prediction of the acoustic wave propagation. To obtain the meaningful analytical solutions, simplifying assumptions are necessary. A reasonable approximation is used to represent the non-uniformity, but no account is taken of temporal variations in the eddy viscosity. The justifications of these simplifications have been described in the preceding chapter.

Fig. 4.1 shows experimental data obtained by Laufer (1954) for steady, turbulent smooth-walled pipe flows. Churchill and Chan (1995) indicated that away from the immediate vicinity of the rough surface, the eddy viscosity could be determined using the same relations as for smooth pipes.

In the present proposed model, the empirical dimensionless viscosity $\nu_T/(u_{st}^* R)$ varies linearly with y/R ($y = R - r$ is the distance from the pipe wall) in the outer annular region $0 \le y/R \le 0.175$, and is kept constant at 0.07 in the core of the flow. As shown in Fig. 4.1, the dash line depicts the Ohmi's eddy viscosity profile for the smooth wall turbulence, and the solid line presents the rough wall approach. At the wall, the present eddy viscosity distribution assumes that the effective viscosity exceeds the kinematic viscosity and can be determined by matching experiments, but Ohmi's approach assumes the effective viscosity at the wall is always equal to the flow kinematic viscosity.

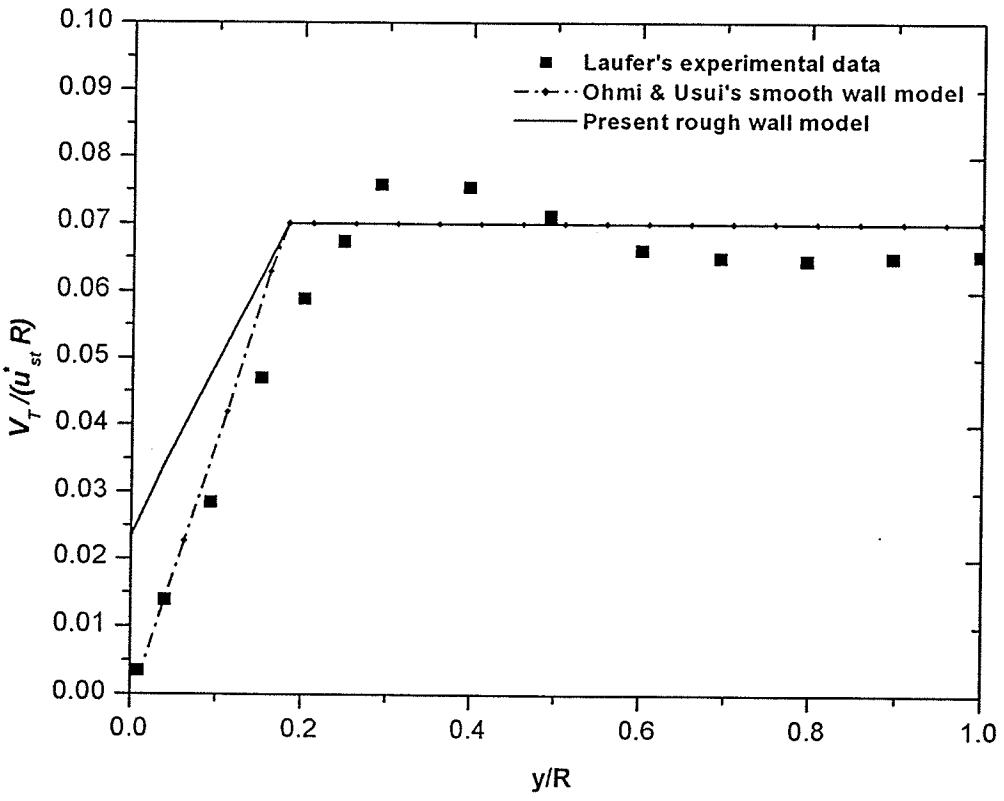

Figure 4.1. Linear-fitted eddy viscosity distributions in an overall pipe cross-section

The remaining task is to find an approximation of the outer annular region (e.g. $0 \le y/R \le 0.175$) eddy viscosity distribution. The eddy viscosity is a function of the steady friction velocity u_{st}^* and the pipe radii. Thus, the assumed total turbulent kinematic viscosity in the annular shear layer at a distance y from the wall is:

$$\nu_T = \nu_w + b\left(yu_{st}^*\right), \qquad 0 \le \frac{y}{R} \le 0.175 \tag{4.17}$$

The parameter b determines the rate of change of ν_T from the effective viscosity ν_w at the wall to the value of $0.07\left(Ru_{st}^*\right)$ at the core / outer-layer interface. Therefore, the total turbulent kinematic viscosity ν_T for the overall conduit cross-section can be expressed by:

$$\nu_T = \begin{cases} \nu_w + b\left(yu_{st}^*\right), & 0 \le \dfrac{y}{R} \le 0.175 \\ 0.07\left(Ru_{st}^*\right), & 0.175 \le \dfrac{y}{R} \le 1 \end{cases} \tag{4.18}$$

Assuming a steady friction velocity, the value of b can be estimated from the friction factor f and the steady mean flow Reynolds number. The Reynolds number is defined here in terms of the mean axial steady flow velocity $\tilde{u}_{m,st}$ (where: $\bar{u}_m(x,t) = \tilde{u}_{m.st}(x) + \tilde{u}'_m(x,t)$) and pipe internal diameter D as:

$$\mathrm{Re}_{st} = \frac{\tilde{u}_{m,st} D}{\nu} \tag{4.19}$$

In pulsatile turbulent flow with a time period of T_p, the axial mean steady velocity is defined as:

$$\tilde{u}_{m,st} = \frac{1}{T_p A} \int_0^{T_p} \int_A \tilde{u}_{st} \, dA \, dT_p \tag{4.20}$$

The friction factor f is defined by:

$$f = \frac{4\tau_{ws}}{\frac{1}{2}\rho_0 \widetilde{U}_{m,st}^{\ 2}} \tag{4.21}$$

And the steady state friction velocity u_{st}^* can be obtained after using Eq. (4.19), as:

$$u_{st}^* = \sqrt{\frac{\tau_{w,st}}{\rho_0}} = \sqrt{\frac{f}{8}}\ \tilde{u}_{m,st} = v\sqrt{\frac{f}{8}}\frac{\mathrm{Re}_{st}}{D} \tag{4.22}$$

with the explicit friction coefficient formula given by Haaland (1983):

$$\frac{1}{\sqrt{f}} = -1.8\log\left[\frac{6.9}{\mathrm{Re}} + \left(\frac{\varepsilon_{rou}}{3.7D}\right)^{1.11}\right] \tag{4.23}$$

where: ε_{rou}/D is the relative roughness, for the commercial steel, the value of ε_{rou} equalling $3.81\times10^{-6}[m]$ is recommended.

A roughness Reynolds number ε_{rou}^* is defined to characterize the wall roughness, as:

$$\varepsilon_{rou}^* = \frac{\varepsilon_{rou}u_{st}^*}{v} \tag{4.24}$$

Experiment shows that the fully smooth wall behaviour exists when $\varepsilon_{rou}^* < 5$, the transitional rough wall behaviour exists when $5 < \varepsilon_{rou}^* < 70$, and that fully rough wall behaviour exists when $\varepsilon_{rou}^* > 70$.

To determine the parameter b, we find that at the outer layer / core interface (e.g. $y/R = 0.175$), the turbulent eddy viscosity ν_T becomes:

$$\nu_T\Big|_{\frac{y}{R}=0.175} = \nu_w + b\left(\frac{y}{R}\right)\Big|_{0.175}\left(Ru_{st}^*\right) = \nu_w + 0.175b\ \left(Ru_{st}^*\right) = 0.07\left(Ru_{st}^*\right)$$

$$\Rightarrow\ 0.07\left(Ru_{st}^*\right) = \nu_w + 0.175b\ \left(Ru_{st}^*\right) \tag{4.25}$$

After rearranging, yields:

$$b\ = \frac{\left(0.07Ru_{st}^*\right) - \nu_w}{\left(0.175Ru_{st}^*\right)} = 0.4 - \frac{\nu_w}{0.175Ru_{st}^*} \tag{4.26}$$

Accordingly, the piece-wise two-region eddy viscosity model proposed here is given in Tab. 4.1, as:

Table 4.1. Present two-region model of eddy viscosity

Present 2-region Model		
y/R	Sub-region j	ν_T distribution
0	$j = 1$	$\nu_w + b\left(yu_{st}^*\right)$
0.175	$j = 2$	$0.07\left(Ru_{st}^*\right)$
1		

4.5 The Transfer Matrix and Specific Impedances

Generally, the solution of the normalized acoustic pressure (the ratio of the pressure at the tube end to the pressure at the tube entrance) is in the form of a 2×2 transfer matrix. To obtain the transfer function, solutions for the cross-sectional velocity distribution,

acoustic wave propagation constant and the line specific acoustic impedances must be derived in advance.

4.5.1 Cross-sectional velocity distribution

Starting from Eq. (4.14) together with the two-region linear eddy viscosity model described above, after Laplace transformation with zero initial value and the replacement of variables, yields (*where* ν_T *is a function of* r *only*):

$$\frac{\partial \tilde{u}'}{\partial t} = -\frac{1}{\rho_0}\frac{\partial \tilde{p}'}{\partial x} + \frac{1}{r}\frac{\partial}{\partial r}\left(r\nu_T \frac{\partial \tilde{u}'}{\partial r}\right)$$

$$\Rightarrow\ s\hat{u}'_j(x,r,s) = -\frac{1}{\rho_0}\frac{\partial \hat{p}'(x,s)}{\partial x} + \nu_T \frac{\partial^2 \hat{u}'_j(x,r,s)}{\partial r^2} + \frac{\partial \hat{u}'_j(x,r,s)}{\partial r}\left(\frac{d\nu_T}{dr} + \frac{\nu_T}{r}\right)$$

$$\Rightarrow\ \nu_T \frac{\partial^2 V}{\partial r^2} + \left(\frac{d\nu_T}{dr} + \frac{\nu_T}{r}\right)\frac{\partial V}{\partial r} - sV = 0 \qquad (4.27)$$

with:
$$V(x,r,s) = \hat{u}'_j(x,r,s) + \frac{1}{\rho_0 s}\frac{d\hat{p}'(x,s)}{dx} \qquad (4.28)$$

where: $j = 1,2$ is the sub-region index, and $s = iw$ ($i \equiv \sqrt{-1}$, $w = angular\ \ frequency$) is the *LaPlacian* variable transformation with respect to time. The hat "$\hat{}$" signifies the Laplace transform, such as: $\hat{u}'_j(x,r,s) = L\left[\tilde{u}'_j(x,r,t)\right]$, $\hat{p}'(x,s) = L\left[\tilde{p}'(x,t)\right]$, and $L\left[\frac{\partial \tilde{u}'_j(x,r,t)}{\partial t}\right] = s\hat{u}'_j(x,r,s)$.

To solve Eq. (4.27), the transformations of variables are defined as $z_1(r)$ *and* $z_2(r)$ which are similarly used by Ohmi *et al.* (1976), including the total turbulence viscosity

ν_T for each sub-region $j = 1,2$ respectively:

$$\begin{cases} z_1(r) = \dfrac{2}{b u_{st}^*}\sqrt{s\,\nu_{T,1}}\ , & 0 \le \dfrac{y}{R} \le 0.175 \\ z_2(r) = r\sqrt{\dfrac{s}{\nu_{T,2}}}\ , & 0.175 \le \dfrac{y}{R} \le 1 \end{cases} \tag{4.29}$$

$$\text{where: } \nu_{T,j} = \begin{cases} \nu_w + b\left(y u_{st}^*\right), & (j=1),\quad 0 \le \dfrac{y}{R} \le 0.175 \\ 0.07\left(R u_{st}^*\right), & (j=2),\quad 0.175 \le \dfrac{y}{R} \le 1 \end{cases} \tag{4.30}$$

Then Eq. (4.27) and arrives the following form for every region (shown in *Appendix A*) as:

$$\frac{\partial^2 V}{\partial\left[z_j(r)\right]^2} + \frac{1}{z_j(r)}\frac{\partial V}{\partial\left[z_j(r)\right]} - V = 0 \tag{4.31}$$

The general solution of Eq. (4.31) is obtained in the form of:

$$V(x,r,s) = f(x,s) \times \left\{ C_j . I_0\left[z_j(r)\right] + D_j . K_0\left[z_j(r)\right] \right\} \tag{4.32}$$

and:

$$\frac{\hat{u}_j'(x,r,s)}{\left[\dfrac{1}{\rho_0 s}\dfrac{d\hat{p}'(x,s)}{dx}\right]} + 1 = \frac{f(x,s)}{\left[\dfrac{1}{\rho_0 s}\dfrac{d\hat{p}'(x,s)}{dx}\right]} \times \left\{ C_j . I_0\left[z_j(r)\right] + D_j . K_0\left[z_j(r)\right] \right\} \tag{4.33}$$

where: I_0 and K_0 are the modified Bessel functions of first and second kinds of order zero, respectively. C_j and D_j are integration constants and can be found from the boundary conditions. $f(x,s)$ is any function that can be decided by any non-zero

forcing function of $d\hat{p}'(x,s)/dx$. For simplicity, $f(x,s)=\frac{1}{\rho_0 s}\frac{d\hat{p}'(x,s)}{dx}$ is chosen as a particular one. Hence, assuming the velocity and pressure profiles vary sinusoidally at every frequency, the cross-sectional velocity (before the average over entire pipe cross-section) is, in terms of axial pressure gradient:

$$\hat{u}'_j(x,r,s)=\left\{C_j.I_0\left[z_j(r)\right]+D_j.K_0\left[z_j(r)\right]-1\right\}.\left[\frac{1}{\rho_0 s}\frac{d\hat{p}'(x,s)}{dx}\right] \qquad (4.34)$$

To decide the integration constants in Eq. (4.34), the relationships of velocity and its derivatives over the entire pipe cross-section are necessary. Applying the boundary conditions described in the assumptions (10) and (11) to Eq. (4.34) gives the following *2n (n=2 here)* relations for C_j and D_j $(j=1,2)$:

$$\begin{cases} (1)\ C_1 I_0\left[z_1(R)\right]+D_1 K_0\left[z_1(R)\right]-1=0 & at\ \ r=R,\ no-slip\ condition \\ (2)\ C_1 I_0\left[z_1(r_2)\right]+D_1 K_0\left[z_1(r_2)\right]=C_2 I_0\left[z_2(r_2)\right]+D_2 K_0\left[z_2(r_2)\right], & velocity\ \ continuity \\ (3)\ \nu_{T,1}\left.\frac{\partial\hat{u}_1'}{\partial r}\right|_{r_2}=-\nu_{T,2}\left.\frac{\partial\hat{u}_2'}{\partial r}\right|_{r_2} & shear\ \ stress\ \ continuity\ \ at\ \ the\ \ interface\ \ r_2=0.825R, \\ (4)\ D_2\equiv 0 & at\ \ r=0,\ velocity\ \ at\ \ the\ \ pipe\ \ axis\ \ must\ \ be\ \ finite. \end{cases}$$

where r_{j+1} is the boundary between *j-th* region and *(j+1)-th* region. The above equation sets are valid for multi-regional model in which *j = 1, 2, ..., n*. The above relations result in *2n-1* algebraic equations that determines 3 unknowns in the present work, C_1, C_2, *and* D_1, since $K_0\left[z_j(r)\right]$ has a pole at the origin $r=0$, one must set

$D_2 = 0$. Relation (3) above also can be rewritten as:

$$\nu_{T,1} \left.\frac{d\left[z_1(r)\right]}{dr}\right|_{r_2} \left\{C_1 I_1\left[z_1(r_2)\right] - D_1 K_1\left[z_1(r_2)\right]\right\} = -\nu_{T,2} \left.\frac{d\left[z_2(r)\right]}{dr}\right|_{r_2} \left\{C_2 I_1\left[z_2(r_2)\right]\right\}$$

$$where: \left.\frac{d\left[z_1(r)\right]}{dr}\right|_{r_2} = -\sqrt{s/\nu_{T,1}(r_2)} \; and \; \left.\frac{d\left[z_2(r)\right]}{dr}\right|_{r_2} = \sqrt{s/\nu_{T,2}(r_2)}$$

C_1, C_2, *and* D_1 are then derived based on above relations, such as:

$$C_1 = \frac{1}{\left\{I_0\left[z_1(R)\right] + \frac{\Delta_1}{\Delta_2} K_0\left[z_1(R)\right]\right\}} \tag{4.35}$$

$$D_1 = \frac{(\Delta_1/\Delta_2)}{\left\{I_0\left[z_1(R)\right] + \frac{\Delta_1}{\Delta_2} K_0\left[z_1(R)\right]\right\}} \tag{4.36}$$

$$C_2 = C_1 \cdot \left\{I_0\left[Z_1(r_2)\right]/I_0\left[Z_2(r_2)\right]\right\} + D_1 \cdot \left\{K_0\left[Z_1(r_2)\right]/I_0\left[Z_2(r_2)\right]\right\} \tag{4.37}$$

where:

$$\begin{cases} \Delta_1 = \sqrt{\dfrac{\nu_{T,1}(r_2)}{\nu_{T,2}(r_2)}} \left\{\dfrac{I_1\left[z_1(r_2)\right]}{I_1\left[z_2(r_2)\right]}\right\} - \left\{\dfrac{I_0\left[z_1(r_2)\right]}{I_0\left[z_2(r_2)\right]}\right\} \\ \Delta_2 = \sqrt{\dfrac{\nu_{T,1}(r_2)}{\nu_{T,2}(r_2)}} \left\{\dfrac{K_1\left[z_1(r_2)\right]}{I_1\left[z_2(r_2)\right]}\right\} + \left\{\dfrac{K_1\left[z_1(r_2)\right]}{I_0\left[z_2(r_2)\right]}\right\} \end{cases} \tag{4.38}$$

4.5.2 Wave propagation constant

The cross-sectional average velocity in the Laplace domain is:

$$\hat{u}'_m(x,s) = \frac{2}{R^2} \sum_{j=1}^{2} \int_{r_{j+1}}^{r_j} \left[\hat{u}'_j(x,r,s)\right] r dr \tag{4.39}$$

Since the pressure distribution is independent of r, applying the Laplace-transformation with zero initial values of Eqs. (4.15) and (4.16), yields:

$$\begin{cases} \hat{p}'(x,s) = -\dfrac{\rho_0 C^2}{s}\dfrac{d\hat{u}'_m(x,s)}{dx} & (4.40) \\ \hat{u}'_m(x,s) = \left[-\dfrac{1}{\rho_0 s}.\dfrac{d\hat{p}'(x,s)}{dx}\right] + \dfrac{2}{Rs}\left(\nu_{T,1}\dfrac{\partial\hat{u}'_1(x,r,s)}{\partial r}\right)\Bigg|_{r=R} & (4.41) \end{cases}$$

The velocity perturbation profile $\tilde{u}'_j(x,r,t)$ is assumed piece-wise continuous over the pipe cross-section. Hence the relation after the Lapalace-transformation of $L\left[\left.\dfrac{\partial\tilde{u}'_j(x,r,t)}{\partial r}\right|_{r=R}\right] \equiv \left[\left.\dfrac{\partial\hat{u}'_j(x,r,s)}{\partial r}\right|_{r=R}\right]$ must be valid at the wall.

Differentiating Eq. (4.40) with respect to x, yields:

$$\frac{d\hat{p}'(x,s)}{dx} = \left(-\frac{\rho_0 C^2}{s}\right)\frac{d^2\hat{u}'_m(x,s)}{dx^2} \qquad (4.42)$$

Differentiating Eq. (4.34) with respect to r at the wall, yields:

$$\left.\frac{\partial\hat{u}'_1(x,r,s)}{\partial r}\right|_{r=R} = \left[\frac{1}{\rho_0 s}\frac{d\hat{p}'(x,s)}{dx}\right].\left(\left.\frac{dZ_1(r)}{dr}\right|_{r=R}\right).\left.\frac{\partial}{\partial Z_1(r)}\left\{C_1.I_0\left[z_1(r)\right]+D_1.K_0\left[z_1(r)\right]-1\right\}\right|_{r=R}$$

$$\therefore \quad \frac{\partial\hat{u}'_1(x,R,s)}{\partial r} = \left[\frac{1}{\rho_0 s}\frac{d\hat{p}'(x,s)}{dx}\right].\left\{\frac{2}{bu^*_{st}}.\frac{d}{dr}\left(\left.\sqrt{s.\nu_{T,1}\left[1+\frac{bu^*_{st}}{\nu}(R-r)\right]}\right)\right|_{r=R}\right\}\left\{C_1.I_1\left[z_1(R)\right]-D_1.K_1\left[z_1(R)\right]\right\}$$

$$\Rightarrow \quad \frac{\partial\hat{u}'_1(x,R,s)}{\partial r} = \left[\frac{1}{\rho_0 s}\frac{d\hat{p}'(x,s)}{dx}\right].\left[-\sqrt{s/\nu_{T,1}\big|_{r=R}}\right].\left\{C_1.I_1\left[z_1(R)\right]-D_1.K_1\left[z_1(R)\right]\right\} \qquad (4.43)$$

Where I_1 and K_1 are the modified Bessel functions of first and second kinds of order one respectively. C_1 and D_1 are integration constants defined in Eqs. (4.35) and (4.36).

Substituting Eq. (4.43) into Eqs. (4.41) and (4.42) gives a simple ordinary differential equation of second order:

$$\frac{d^2\hat{u}'_m(x,s)}{dx^2} - \left\{ \frac{\left(s^2/C^2\right)}{\left\{1+\frac{2}{R}\sqrt{\frac{\nu_w}{s}}\left\{C_1.I_1\left[z_1(R)\right]-D_1.K_1\left[z_1(R)\right]\right\}\right\}} \right\} \hat{u}'_m(x,s) = 0 \qquad (4.44)$$

The wave propagation constant is therefore:

$$\Gamma(s) = \left(\frac{s}{C}\right)\left\{1+\frac{2}{R}\sqrt{\frac{\nu_w}{s}}\left\{C_1.I_1\left[z_1(R)\right]-D_1.K_1\left[z_1(R)\right]\right\}\right\}^{-1/2} \qquad (4.45)$$

4.5.3 Specific acoustic impedance

The specific acoustic impedance is given by taking the ratio of the pressure perturbation to the mean velocity perturbation at the boundary:

$$\tilde{Z} = \hat{p}' \,/\, \hat{u}'_m \qquad (4.46)$$

In general, $\tilde{Z}$ will depend on the properties of the boundary, the properties of the fluid, the frequency of the wave, and so on, but not on time. Also, it may vary from point to point on the boundary. It should be clear that $\tilde{Z}$ is introduced as a specific impedance because the term *"acoustic impedance"* is usually reserved for the ratio of pressure to the volume flow rate.

In many practical situations, the conditions imposed on the acoustic variables at the boundary are not known a priori. Therefore the specific acoustic impedance at the boundary is usually obtained from experiments. Theoretically, to determine the inlet and outlet specific acoustic impedance, it is assumed that the upstream specific acoustic impedance can be modeled by Thurston's (1952) analogous specific acoustic impedance per unit length Z_α:

$$Z_\alpha = \psi / \theta \tag{4.47}$$

$$where: \begin{cases} \psi: \textit{ is the negative pressure gradient down the tube;} \\ \theta: \textit{ is average particle velocity over the tube cross} - \text{section.} \end{cases}$$

According to the definition of Z_α and $\hat{u}_m'$, it is obtained:

$$Z_\alpha = \frac{\left(-d\hat{p}'/dx\right)}{\hat{u}_m'} = \frac{\left(-d\hat{p}'/dx\right)}{\left[\theta^* \frac{1}{\rho_0 s}\frac{d\hat{p}'}{dx}\right]} \doteq -\left[\frac{\rho_0 s}{\theta^*}\right] \tag{4.48}$$

where:

$$\theta^* = \frac{2}{R^2}\sum_{j=1}^{2}\int_{r_{j+1}}^{r_j}\left\{C_j.I_0\left[z_j(r)\right] + D_j.K_0\left[z_j(r)\right] - 1\right\} r dr \tag{4.49}$$

The averaged mean velocity $\hat{u}_m'$ can be solved by directly integrating Eq. (4.49) over the pipe cross section. Details of the integral are presented in *Appendix A*, and becomes:

$$\theta = \frac{\theta^*}{\rho_0 s}\frac{d\hat{p}'}{dx} = \left(\theta_1^* + \theta_2^* - \frac{2}{R^2}\sum_{j=1}^{2}\int_{r_{j+1}}^{r_j} r dr\right).\frac{1}{\rho_0 s}\frac{d\hat{p}'}{dx} \tag{4.50}$$

where: $$\theta^* = \left(\theta_1^* + \theta_2^* - 1\right)$$

$$\theta_1^* = \frac{2}{R^2} \times \left\langle \left(-C_1 \frac{bu_{st}^*}{2s} \right) \left\{ \left(r Z_1(r) \; I_1\left[Z_1(r) \right] \right) \right|_{0.825R}^{R} + \left(\frac{bu_{st}^*}{2s} \right) \left(Z_1^2(r) \; I_2\left[Z_1(r) \right] \right) \Big|_{0.825R}^{R} \right\}$$

$$+ \left(D_1 \frac{bu_{st}^*}{2s} \right) \left\{ \left(r Z_1(r) \; K_1\left[Z_1(r) \right] \right) \right|_{0.825R}^{R} - \left(\frac{bu_{st}^*}{2s} \right) \left(Z_1^2(r) \; K_2\left[Z_1(r) \right] \right) \Big|_{0.825R}^{R} \right\} \Bigg\rangle$$

$$\theta_2^* = \frac{2}{R^2} \times C_2 \int_0^{0.825R} I_0\left[Z_2(r) \right] r dr = \frac{2}{R^2} \times \left\langle \left(C_2 \frac{0.07 R u_{st}^*}{s} \right) \left(Z_2(r) \; I_1\left[Z_2(r) \right] \right) \Big|_0^{0.825R} \right\rangle .$$

In which I_2, K_2 are the modified Bessel functions of first and second kinds of order 2 respectively.

4.5.4 Transfer function

Starting from Eq. (4.44), the general solution to the axial propagation velocity distribution is:

$$\hat{u}'_m(x,s) = A.e^{\Gamma(s).x} + B.e^{-\Gamma(s).x} \text{ (where A and B are integration constants)} \tag{4.51}$$

The general solution to the acoustic pressure distributions then can be obtained by differentiating Eq. (4.51) with respect to x:

$$\hat{p}'(x,s) = \left(-\frac{\rho_0 C^2}{s} \right) \left[(A.\Gamma) e^{\Gamma.x} - (B.\Gamma) e^{-\Gamma.x} \right] \tag{4.52}$$

Eqs. (4.51) and (4.52) then can be used to derive the standard transfer function solution. Assuming the axial boundary conditions ($x = 0$ *and* $x = L$) as:

$$\begin{cases} \hat{p}'(0,s) = \hat{p}'_1 \\ \hat{p}'(L,s) = \hat{p}'_2 \end{cases} \qquad \begin{cases} \hat{u}'_m(0,s) = \hat{u}'_1 \\ \hat{u}'_m(L,s) = \hat{u}'_2 \end{cases} \tag{4.53}$$

Above equations represent the acoustic pressure and velocity values at the pipe inlet and outlet, L indicating the distance between the pipe upstream and downstream. Substituting Eq. (4.53) into Eqs. (4.51) and (4.52), yields:

$$\begin{cases} \hat{u}'_1 = A + B \\ \hat{u}'_2 = A.e^{\Gamma.L} + B.e^{-\Gamma.L} \end{cases} \quad and \quad \begin{cases} \hat{p}'_1 = \left(-\frac{\rho_0 C^2}{s}.\Gamma\right)[A - B] \\ \hat{p}'_2 = \left(-\frac{\rho_0 C^2}{s}.\Gamma\right)\left[A.e^{\Gamma.L} - B.e^{-\Gamma.L}\right] \end{cases} \tag{4.54}$$

where: $$A = \frac{1}{2}\left(\hat{u}'_1 + \frac{1}{\beta}\hat{p}'_1\right),\ B = \frac{1}{2}\left(\hat{u}'_1 - \frac{1}{\beta}\hat{p}'_1\right),\ and\ \beta = \left(-\frac{\rho_0 C^2}{s}.\Gamma\right) \tag{4.55}$$

Hence, solutions for $\hat{u}'_m(x,s)$ and $\hat{p}'(x,s)$ can be obtained on the basis of the axial boundary conditions by:

$$\begin{cases} \hat{u}'_m(x,s) = \hat{u}'_1.\cosh(\Gamma.x) + \frac{\hat{p}'_1}{\beta}.\sinh(\Gamma.x) & (4.56) \\ \hat{p}'(x,s) = \left(\beta\hat{u}'_1\right).\sinh(\Gamma.x) + \hat{p}'_1.\cosh(\Gamma.x) & (4.57) \end{cases}$$

and:

$$\begin{cases} \hat{u}'_1 = \frac{\hat{u}'_2}{\cosh(\Gamma.L)} - \frac{\hat{p}'_1}{\beta}\frac{\sinh(\Gamma.L)}{\cosh(\Gamma.L)} & (4.58) \\ \hat{p}'_1 = \frac{\hat{p}'_2}{\cosh(\Gamma.L)} + \left(\beta\hat{u}'_1\right)\frac{\sinh(\Gamma.L)}{\cosh(\Gamma.L)} & (4.59) \end{cases}$$

Substituting Eq. (4.58) into Eq. (4.59), and substituting Eq. (4.59) into Eq. (4.58), yields two relations as:

$$\begin{cases} \hat{u}_1' = \hat{u}_2' \cosh(\Gamma L) - \dfrac{\hat{p}_2'}{\beta} \sinh(\Gamma L) & (4.60) \\ \hat{p}_1' = \hat{p}_2' \cosh(\Gamma L) - \left(\beta \hat{u}_2'\right) \sinh(\Gamma L) & (4.61) \end{cases}$$

A 2×2 transfer matrix of single piping system is then obtained as:

$$\begin{bmatrix} \hat{u}_1' \\ \hat{p}_1' \end{bmatrix} = \begin{bmatrix} \cosh(\Gamma L) & -\dfrac{1}{\beta} \sinh(\Gamma L) \\ -\beta \sinh(\Gamma L) & \cosh(\Gamma L) \end{bmatrix} \begin{bmatrix} \hat{u}_2' \\ \hat{p}_2' \end{bmatrix} \tag{4.62}$$

or in the form of the transfer function, as:

$$\frac{\hat{p}_2'(s)}{\hat{p}_1'(s)} = \frac{1}{\cosh(\Gamma L) - \beta . \dfrac{\hat{u}_2'(s)}{\hat{p}_2'(s)} \sinh(\Gamma L)} \tag{4.63}$$

At the line inlet and outlet, the specific acoustic impedances are defined as:

$$\begin{cases} \tilde{Z}_0 = \dfrac{\hat{p}_1'(s)}{\hat{u}_1'(s)} & (4.64) \\ \tilde{Z}_L = \dfrac{\hat{p}_2'(s)}{\hat{u}_2'(s)} = \dfrac{\tilde{Z}_0 - \beta . \tanh(\Gamma L)}{1 - \left(\tilde{Z}_0 / \beta\right) . \tanh(\Gamma L)} & (4.65) \end{cases}$$

Correspondingly, the inlet specific acoustic impedance is expressed in terms of the Z_α by introducing a resistance coefficient λ (Rzentkowski *et al.* (1993)), as:

$$\tilde{Z}_0 \doteq \left. \frac{\hat{p}_1'(s)}{\hat{u}_1'(s)} \right|_{x=0} = \lambda . Z_\alpha = -\lambda \left[\frac{\rho_0 s}{\theta^*} \right] \tag{4.66}$$

The resistance coefficient λ is believed to capture any line inlet imperfections such as

flow restrains, line vibrations, and boundary conditions to some extent. The exact tuning of the resonance amplitude of the transfer function Eq. (4.63) requires using λ, which can be determined by matching the experiments.

Substituting the axial mean velocity solution of Eq. (4.50) into Eqs. (4.64) and (4.65), the downstream specific acoustic impedance $\hat{p}_2(s)/\hat{u}_2(s)$ can be theoretically solved. Consequently, the transfer function Eq. (4.63) can be solved analytically. Therefore, the linear impedance transfer function yields a final form of following equation:

$$\frac{\hat{p}_2(s)}{\hat{p}_1(s)} = \frac{1}{\cosh(\Gamma.L) - \beta.\left\{\dfrac{1-\left(-\lambda\left[\dfrac{\rho_0 s}{\theta^*}\right]\Big/\beta\right).\tanh(\Gamma.L)}{-\lambda\left[\dfrac{\rho_0 s}{\theta^*}\right]-\beta.\tanh(\Gamma.L)}\right\}\sinh(\Gamma.L)} \qquad (4.67)$$

The modulus of this formula is then used to evaluate the acoustic pressure amplification in high mean Reynolds number turbulent flows. Recalling that the turbulence propagation constant Γ and parameter β contain the steady and unsteady parts, hence the above transfer function can be easily revised to its steady flow model.

4.6 Turbulence Volumetric Drag

As discussed in preceding chapter, the volumetric drag has been used in the ABAQUS code as the damping parameter, which is determined from experimental data. The shortcoming is obviously if the experimental data are not available a priori. Thus, a

systematic development of the volumetric drag formula becomes necessary, especially in turbulent flow. In ABAQUS, the axial momentum equation is derived in the time-domain analogous to Eq. (4.16) as:

$$\frac{\partial \tilde{u}_m'}{\partial t} + \frac{1}{\rho_0}\frac{\partial \tilde{p}'}{\partial x} + R_v \frac{\tilde{u}_m'}{\rho_0} = 0 \tag{4.68}$$

R_v is termed the turbulence volumetric drag herein, and other parameters have the same meanings as aforementioned.

4.6.1 Time-harmonic solution

For systems subjected to a continuous harmonic excitation, the flow parameters are feasibly assumed to vary sinusoidally. Therefore, the solutions of the 1-D continuity equation Eq. (4.15) and axial momentum equation Eq. (4.16) are simultaneous functions of x and t. For a linear system driven sinusoidally, the output must be a sinusoid of the same frequency as the driven signal. Hence, the solutions can be assumed of the form:

$$\begin{cases} \tilde{u}_m'(x,t) = \left[U(x).e^{i\omega t}\right] & (4.70) \\ \tilde{p}'(x,t) = \left[P(x).e^{i\omega t}\right] & (4.71) \end{cases}$$

Where $U(x)$ and $P(x)$ are any particular functions of x. The harmonic time-derivative relations are given by:

$$\begin{cases} \dfrac{\partial \tilde{u}_m'(x,t)}{\partial t} = U(x)\dfrac{de^{iwt}}{dt} = (iw).\tilde{u}_m'(x,t) & (4.72) \\ \dfrac{\partial \tilde{p}'(x,t)}{\partial t} = P(x)\dfrac{de^{iwt}}{dt} = (iw).\tilde{p}'(x,t) & (4.73) \end{cases}$$

It is herein considered $\hat{u}_m'$ and $\hat{p}'$ representing the axial velocity and pressure distributions with respect to x and w in *LaPlacian* domain at certain time. Therefore, the exponential function e^{iwt} is assumed to be a particular solution for time-harmonic oscillations at certain frequency. In other words, defining:

$$\begin{cases} \tilde{u}_m'(x,t) = \hat{u}_m'.e^{iwt} & (4.74) \\ \tilde{p}'(x,t) = \hat{p}'.e^{iwt} & (4.75) \end{cases}$$

Using the relations of axial velocity distribution in *LaPlacian* domain of Eq. (4.50), $\tilde{u}_m'(x,t)$ becomes:

$$\tilde{u}_m'(x,t) = \theta^* \frac{1}{\rho_0 iw}\frac{d\left[\hat{p}'.e^{iwt}\right]}{dx} \qquad (4.76)$$

This formula is then referred to the time-harmonic solution of axial velocity distribution, and is used to derive the turbulence volumetric drag in the next section.

4.6.2 Similarity analysis

Substituting Eq. (4.75) into Eq. (4.76), and after rearrangements, yields:

$$(iw)\rho_0 \tilde{u}_m'(x,t) = \theta^* \frac{d\tilde{p}'(x,t)}{dx} \qquad (4.77)$$

Let $\theta^* = \theta^*_{real} + i\theta^*_{imag}$, where θ^*_{real} and θ^*_{imag} are the real and imaginary parts, respectively, Eq. (4.77) becomes:

$$\frac{(iw)\rho_0 \tilde{u}_m'(x,t)}{\left[\theta^*_{real} + i\theta^*_{imag}\right]} = \frac{d\tilde{p}'(x,t)}{dx} \tag{4.78}$$

Applying the complex function algebra rule of $\frac{a+ib}{c+id} = \frac{ac+bd}{c^2+d^2} + \frac{bc-ad}{c^2+d^2}$, where $a, b, c,$ *and* d are any real variables. Eq. (4.78) becomes:

$$\left\{\rho_0 \frac{\theta^*_{real}}{\theta^{*\,2}_{real} + \theta^{*\,2}_{imag}}\right\}(iw)\tilde{u}_m'(x,t) + \left\{\rho_0 \frac{w\theta^*_{imag}}{\theta^{*\,2}_{real} + \theta^{*\,2}_{imag}}\right\}\tilde{u}_m'(x,t) = \frac{d\tilde{p}'(x,t)}{dx} \tag{4.79}$$

Using the time-derivative relation of Eq. (4.72) in which $(iw)\tilde{u}_m'(x,t) = d\tilde{u}_m'(x,t)/dt$, we obtain the time-harmonic x-momentum equation:

$$\left\{-\rho_0 \frac{\theta^*_{real}}{\theta^{*\,2}_{real} + \theta^{*\,2}_{imag}}\right\}\frac{d\tilde{u}_m'(x,t)}{dt} + \frac{d\tilde{p}'(x,t)}{dx} + \left\{-(\rho_0 w)\frac{\theta^*_{imag}}{\theta^{*\,2}_{real} + \theta^{*\,2}_{imag}}\right\}\tilde{u}_m'(x,t) = 0 \tag{4.80}$$

Comparing the coefficients of Eq. (4.68) with Eq. (4.80), it is clear that the turbulence volumetric drag R_v is given by the last term in bracket. However, the total turbulence volumetric drag is the sum of its steady part and unsteady part as emphasized by Vardy *et al.* (1995). Consequently R_v is modified as:

$$R_v = \left\{-(\rho_0 w)\frac{\theta^*_{imag}}{\theta^{*\,2}_{real} + \theta^{*\,2}_{imag}}\right\} + \frac{f.\mathrm{Re}_{st}\,\nu.\rho_0}{D^2} \tag{4.81}$$

It should be stressed that, in the past, the volumetric drag is a constant estimated by tuning with the experimental data. On the contrary, the derived formula herein is

obviously a frequency dependent function, which provides more systematic and fundamental estimations if there are no experimental data available a priori. A computer program is written to evaluate the acoustic model developed above.

Chapter 5
Results and Discussions

5.1 Introduction

This chapter presents the results of simulation of the outer feeder of the STERN Loop experiments (Chatoorgoon *et al.* (1993), Kar (1993) and Zhou (1995)). Six different eddy viscosity models are applied and compared with the STERN experimental measurements, including four time-invariant models, such as:

(1) Ohmi & Usui's (1976) two-region model for smooth-walled turbulence;

(2) Brown's (1981) zero-perturbation (time-invariant) single region eddy viscosity model for smooth-walled turbulence;

(3) Zhou's (1995) two-region model for rough-walled turbulence;

(4) A new proposed two-region linear model for rough-walled turbulence.

In addition, Brown's (1981) quasi-steady and his time-dependent single layer eddy viscosity model are also investigated. Computed results using above models are compared against those computed using the reference value of volumetric drag of 13200, which was obtained by "best" fitting the experimental data. To evaluate and qualify the performances of these models, the volumetric drag values calculated from each case is also compared with the reference value of "13200".

5.2 Comparisons of Eddy Viscosity Models

The past work of different eddy viscosity models, and of the time-invariant assumption, on the accuracy of modeling the turbulent flows has been reviewed in chapter 3. To validate their applicability to the acoustic wave propagation in turbulence, comparisons with experimental measurements between various eddy viscosity models are necessary.

Fig. 5.1 graphs the experimental data obtained by Laufer (1954) for steady, turbulent, smooth-walled pipe flow together with four different time-invariant eddy viscosity distributions.

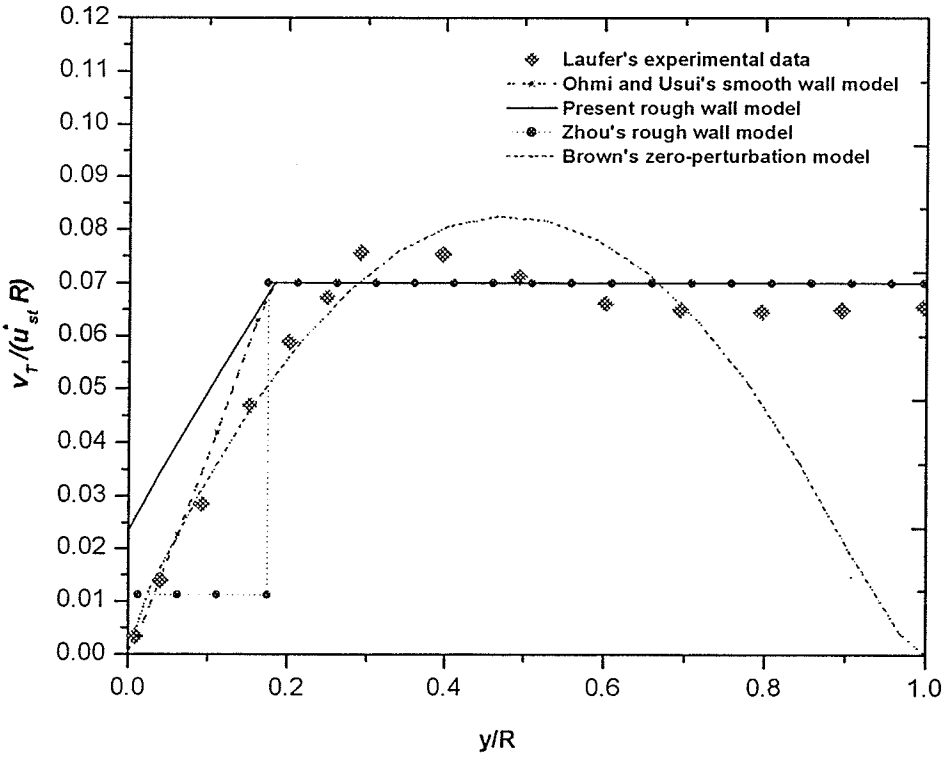

Figure 5.1. Comparisons of various time-invariant eddy viscosity profiles

Present proposed eddy viscosity model follows the Ohmi *et al.*'s (1976) two-region linear approximations with the different effective viscosity at the wall, and better suited for analyzing the rough-walled turbulence. The 1-D acoustic equations (i.e. Eqs. (4.15) ~ (4.16)) were described in chapter 4. Generally, analytical solutions to the 1-D acoustic wave propagation can be obtained from Eqs. (4.15) and (4.16) assuming appropriate eddy viscosity models. The results from various authors' eddy viscosity models are described below.

Ohmi & Usui's (1976) and Zhou's (1995) two-region time-invariant eddy viscosity profiles ν_T in each sub-region are tabulated in Tab. 5.1 as:

Table 5.1. Comparisons of Ohmi *et al.*'s & Zhou's eddy viscosity models

Two-region models		Ohmi & Usui 's model	Zhou's model
y/R	Sub-region j	Time-mean eddy viscosity distribution	Time-mean eddy viscosity distribution
0	$j = 1$	$\nu_{T,1} = \nu + 0.4\left(yu_{st}^*\right)$	$\nu_{T,1} = 0.0112\ Ru_{st}^*$
0.175	$j = 2$	$\nu_{T,2} = 0.07\ Ru_{st}^*$	$\nu_{T,2} = 0.07\ Ru_{st}^*$
1			

Ohmi's model

Using the time-invariant eddy viscosity distribution described in Tab. 5.1, the acoustic momentum equation in the Laplace domain becomes:

$$\nu_T \frac{d^2\hat{u}'}{dr^2} + \left(\frac{\nu_T}{r} + \frac{d\nu_T}{dr}\right)\frac{d\hat{u}'}{dr} = s\hat{u}' + \frac{1}{\rho_0}\frac{d\hat{p}'}{dx} \tag{5.1}$$

The solutions of Ohmi's model (1976) for acoustic pressure, radial velocity and wave propagation constant are summarized below (x and r are axial and radial coordinates, respectively).

$$\hat{p}'(x,s) = Ae^{\gamma x} + Be^{-\gamma x} \tag{5.2}$$

$$\hat{u}_j'(x,r,s) = \frac{\gamma}{\rho_0 s}\left(Ae^{\gamma x} - Be^{-\gamma x}\right)\left\{C_j I_0\left[z_j(r)\right] + D_j K_0\left[z_j(r)\right] - 1\right\} \quad (j=1,2) \tag{5.3}$$

$$\gamma = \frac{s/C}{\sqrt{1 + 2\left\{C_1 I_1\left[z_1(R)\right] - D_1 K_1\left[z_1(R)\right]\right\}\Big/\left(R\sqrt{s/\nu}\right)}} \tag{5.4}$$

In which $\hat{u}_j'(x,r,s)$ and $\hat{p}'(x,s)$ is the acoustic velocity and pressure distribution in the *LaPlacian* domain (e.g. $\hat{u}_j'(x,r,s) = L\left[\tilde{u}_j'(x,r,t)\right]$ and $\hat{p}'(x,s) = L\left[\tilde{p}'(x,t)\right]$) respectively. $z_j(r)$ are the transformation of variables, while $z_1(r) = \frac{2}{0.4u_{s1}^*}\sqrt{s\,\nu_T^1}$ and $z_2(r) = r\sqrt{s/\nu_T^2}$. γ is the wave propagation constant. A, B, C_j, D_j are integration constants obtained from the boundary conditions (i.e. no-slip on the pipe wall and finite velocity at the pipe axis etc.), while j refers to a sub-region number. I_0, K_0, I_1, K_1 are the modified Bessel functions of first and second kinds of order zero and order one, respectively.

Zhou's model

Similarly, the solutions of Zhou's model (1995) for acoustic radial velocity and volumetric drag term can be obtained by using the eddy viscosity distribution in Tab. 5.1. The acoustic momentum equation in the time domain is:

$$\frac{\partial \tilde{u}'}{\partial t} = -\frac{1}{\rho_0}\frac{\partial \tilde{p}'}{\partial x} + \frac{1}{r}\frac{\partial}{\partial r}\left(r\, \nu_T \frac{\partial \tilde{u}'}{\partial r} \right) \tag{5.5}$$

The results are summarized below (x, r are axial and radial coordinates, respectively, and t is time).

$$\tilde{u}_j'(r,x,t) = \left\{ C_j B\left[r\sqrt{\frac{\omega}{\nu_T{}^j}} \right] + D_j K\left[r\sqrt{\frac{\omega}{\nu_T{}^j}} \right] + 1 \right\} \frac{i}{\rho_0 \omega}\frac{\partial \tilde{p}'(x,t)}{\partial x} \quad (j=1,2) \tag{5.6}$$

$$R_V = \frac{\rho_0 \omega \alpha_{imag}}{|\alpha|^2} + \frac{f\,\mathrm{Re}_{st}\,\mu}{D^2} \tag{5.7}$$

$$\text{where: } \alpha = \frac{2}{R^2}\sum_{j=1}^{2}\int_{r_{j+1}}^{r_j} \left\{ C_j B\left[r\sqrt{\frac{\omega}{\nu_T{}^j}} \right] + D_j K\left[r\sqrt{\frac{\omega}{\nu_T{}^j}} \right] + 1 \right\} r\,dr$$

$$and: \ \alpha = \alpha_{imag} + \alpha_{real} = \frac{2}{R^2}\sum_{j=1}^{2}\alpha_j + 1 \tag{5.8}$$

$$\alpha_j = i\sqrt{\frac{\nu_T{}^{j+1}}{\omega}}\, r_{j+1}\left[C_{j+1}\, B'\left(r_{j+1}\sqrt{\frac{\omega}{\nu_T{}^{j+1}}} \right) + D_{j+1}\, K'\left(r_{j+1}\sqrt{\frac{\omega}{\nu_T{}^{j+1}}} \right) \right]$$
$$-i\sqrt{\frac{\nu_T{}^{j}}{\omega}}\, r_j\left[C_j\, B'\left(r_j\sqrt{\frac{\omega}{\nu_T{}^{j}}} \right) + D_j\, K'\left(r_j\sqrt{\frac{\omega}{\nu_T{}^{j}}} \right) \right] \quad \left(where: i = \sqrt{-1} \right) \tag{5.9}$$

Where: $\tilde{u}_j'(x,r,t)$ *and* $\tilde{p}'(x,t)$ are the time-dependent acoustic velocity and pressure distributions, respectively. R_V is Zhou's volumetric drag obtained by comparing the coefficients of Eq. (5.5) with the axial momentum equation used in ABAQUS (e.g.

$\frac{\partial \tilde{u}_m'}{\partial t} + \frac{1}{\rho_0}\frac{\partial \tilde{p}'}{\partial x} + R_v \frac{\tilde{u}_m'}{\rho_0} = 0$). α, α_j are definitions, while $|\alpha|$ is referred to the modulus, and α_{imag}, α_{real} are corresponding imaginary and real parts. In Eqs. (5.6), (5.8) and (5.9), $B(z) = ber(z) + i\, bei(z)$, $K(z) = ker(z) + i\, kei(z)$ are the Kelvin's functions of the first-kind and second-kind, and $B'(z)$, $K'(z)$ are their derivatives respectively.

Tab. 5.2 summarizes Brown's quasi-steady, zero and uniform dynamic perturbation eddy viscosity distributions.

Table 5.2. Comparisons of Brown's perturbation eddy viscosity models

	Steady eddy viscosity distribution	Brown's zero perturbation model	Brown's quasi-steady perturbation model	Brown's uniform-dynamic perturbation model
Sigle-region models		Perturbation of eddy viscosity	Perturbation of eddy viscosity	Perturbation of eddy viscosity
	$\nu_T = \nu \left\{ \frac{1}{2} + \sqrt{\frac{1}{4} + g(r)\left[1 - \exp\left(-h_0(r)\right)\right]^2} \right\}$	$\nu_T' = 0$	$\nu_T' = k(r)\frac{d\tilde{u}'}{dr}$	$\nu_T' = \left(m_0 e^{i\varphi}\right)\, k(r)\frac{d\tilde{u}'}{dr}$

Brown's zero perturbation model

Brown's model (1981) using the modified Nikuradse's single region eddy viscosity distribution (e.g. Schlicting (1968)), which is corrected near the wall by employing the popular Van Driest correction (e.g. Cebeci *et al.* (1977)). The zero perturbation assumption (i.e. $\nu_T' = 0$) in the eddy viscosity has been shown to be meaningful for a

significant frequency band for Reynolds numbers above 10^4. The time invariant eddy viscosity ν_T is defined as:

$$\nu_T = \nu \left\{ \frac{1}{2} + \sqrt{\frac{1}{4} + g(r)\left[1 - \exp\left(-h_0(r)\right)\right]^2} \right\} \tag{5.10}$$

$$\text{where: } g(r) = \frac{\mathrm{Re}_{st}\, f}{32} r l^2, \quad h_0(r) = \frac{R(1-r)}{4N}\sqrt{\frac{f r}{2}} \tag{5.11}$$

$$l = 0.14R - 0.075\frac{r^2}{R} - 0.065\frac{r^4}{R^3} \tag{5.12}$$

where, l denotes the Prandtl mixing length and N is a constant. Using Brown's eddy viscosity model, the acoustic momentum equation (e.g. Eq. (5.1)) becomes a two-point boundary value problem and cannot be obtained analytically. Therefore, it is solved using a fourth-order Runge-Kutta algorithm by a two-variable Newton Raphson procedure in which the gradient is determined numerically.

Brown's quasi-steady perturbation model

This model assumed quasi-steady perturbations in the eddy viscosity and applied originally by definition in the limit of zero frequency. The time-mean part of the eddy viscosity is the same as that in the zero perturbation model. The quasi-steady perturbation in the eddy viscosity ν_T' is given by:

$$\nu_T' = k(r)\frac{d\tilde{u}'}{dr} \tag{5.13}$$

$$\text{where: } k(r)=\frac{-\frac{l^2}{\nu}\left(1-e^{-h_0(r)}\right)\left(1-e^{-h_0(r)}+h_0(r)e^{-h_0(r)}\right)}{1+\frac{l^2}{\nu}\left(1-e^{-h_0(r)}\right)h_0(r)e^{-h_0(r)}\left(\frac{\mathrm{Re}_{st}\,f}{16}\right)\frac{\nu.r}{\nu_T}} \tag{5.14}$$

The transformed momentum equation in the LaPlacian domain becomes:

$$A_q\frac{d^2\hat{u}'}{dr^2}+B_q\frac{d\hat{u}'}{dr}=s\hat{u}'+\frac{1}{\rho_0}\frac{d\hat{p}'}{dx} \tag{5.15}$$

$$\text{where: } A_q=\nu_T+\left(\nu.k(r)\right)\left[-\frac{f\,\mathrm{Re}_{st}{}^2\nu^2}{32R^3}\left(\frac{1}{\nu_T}-\frac{r}{\nu_T{}^2}\frac{d\nu_T}{dr}\right)\right] \tag{5.16}$$

$$B_q=\left(\frac{\nu_T}{r}+\frac{d\nu_T}{dr}\right)+\left[-\frac{f\,\mathrm{Re}_{st}{}^2\nu^2}{32R^3}\left(\frac{1}{\nu_T}-\frac{r}{\nu_T{}^2}\frac{d\nu_T}{dr}\right)\right]\left[\left(\nu.k(r)\right)+\frac{\nu.k(r)}{r}+\frac{dk(r)}{dr}\right] \tag{5.17}$$

In which $\frac{d\tilde{u}'}{dr}$ is the perturbation in the cross-sectional velocity gradient. Again, the acoustic equations can be solved numerically using the methods described for the zero perturbation model.

Brown's uniform dynamic perturbation model

Brown (1981) further developed an improved eddy viscosity perturbation model, which was achieved by multiplying the factor $k(r)$ with $m_0e^{i\varphi}$. That is, the magnitude of the eddy viscosity perturbation is set as m_0 times its quasi-steady value, and its phase angle is set at φ. Brown indicated that the ratio of the local perturbations in the eddy viscosity to the local perturbations in the velocity gradient could be assumed to be invariant for all radii and became a frequency-dependent complex number. Therefore, the uniform dynamic perturbations in the eddy viscosity ν_T' becomes:

$$\nu_T' = m_0 e^{i\varphi} k(r) \frac{d\tilde{u}'}{dr} \tag{5.18}$$

The transformed momentum equation in the LaPlacian domain is given by:

$$A_d \frac{d^2\hat{u}'}{dr^2} + B_d \frac{d\hat{u}'}{dr} = s\hat{u}' + \frac{1}{\rho_0}\frac{d\hat{p}'}{dx} \tag{5.19}$$

$$\text{where: } A_d = \nu_T + \left(\nu.\left\{m_0 e^{i\varphi} k(r)\right\}\right)\left[-\frac{f\,\mathrm{Re}_{st}{}^2 \nu^2}{32R^3}\left(\frac{1}{\nu_T} - \frac{r}{\nu_T{}^2}\frac{d\nu_T}{dr}\right)\right] \tag{5.20}$$

$$B_d = \left(\frac{\nu_T}{r} + \frac{d\nu_T}{dr}\right) + \left[-\frac{f\,\mathrm{Re}_{st}{}^2 \nu^2}{32R^3}\left(\frac{1}{\nu_T} - \frac{r}{\nu_T{}^2}\frac{d\nu_T}{dr}\right)\right]\left[\left(\nu.\left\{m_0 e^{i\varphi} k(r)\right\}\right) + \frac{\nu.\left\{m_0 e^{i\varphi} k(r)\right\}}{r} + \frac{d\left\{m_0 e^{i\varphi} k(r)\right\}}{dr}\right] \tag{5.21}$$

Finally, a fourth-order Runge-Kutta algorithm by a two-variable Newton Raphson approximation is applied to solve the above equation. The same values of m_0 and φ are applied at all radii and reveal the effects of the magnitude and phase on the eddy viscosity perturbations.

5.3 STERN Experiments

The schematic of STERN Loop (Chatoorgoon *et al.* (1993)) is shown in Fig. 5.2, in which the outlet feeder is from the outlet flange to the separator. The configuration of the outlet feeder is shown in Fig. 5.3, which consists of three pipes in series. The geometric dimensions are also shown in Fig. 5.3. The measurements were done for the frequency sweeping from 70 Hz to 270 Hz at 129 frequency values for the temperature of 60.6 $^{\circ}C$. The pipe wall was made of commercial steel. For both cases, the mass flow rate was 28 kg/sec and the static pressure was $10MPa$. Parameters used in this study,

including the relative roughness ε_{rou}/D (Zhou (1995)), measured sonic velocity, fluid density and dynamic viscosity are listed in Tab. 5.3.

Table 5.3: Parameters used in the simulation of the outlet feeder of the STERN Loop

Pipe	ε_{rou}/D [-]	$T = 60.6\ °C,\ P = 10MPa$		
		ρ $[kg/m^3]$	C $[m/s]$	μ $[N \cdot s/m^2]$
1	0.00085	983.0	1495.0	4.61×10^{-4}
2	0.00063	983.0	1484.0	4.61×10^{-4}
3	0.00045	983.0	1471.0	4.61×10^{-4}

5.4 Results

5.4.1 Amplitudes

Figs. 5.4 ~ 5.11 show the comparisons of the results of various models with the experimental measurements at channel 30 (Ch30), as explained in Fig. 5.3. Correspondingly, Figs. 5.12 ~ 5.19 show the results calculated using different models compared with the experimental data at channel 31 (Ch31). The analytical results are obtained using the frequency step of 1 Hz. The steady Reynolds numbers of all cases are 1.31×10^6 and 1.05×10^6 for the first and second pipes, respectively. The roughness Reynolds numbers ε^*_{rou} are 21.6 and 17.5 for the first and second pipe, correspondingly.

It is seen that for the available experimental data of two pressure taps, the computed results (such as: Figs. 5.4, 5.8, 5.9, 5.12, 5.16, and 5.17) using Ohmi & Usui's two-region time independent eddy viscosity model (1976), Brown's quasi-steady perturbation eddy viscosity model and his zero perturbation eddy viscosity model (1981) overpredict the pressure amplitudes at all three resonant frequencies. Plots of normalized resonant pressures in Figs. 5.8 and 5.16 indicate that the quasi-steady model of Brown overpredicts the pressure amplitudes at each resonance mode compared with those computed using Ohmi & Usui's two-region time invariant eddy viscosity model. Figs. 5.9 and 5.17 show that for measurements of Ch30 and Ch31, Brown's zero perturbation eddy viscosity model (1981) slightly overpredicts the amplitudes at the first and second resonant frequencies than those obtained from Ohmi & Usui's model (1976), and it gives better estimations on the pressure amplitudes at the third resonant mode. It is also shown from Figs. 5.4 and 5.12 that, Ohmi & Usui's model (1976) causes significant overestimations of the resonant amplitudes than the empirical volumetric drag of 13200 obtained by "best fit" of the experiments.

Figs. 5.5, 5.6, 5.10, 5.13, 5.14 and 5.18 show the comparisons of computed results obtained from Zhou's two-region model (1995), the proposed two-region linear model and Brown's uniform dynamic perturbation model with the experimental data at each channel location and those computed using the empirical volumetric drag value of 13200. The normalized pressure amplitudes at Ch30 and Ch31, sketched in Figs. 5.5 and 5.13,

show that Zhou's two-region rough-walled model (1995) results in lower amplitudes for all three resonant frequencies than those calculated using the empirical value of volumetric drag of 13200. Likewise, Figs. 5.6 and 5.14 also show the similar trend for all resonant modes by using the present two-region rough-walled model when comparing with the amplitudes computed using the volumetric drag of 13200. Figs. 5.10 and 5.18 show that Brown's uniform dynamic perturbation model (1981) results in higher amplitudes at the first resonant frequency than those given by the empirical volumetric drag of 13200, and it results in lower amplitudes for the last two resonant frequencies. The performances of above three models are better than others discussed in the preceding section. However, all three models apparently overpredict the amplitudes for the first resonant frequency at Ch30 and Ch31.

To further qualify the present model's performance, several simulations using Zhou's (1995), Brown's uniform dynamic perturbation (1981) and present models are compared with the empirical measurements at two pressure taps. Figs. 5.7 and 5.15 indicate that the present model results in slightly higher amplitudes at all three resonant frequencies than Zhou's model (1995). Apparently, Zhou's model (1995) underpredicts the amplitudes for the second and third resonant frequencies compared with the measurement data. Figs. 5.11 and 5.19 show that Brown's uniform dynamic model (1981) produces higher amplitudes at the first and second resonant frequencies than the present model, and gives nearly the same predictions for the third acoustic mode. These observations

suggest that the overall performance of present model is somewhat superior to Zhou's model (1995) and Brown's uniform dynamic model (1981).

5.4.2 Volumetric drag

Plots of volumetric drag values calculated using various models for the first and second pipes of STERN Loop Outlet Feeder are shown in Figs. 5.20 and 5.21. It is seen from Fig. 5.20 that, (1) the volumetric drag values computed from Brown's quasi-steady perturbation model are frequency-independent, (2) the volumetric drag becomes frequency dependent by using either Ohmi & Usui's model (1976) or Brown's zero perturbation model (1981). The plot also shows a trend that the volumetric drag values computed from each model for the first pipe are greater than that of the second pipe. This means there is more damping in the smaller pipe than in the larger pipe. It is also observed that Brown's zero perturbation model (1981) results in lower volumetric drag values for the first resonant frequency than the Ohmi & Usui's model (1976), and it results in the higher volumetric drag values for the third resonant frequency. Corresponding influences on the amplitudes can be seen in Figs. 5.9 and 5.17. However, all volumetric drag values are smaller than the value of 6000, which therefore imply the above three models behave poorly on predicting the pressure amplitudes.

Fig. 5.21 shows the volumetric drag values calculated from Zhou's two-region model (1976), Brown's uniform dynamic perturbation model and present two-region linear

model. The empirical volumetric drag of 13200 is also shown for reference. For these models, it is observed that the computed volumetric drag values are dependent upon the frequency, and become comparable with the reference value of 13200. For the first pipe, Zhou's model (1995) and the present model result in higher volumetric drag values for all frequencies than the empirical value of 13200, whereas Brown's uniform dynamic perturbation model (1981) results in lower volumetric drag at the first resonant frequency and higher volumetric drag values for the last two resonant frequencies compared with 13200. For the second pipe, Zhou's model (1995) still gives higher volumetric drag values for all acoustic modes than the reference volumetric drag of 13200. Unlike Zhou's model (1995), the present model results in higher volumetric drag values for the second and third resonant frequencies than 13200, but gives slightly lower value at the first resonant frequency. Brown's model (1981) causes higher volumetric drag than 13200 only at the third resonance. The same trend of more damping in the smaller pipe than in the larger pipe is also observed. As we known, the empirical volumetric drag of 13200 was obtained by "best fit" the experiments and might be suggested as a measure of the performance of any acoustic model. Therefore, these three models performed better for current analysis than Ohmi & Usui's model (1976) and Brown's quasi-steady perturbation & zero perturbation models (1981).

For Brown's uniform dynamic perturbation model (1981), several simulations are carried out to further investigate the effects of magnitude perturbation m_0 and phase angle

perturbation $e^{i\varphi}$ in the eddy viscosity. Fig. 5.22 shows:

(1) With zero phase angle perturbations, the volumetric drag values computed using different magnitude perturbations m_0 are the same as those computed from Brown's quasi-steady perturbation model, and are independent of frequency,

(2) With a uniform magnitude perturbation in eddy viscosity, the calculated volumetric drag values are frequency dependent and increase as the phase angle increase (i.e. volumetric drag values calculated using a phase of 0.06 are higher than those using a phase of 0.01 for all resonant frequencies).

The corresponding influences of phase angles on the resonant amplitudes at Ch31 are shown in Fig. 5.23. These observations suggest that the phase angle perturbation in the eddy viscosity significantly alter the volumetric drag, while the magnitude has no influences on the damping. However, the proper phase angle value of 0.06 here was obtained by tuning to the experiments.

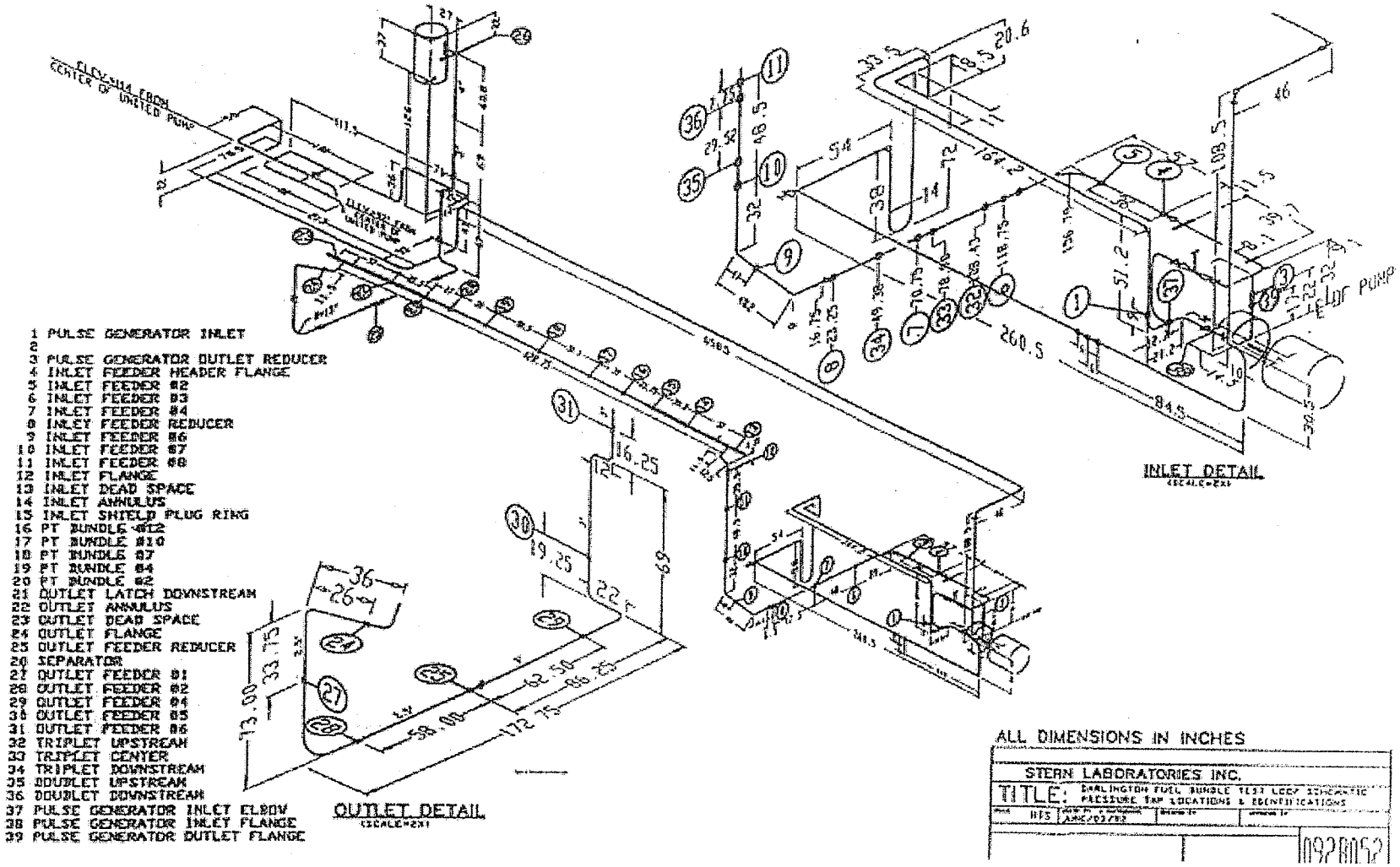

Figure 5.2: Schematic of STERN Loop

STERN Benchmark Cases

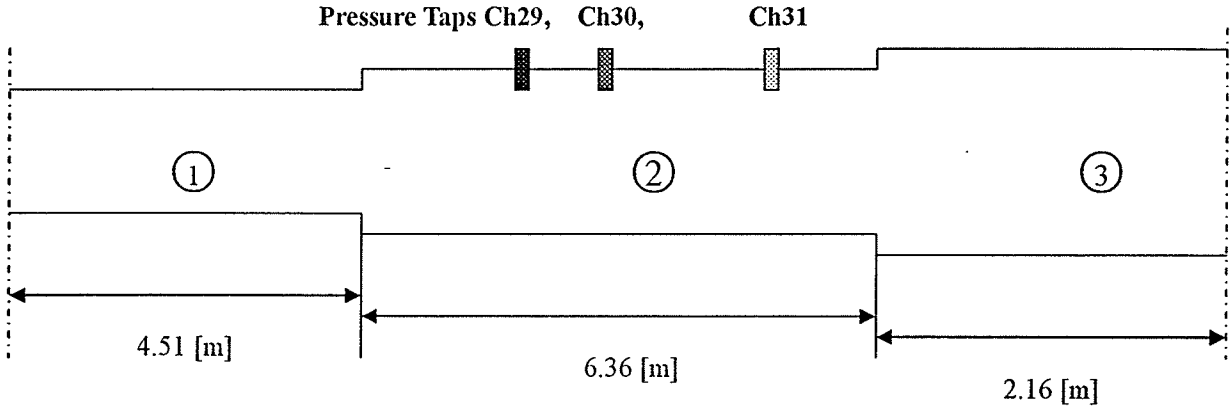

Area ① = 0.002734 $[m^2]$

Area ② = 0.004261 $[m^2]$

Area ③ = 0.007417 $[m^2]$

Location of pressure taps, given as distance from the inlet

5.99 [m] (Ch29), 7.65 [m] (Ch30), 9.76[m] (Ch31)

Outlet boundary condition is p' = 0.

Figure 5.3: Configuration and dimensions of the outlet feeder of the STERN Loop

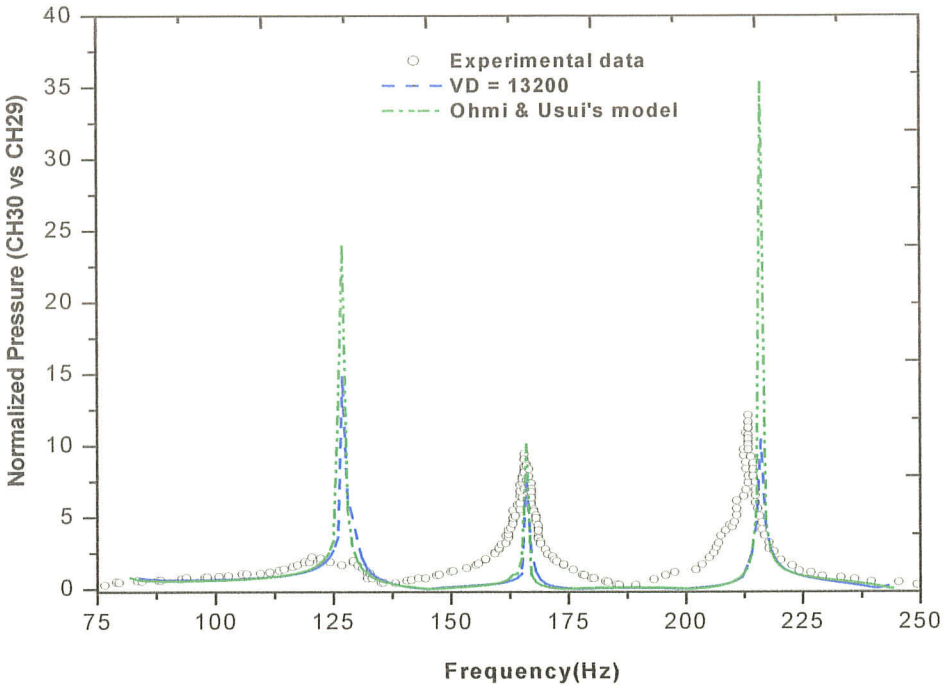

Figure 5.4: Comparison of Ohmi & Usui's model and VD=13200 (Ch30 vs. Ch29)

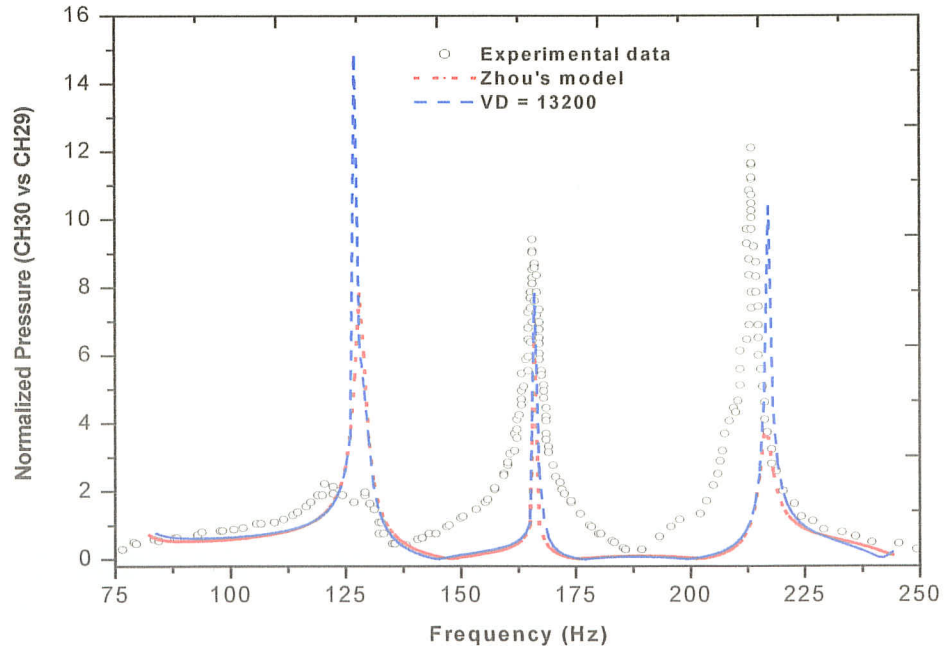

Figure 5.5: Comparison of Zhou's model and VD=13200 (Ch30 vs. Ch29)

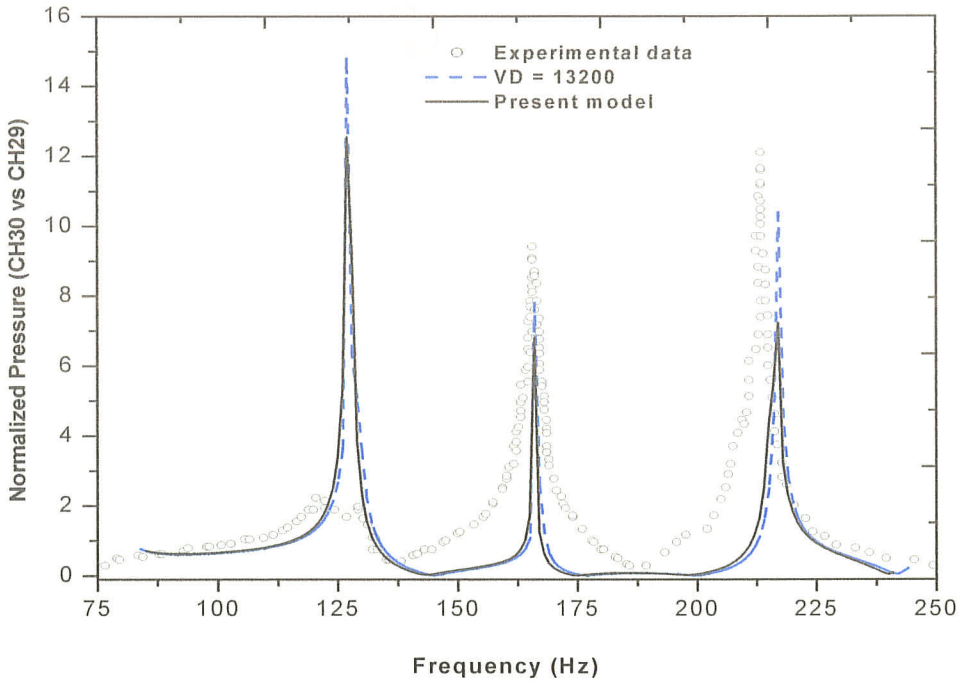

Figure 5.6: Comparison of present model and VD=13200 (Ch30 vs. Ch29)

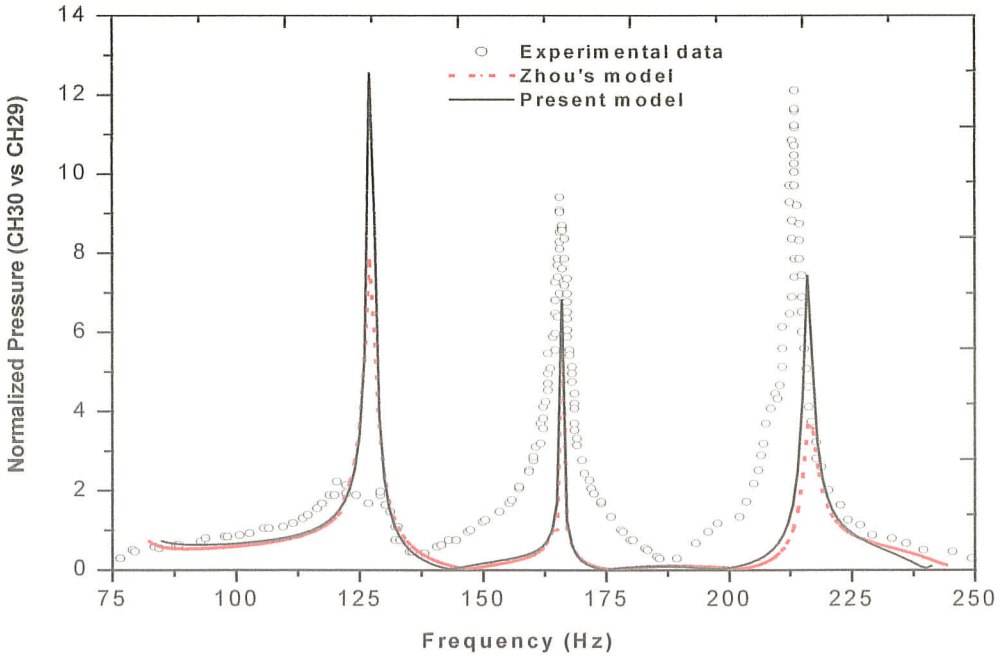

Figure 5.7: Comparison of present model and Zhou's model (Ch30 vs. Ch29)

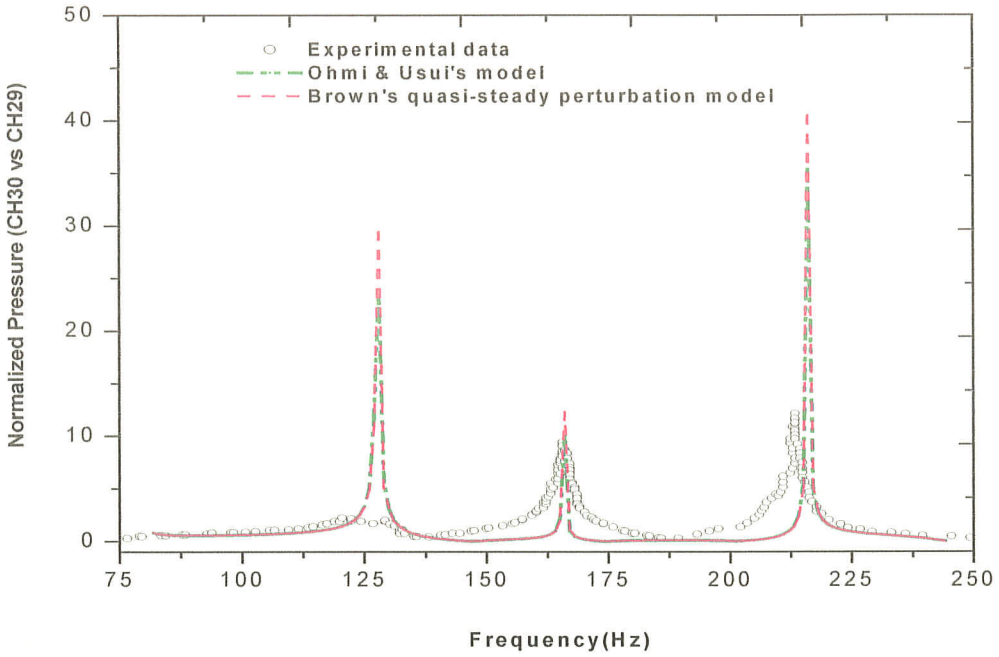

Figure 5.8: Comparison of Ohmi & Usui's model and Brown's quasi-steady perturbation model (Ch30 vs. Ch29)

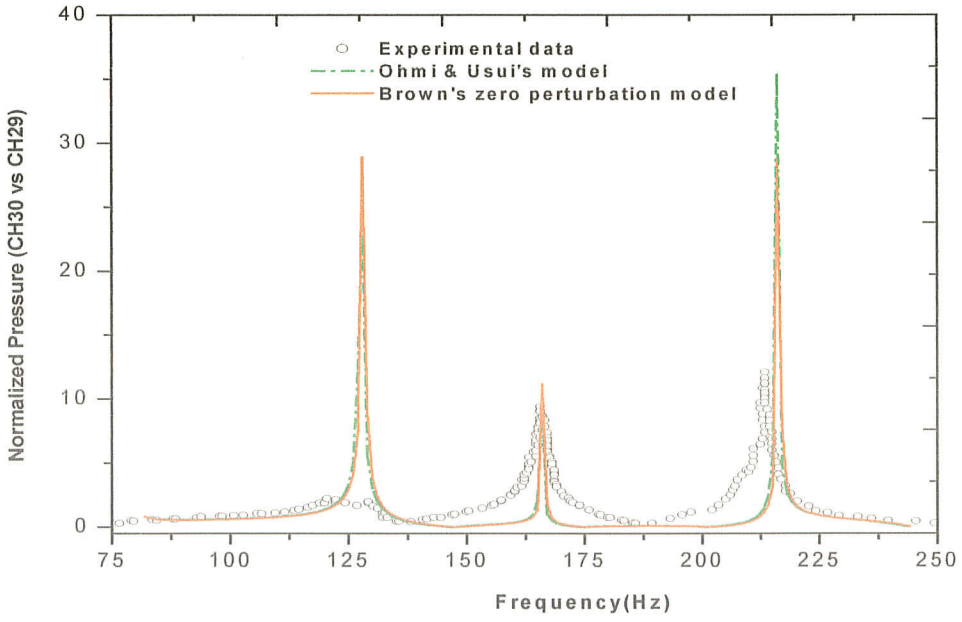

Figure 5.9: Comparison of Ohmi & Usui's model and Brown's zero perturbation **model (Ch30 vs. Ch29)**

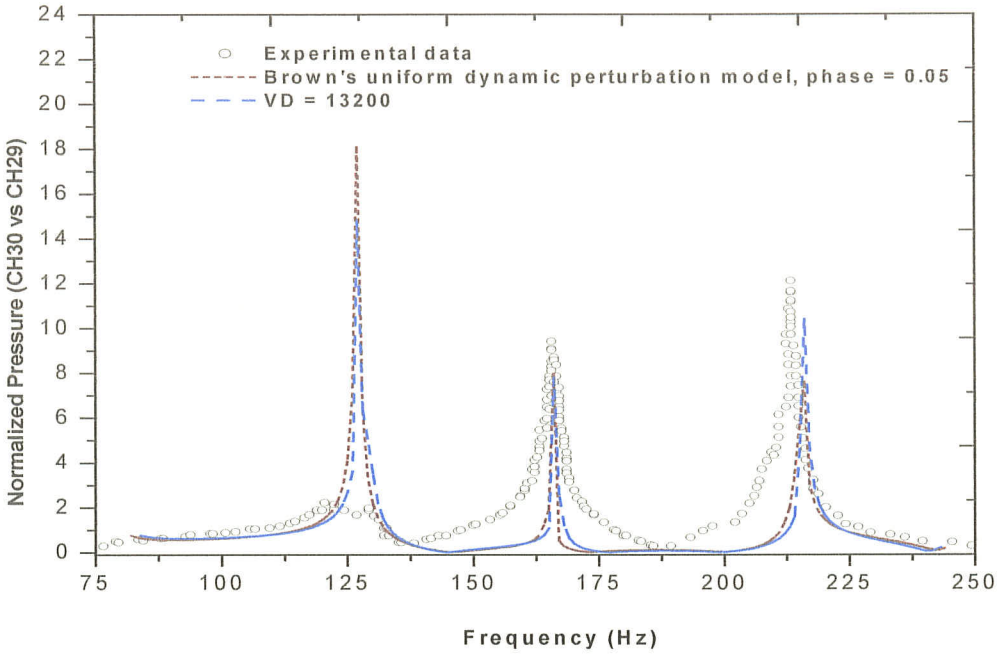

Figure 5.10: Comparison of VD =13200 and Brown's uniform dynamic perturbation model (Ch30 vs. Ch29)

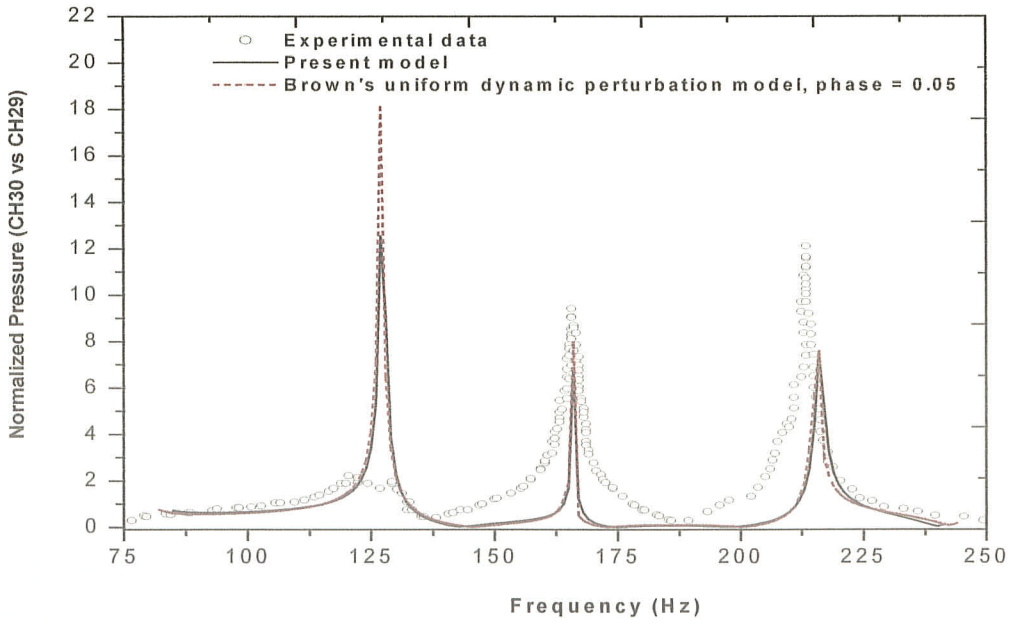

Figure 5.11: Comparison of present model and Brown's uniform dynamic perturbation model (Ch30 vs. Ch29)

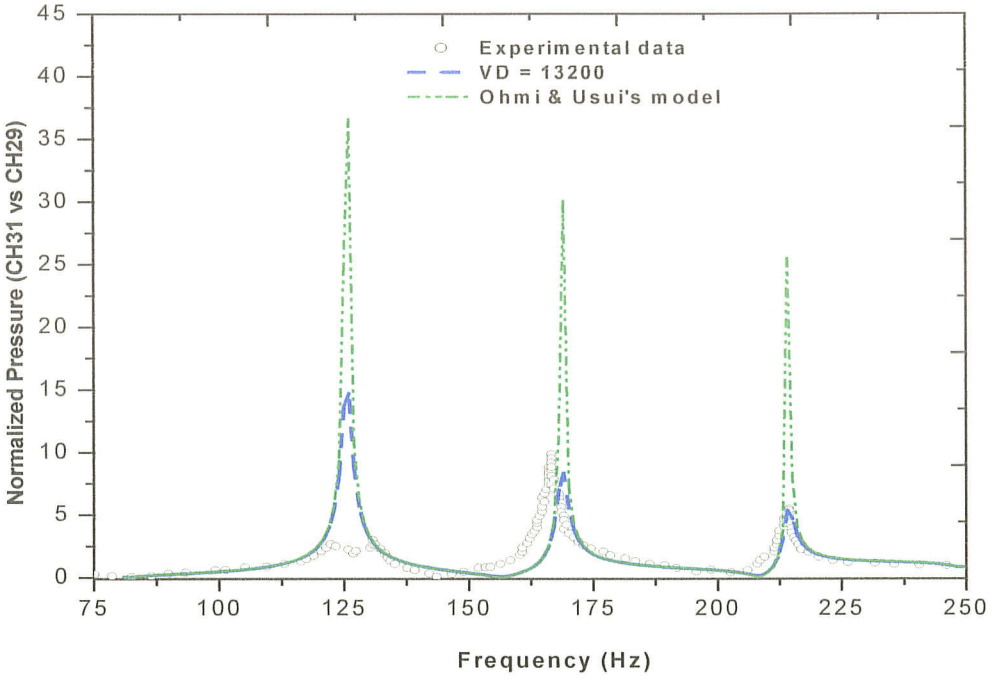

Figure 5.12: Comparison of Ohmi & Usui's model and VD=13200 (Ch31 vs. Ch29)

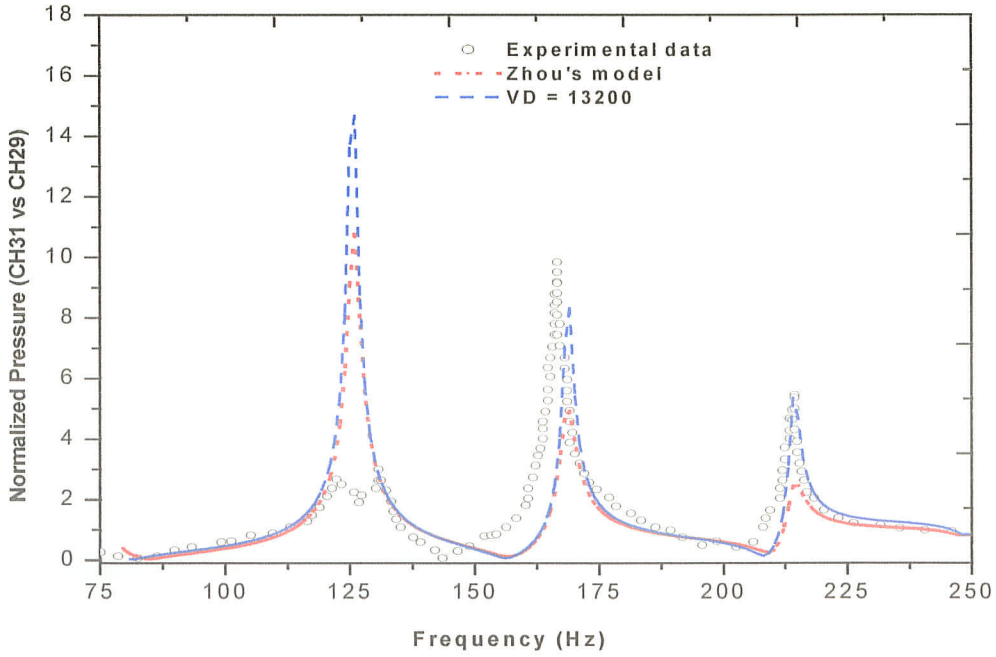

Figure 5.13: Comparison of Zhou's model and VD=13200 (Ch31 vs. Ch29)

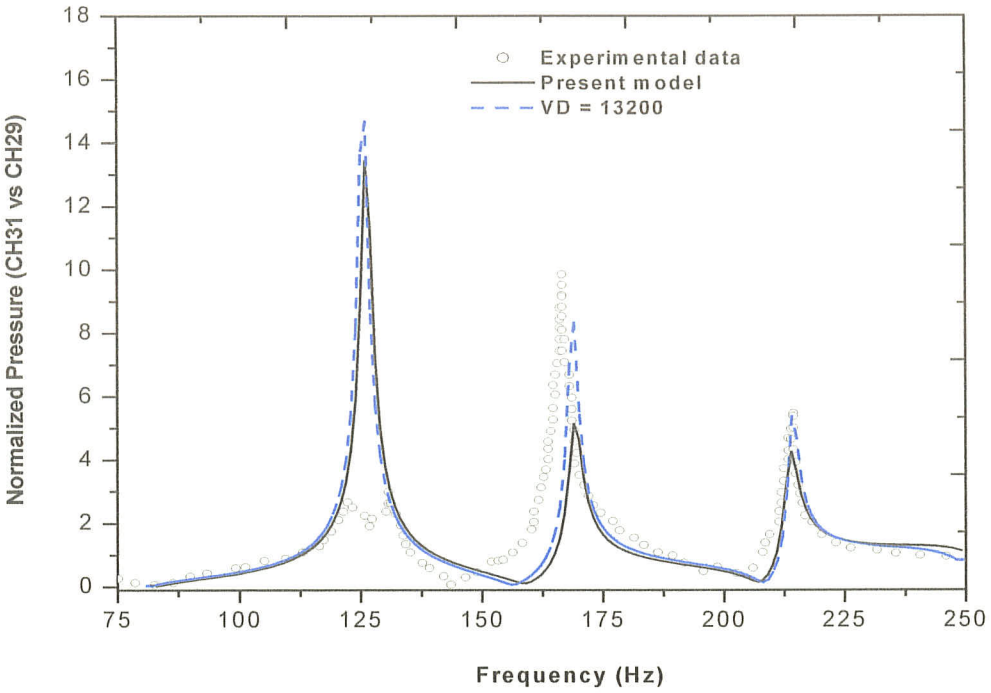

Figure 5.14: Comparison of present model and VD=13200 (Ch31 vs. Ch29)

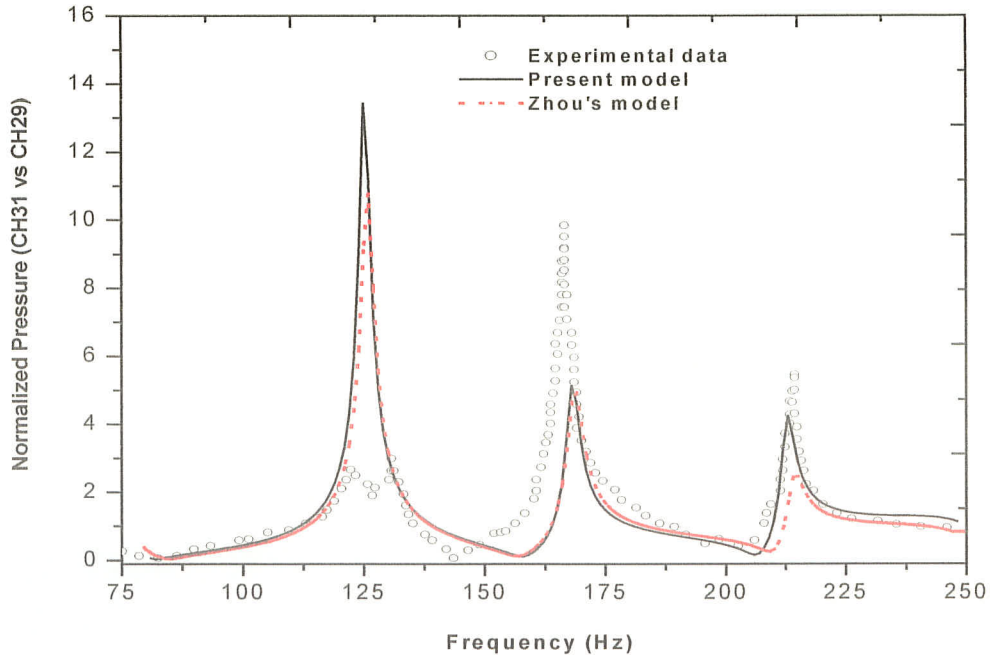

Figure 5.15: Comparison of present model and Zhou's model (Ch31 vs. Ch29)

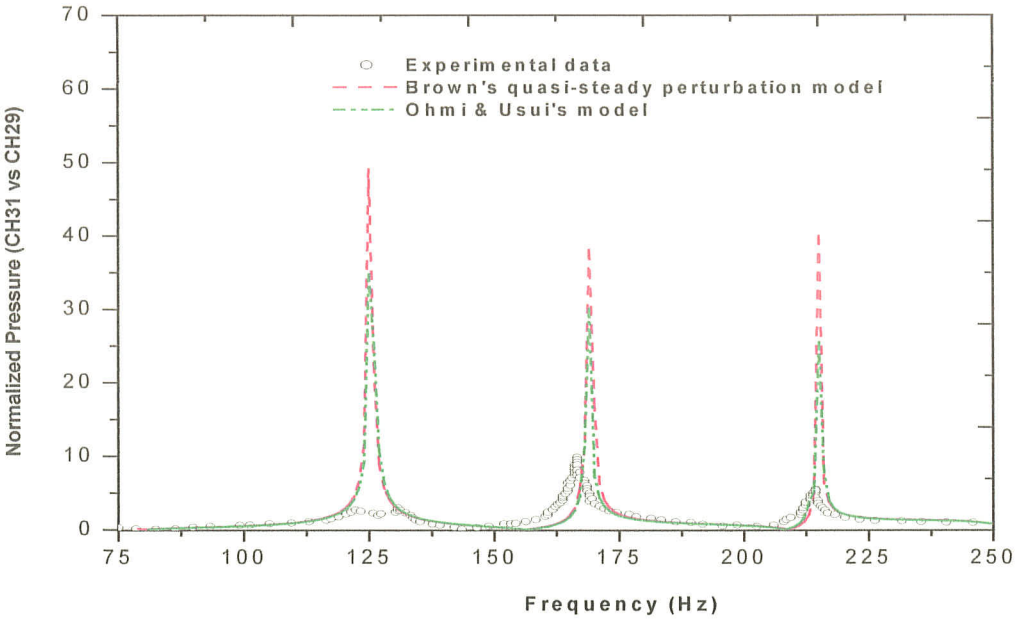

Figure 5.16: Comparison of Ohmi & Usui's model and Brown's quasi-steady perturbation model (Ch31 vs. Ch29)

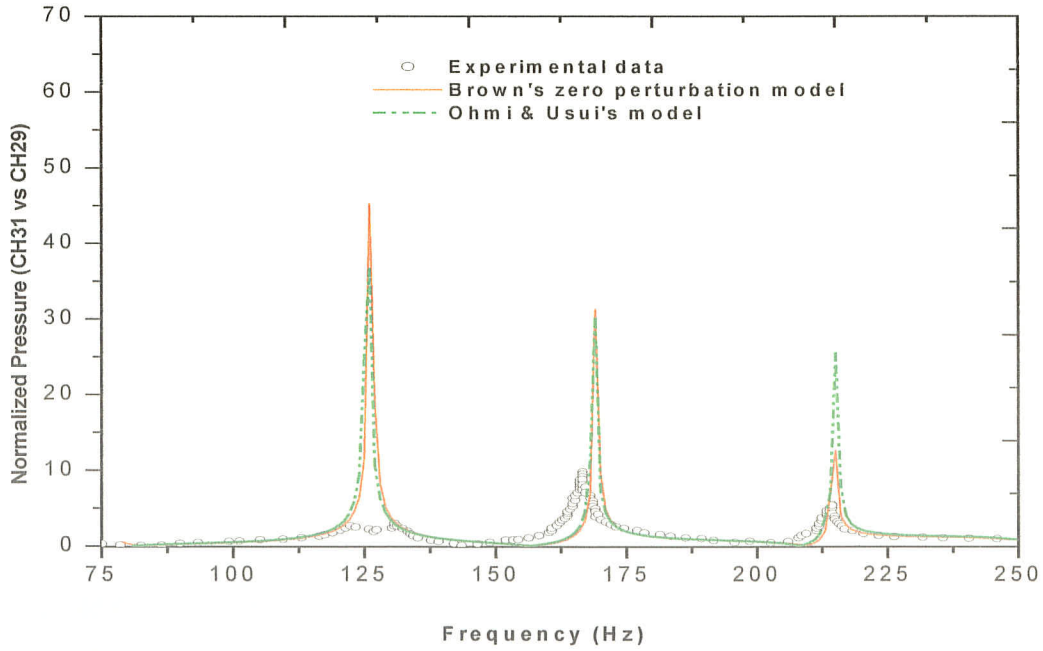

Figure 5.17: Comparison of Ohmi & Usui's model and Brown's zero perturbation model (Ch31 vs. Ch29)

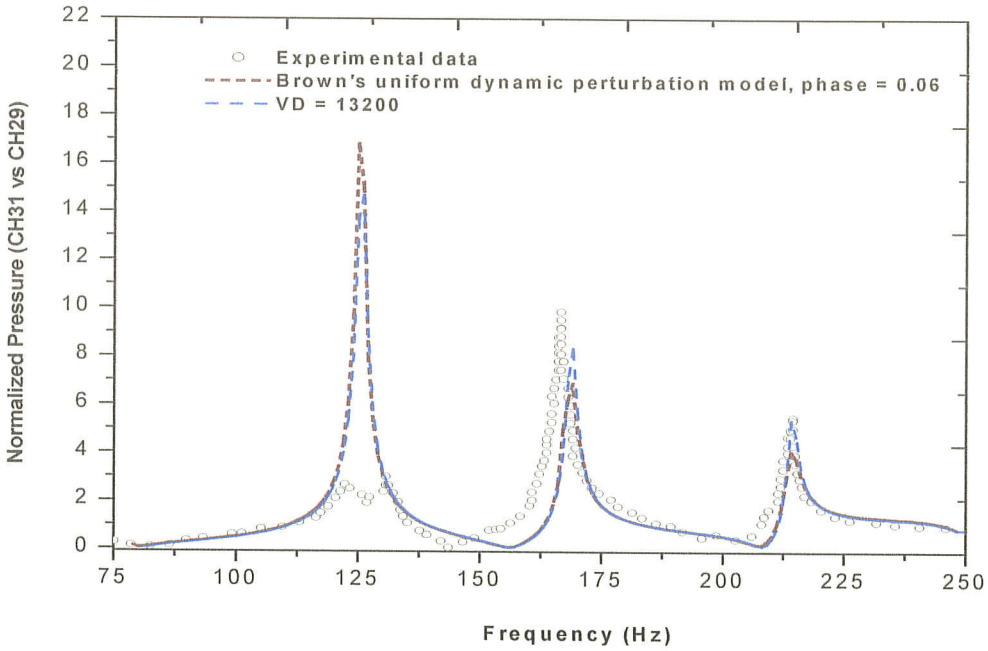

Figure 5.18: Comparison of VD =13200 and Brown's uniform dynamic perturbation model (Ch31 vs. Ch29)

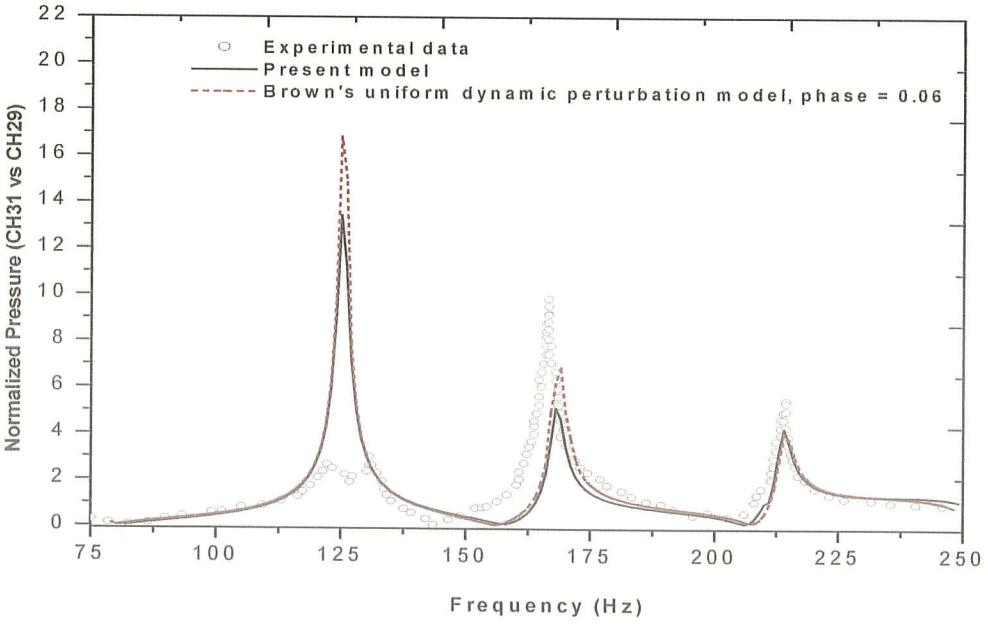

Figure 5.19: Comparison of present model and Brown's uniform dynamic perturbation model (Ch31 vs. Ch29)

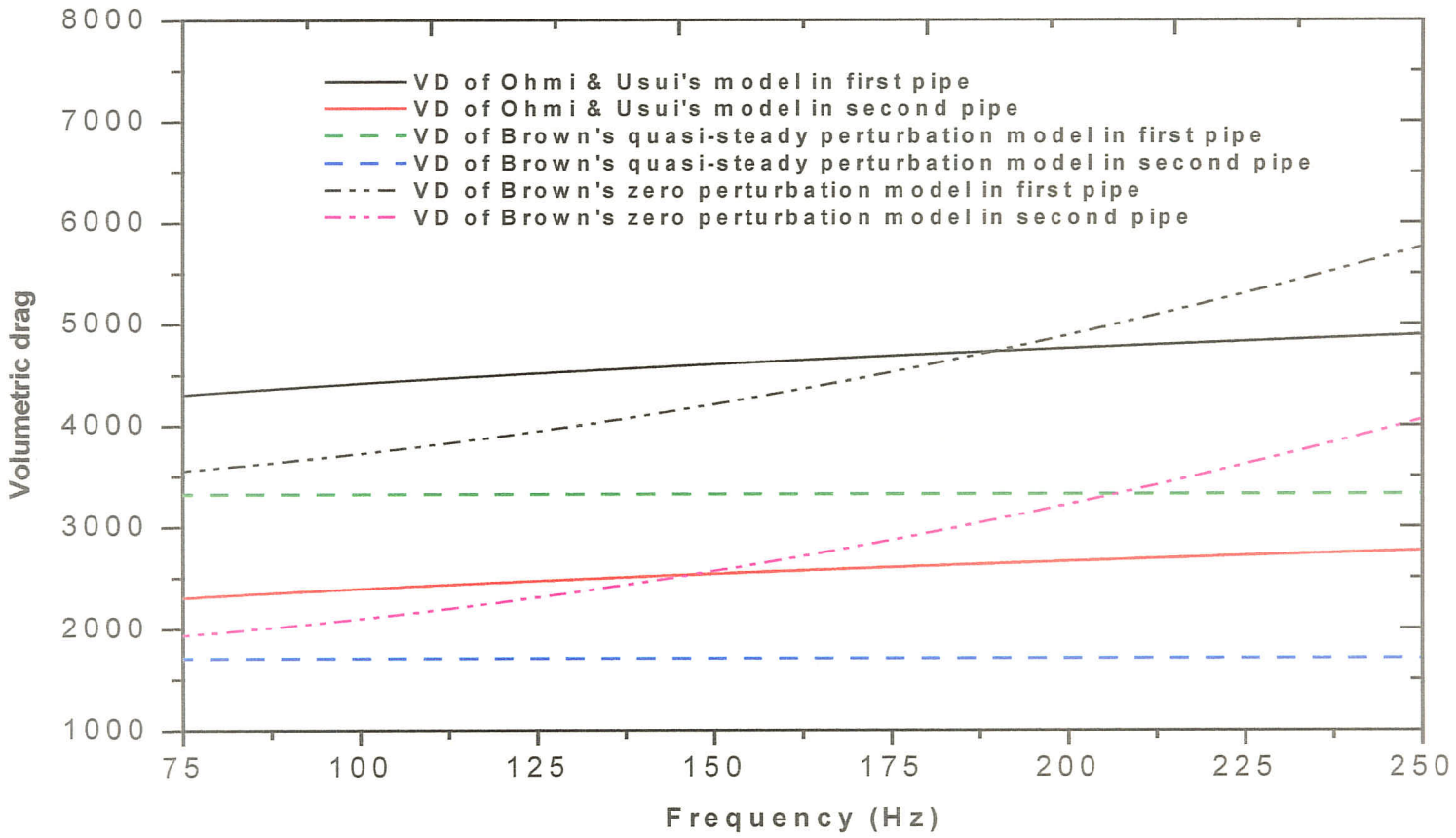

Figure 5.20: The volumetric drag values based on Ohmi *et al.*'s & Brown's models for first and second pipes of STERN Loop Outlet Feeder

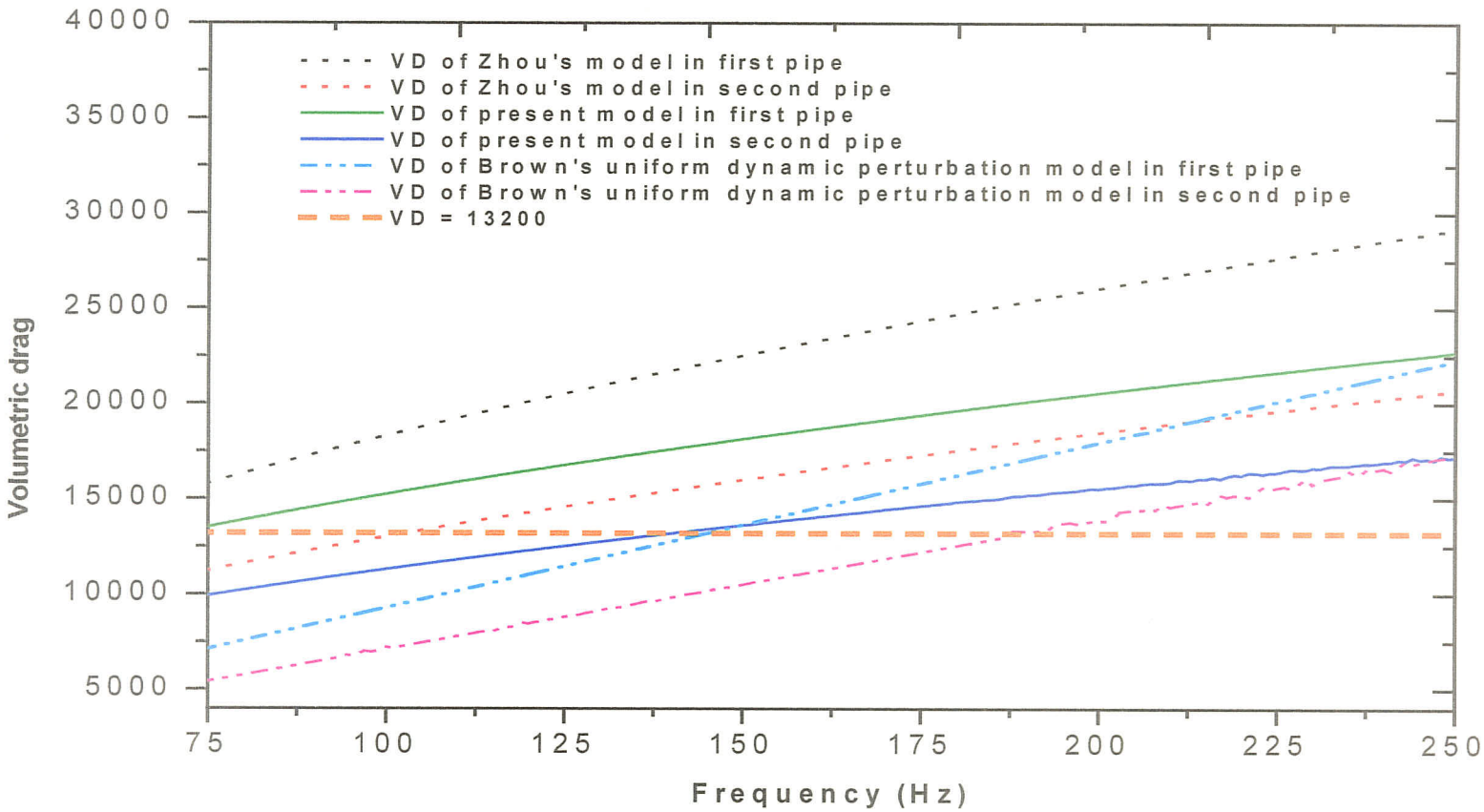

Figure 5.21: The volumetric drag values based on the present and other models for first and second pipes of STERN Loop Outlet Feeder

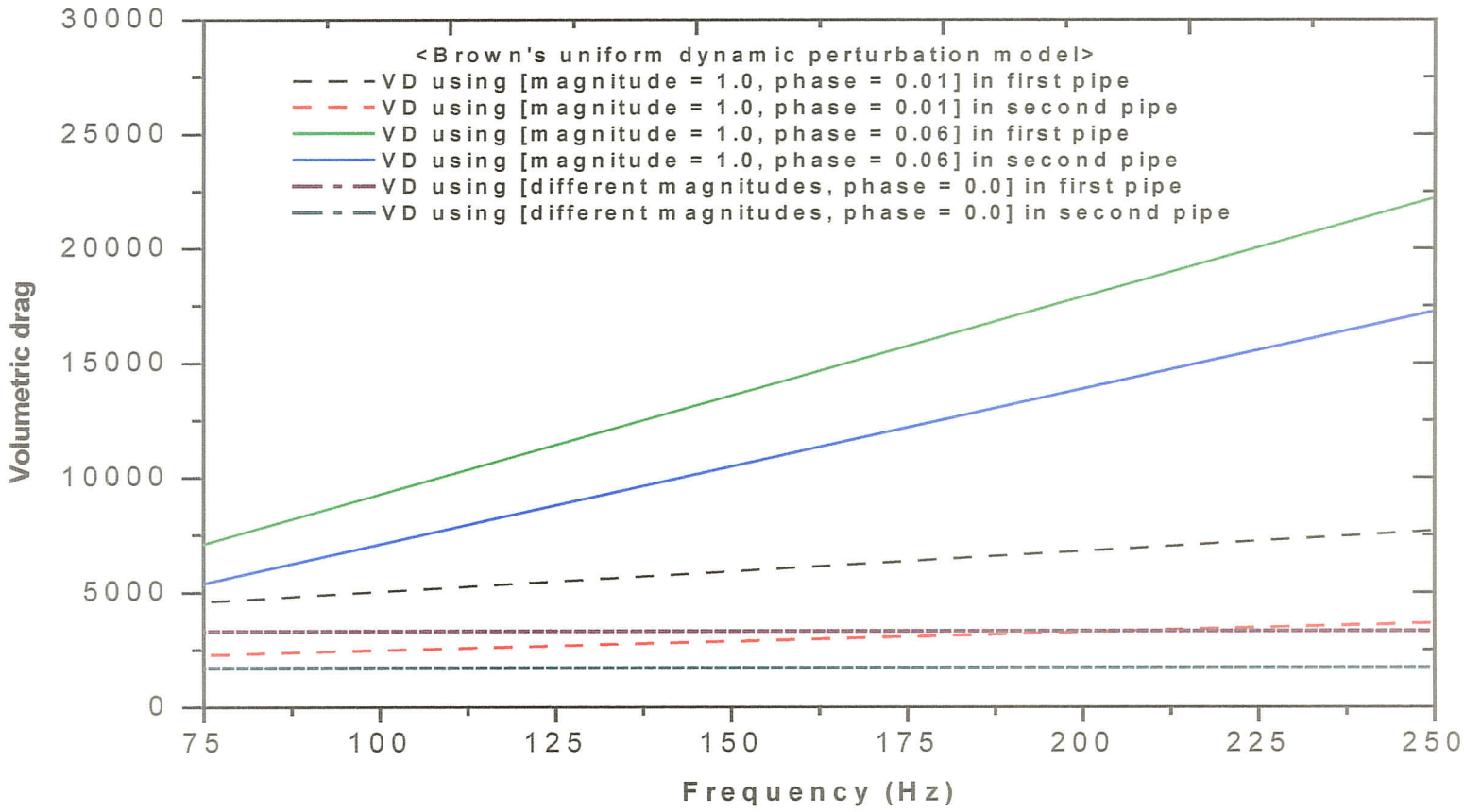

Figure 5.22: Effects of magnitude & phase angle perturbations in the eddy viscosity on the volumetric drag values for first and second pipes of STERN Loop Outlet Feeder

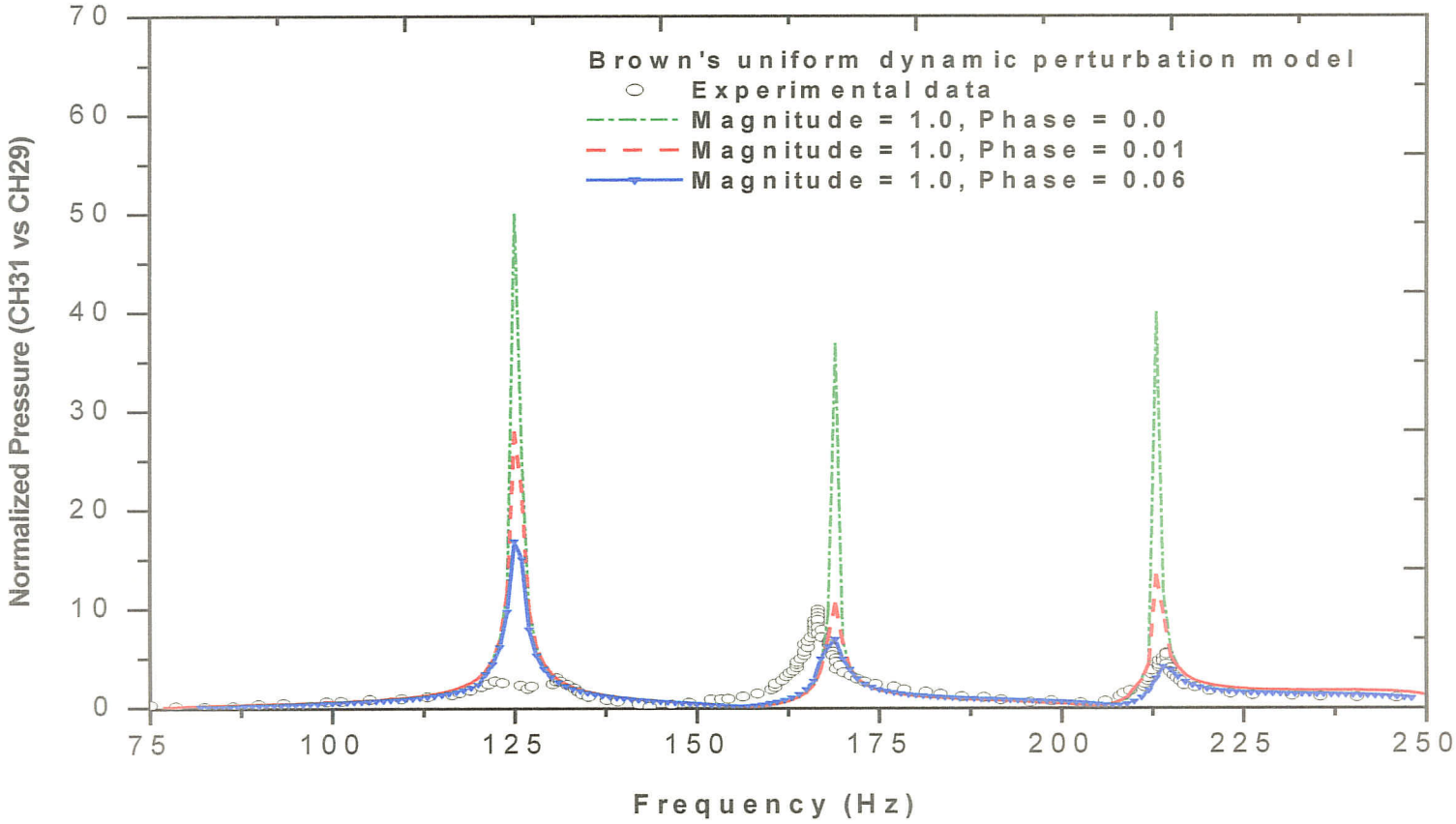

Figure 5.23: Effects of phase angle perturbation in the eddy viscosity on the resonant amplitudes (Ch31 vs. Ch29)

Chapter 6
Conclusions

6.1 Conclusions

An analytical 1-D linear model for predicting acoustic wave propagation in turbulent flows has been developed. A two-region linear time-invariant eddy viscosity distribution for rough-walled turbulence is employed for present work. Corresponding frequency-dependent acoustic parameters such as acoustic wave propagation constant, specific acoustic impedance per unit length, and the transfer function are derived for high mean Reynolds number turbulent flows. A fundamental formula to calculate the volumetric drag of turbulence has also been developed. Six different turbulent models including the present model have been applied to simulate the experiments of the outlet feeder of the STERN Loop at temperature of 60.6 degrees (Chatoorgoon *et al.* (1993), Kar (1993) and Zhou (1995)). The influences on the volumetric drag of each model are also investigated. For these experiments, the steady mean Reynolds numbers are greater than 1.0×10^6.

Performances of various models on predicting the resonant amplitudes are first investigated. Ohmi & Usui's two-region time-invariant eddy viscosity model (1976), Brown's zero perturbation (time-invariant) and quasi-steady perturbation eddy viscosity models (1981) result in substantial overestimated amplitudes for all resonant frequencies

compared with the experimental data. Brown's quasi-steady perturbation model (1981), however, has the worst performance for the current analysis among these models. The amplitudes computed using Zhou's two-region rough-walled model (1995), Brown's uniform dynamic perturbation model (1981) and present two-region linear rough-walled model all agree well with the experimental measurements and the results obtained using the empirical volumetric drag of 13200. The effective eddy viscosity at the wall in Zhou's model (i.e. $0.0112\ Ru_{st}^{*}$) is approximately 600 times of the laminar viscosity, and the present model is found to be 250 times the laminar viscosity value. Both approximations in the effective viscosity at the wall provide good agreements on resonant amplitudes compared with the existing experimental measurements. Comparisons of above models indicate that:

(1) Brown's quasi-steady perturbation eddy viscosity model has shown to be not applicable for the current analysis,

(2) For time-invariant eddy viscosity models, the rough-walled models (i.e. Zhou's (1995) & present models) behave better than those smooth-walled models (Ohmi & Usui's model (1976) and Brown's zero perturbation model (1981)),

(3) Brown's uniform dynamic perturbation eddy viscosity model (1981) for smooth-walled turbulence performs at least as good as those rough-walled time-invariant models,

(4) The model proposed here performs relatively superior or at least as good as Zhou's model (1995).

(5) The present proposed model, Zhou's model (1995) and Brown's uniform dynamic model (1981) have a disadvantage that they need experiments to determine the empirical constants used in the eddy viscosity distributions.

As a measure of acoustic damping, the volumetric drag values computed from each model are investigated. The conclusions are:

(1) The volumetric drag values calculated using Brown's quasi-steady perturbation mode (1981) are frequency-independent and less than 3300,

(2) Two smooth-walled time-invariant eddy viscosity models (Ohmi & Usui's model (1976) and Brown's zero perturbation model (1981)) result in frequency-dependent volumetric drags with the values less than 6000,

(3) The volumetric drag values computed using two rough-walled time-invariant models (Zhou's (1995) & present) and Brown's smooth-walled uniform dynamic perturbation model (1981) are frequency-dependent, and compared well with the reference value of 13200,

(4) For Brown's smooth-walled uniform dynamic perturbation model (1981), the magnitude in the eddy viscosity has no influence on the volumetric drag values and behaves the same as Brown's quasi-steady perturbation model (1981). On the contrary, the phase angle substantially influences the volumetric drag values and increase the damping with the increased phase angles,

(5) Higher volumetric drag values are obtained in the smaller pipe than those in the larger

pipe from each model.

The computational costs from the four time-invariant eddy viscosity models (i.e. Ohmi & Usui's (1976), Brown's zero perturbation (1981), Zhou's (1995) and present models) are much lower than the other two models of Brown's. Brown's quasi-steady and dynamic models (1981) are more complicated to solve and require more advanced modeling skills. Therefore, the model proposed in the thesis is suggested to be an economic and effective tool for acoustic wave propagation analysis.

Furthermore, current turbulence model provides an advanced methodology for the computation of the volumetric drag in ABAQUS acoustic analysis. It is possible to obtain the volumetric drag values from the proposed two-region model than tune to experiments. The limitation of the proposed model is that it valid only for high mean Reynolds number turbulent pipe flows. It is not applicable to zero mean velocity flow.

The proposed two-region turbulence model is a rather crude estimate of the near wall turbulence. More experiments are needed to verify this model. Note that this model is developed only for one-dimensional turbulent flow. When multi-dimensionality is non-negligible, such as in very large pipes, pipe with significant bend, etc., the formula of volumetric drag or the approximation of specific acoustic impedance should be used with caution under those cases.

6.2 Recommendations for Future Study

Recommendations for future work to further assess present 1-D turbulence model, or to develop more systematic and sophisticated acoustic model are:

(1) The approach involving the time-variant eddy viscosity distributions in the rough-walled turbulence may need to be further investigated.

(2) A nonlinear numerical model (including the convection terms) using the method of characteristics needs to be developed for the rough–walled turbulence.

(3) Since the fluid velocity distributions are believed to affect the accuracy of predicting the resonance pressure amplitudes, developing a 2-D nonlinear turbulence model becomes an attractive issue.

Future work as outlined would allow the acoustic model to simulate the complex piping system (e.g. branched configurations) as well as the heat transfer applications. The work in this thesis has been one of the steps in achieving this process.

REFERENCES

Brown, F.T., Morgolis, D.L., and Shah, P.P. (1969). *"Small amplitude frequency behaviour of fluid lines with turbulent flow"*. J. Basic Eng., Trans. ASME, Vol. 9(4), pp. 67 - 81.

Brown, F.T. (1981). *"Wave propagation in tubes with turbulent flow. Part I: Analytical models; Part II: Experimental results"*, Proc. Symp. on Fluid Transmission Line Dynamics, ASME Winter Annual Meeting, pp. 1 – 15 (Part I), pp. 17 – 32 (Part II).

Brown, F.T. (1984). *"On weighting functions for the simulation of unsteady turbulent flow"*, Forum on Unsteady Flow, ASME, New Orleans, USA, FED-Vol. 15, pp. 26 – 28.

Bergant, A., Simpson, A.R., and Vitkovský, J. (2001). *"Developments in unsteady pipe flow friction modelling"*, Journal of Hydraulic Research, Vol. 39(3), pp. 249 – 257.

Cebeci, T. and Bradshaw, P. (1977). *"Momentum transfer in boundary layers"*, McGraw-Hill, N. Y. and Hemisphere, Washington, D.C.

Chaudhry, M.H. (1987). *"Applied hydraulic transients"*, Second Edition, Van Nostrand Reinhold, N. Y.

Chatoorgoon, V., Hau, K., Lee, N. and Reesor, G. (1993). *"Modelling of acoustic phenomena in reacting piping, Part I : Fundamental studies"*, AECL Report, ARD-TD-465, COG-93-402.

Chatoorgoon, V. and Zhou, R.Q.N., (1995). *"Modelling of acoustic phenomena in reacting pipe, Part III: "Acoustic damping"*, AECL Report, ARD-TD-511, COG-94-464.

Churchill, S.W. and Chan, C.C. (1995). *"Theoretically based correlating equations for the local characteristics of fully turbulent flow in round tubs and between parallel plates"*, Indus. And Eng. Chemistry Res., Vol. 34, pp. 1332 – 1341.

D'Souza, A.F., and Oldenburger, R. (1964). *"Dynamic response of fluid lines"*, J. Basic Eng., Trans. ASME, Sept. Vol. 86, pp 589 - 598.

Eichinger, P., and Lein, G. (1992). *"The influence of friction on unsteady pipe flow"*, Proc. Int. Conf. On Unsteady Flow and Fluid Transients, Durham, England, pp. 41 – 50.

Foster, K. and Parker G.A. (1964). *"Transmission of power by sinusoidal wave motion through hydraulic oil in a uniform pipe"*. Proc. Instn. Mech. Engs. (1964 – 65), Vol. 179: Pt. 1(19), pp. 599 – 612.

Holmboe, E.L., Rouleau W.T. (1967). *"The effect of viscous shear on transients in liquid lines"*, Transaction of ASME, J. of Basic Eng., Vol. 68, pp. 174 – 180.

Hinze, J.O. (1975). *"Turbulence"*, 2nd Edition, McGraw-Hill, Inc.

Haaland, S. E. (1983). *"Simple and explicit formulas for the friction factor in turbulent pipe flow"*, J. of Fluids Eng., Vol. 105, pp. 89 – 90.

He, S. and Jackson, J.D. (2000). *"A study of turbulence under structure of transient flow in a pipe"*, J. of Fluid Mechanics, Vol. 408, pp. 1 - 38.

Kita, Y., Adachi, Y. and Hirose, K. (1980). *"Periodically oscillating turbulent flow in a pipe"*, Bull. of JSME, Vol. 23(179), pp. 656 – 664.

Kar, P.K. (1993). *"Reactor fuel damage computer modelling and analysis work program review"*, AECL-CANDU, Nuclear Support Service Department, Report No. 938011.

Laufer, J. (1954). *"The structure of turbulence in fully developed pipe flow"*, NACA TR 1174.

Lighthill, M.J. Sir. (1978). *"Waves in fluids"*, Cambridge University Press.

Munjal, M. L., and Thawani, P. T. (1997). *"Acoustic performance of hoses – a parametric study"*, Noise Control Engineering Journal, Vol. 44, pp. 274 - 280.

Ohmi, M., Usui, T., Tanaka, O., and Toyama, M. (1976). *"Pressure and velocity distributions in pulsating turbulent pipe flow, Part I: Theoretic treatments; Part II: Experimental investigations "*, Bull. of JSME, Vol. 19(129), pp. 307 – 313 (part I); Vol. 19(134), pp. 951 – 957 (part II).

Ohmi, M., Kyomen, S., and Usui T., (1978). *"Analysis of velocity distribution in pulsating turbulent pipe flow with Time-dependent friction velocity"*, Bull. of

JSME, Vol. 21(157), pp. 1137 - 1143.

Ohmi, M., Iguchi, M., Usui, T. and Minami, H. (1980). *"Flow pattern and frictional losses in pulsating pipe flow: Part 1 - 3"*, Bull. JSME, Vol. 23(186), pp. 2013 - 2036.

Ohmi, M., Iguchi, M. and Usui, T. (1981). *"Flow pattern and frictional losses in pulsating pipe flow: Part 4 - 6"*, Bull. JSME, Vol. 24(187), pp. 67 – 81, pp. 1756 - 1763.

Ohmi, M. and Iguchi, M. (1982). *"Flow pattern and frictional losses in pulsating pipe flow: Part 7"*, Bull. JSME, Vol. 24(196), pp. 1537 - 1543.

Ohmi, M., Kyomen, S., and Usui T. (1981). *"Numerical analysis of pressure and velocity distributions for a pulsating turbulent flow in a circular tube containing a slightly compressible fluid"*, Bull. of JSME, Vol. 24(187), pp. 60 - 66.

Ohmi, M., Kyomen, S., and Usui T. (1985). *"Numerical analysis of transient turbulent flow in a liquid line"*, Bull. of JSME, Vol. 28(239), pp. 799 - 806.

Pezzinga, G. (1999). *"Quasi-2D model for unsteady flow in pipe networks"*, J. of Hydr. Eng., ASCE, Vol. 125(7), pp. 676 – 685.

Prek, M. (2004). *"Wavelet analysis of sound signal in fluid-filled viscoelastic pipes"* J. of Fluids and Structures, Vol. 19, pp. 63 -72.

Rzentkowski, G., Forest, J.W. and Martin, D.G. (1993). *"Acoustical characterization of the heat transport system of Darlington Nuclear Generation Station: Analysis technique and results"*, 1st International Symposium on Pump Noise and Vibrations, Clamart, France, pp. 289 - 300.

Rzentkowski, G., Forest, J.W., and Russel, J.H. (1993). *"Estimation of pump-generated pressure pulsations from instrument line measurements"*, Pump Noise and Vibrations, 1st International Symposium, Clamart, France, July 7 - 9.

Schlicting, H. (1968). *"Boundary layer theory"*, Sixth Edition, McGraw-Hill, N. Y.

Samuel, T. (1981). *"Elements of acoustics"*, John Wiley & Sons, Inc.

Sou, L., and Wylie, E. B. (1990). *"Complex wavespeed and hydraulic transients in viscoelastic pipes"*, J. of Flu. Eng., Vol. 112, pp. 496 – 500.

Suzuki, K., Taketomi, T., and Sato, S. (1991). *"Improving Zielke's method of simulating frequency-dependent friction in laminar liquid pipe flow"*, J. Fluids Eng., ASME, Vol. 113(4), pp. 569 – 573.

Schohl, G.A. (1993). *"Improved approximation for simulating frequency-dependent friction in transient laminar flow"*, J. Fluids Eng., ASME, Vol. 115(3), pp. 420 – 424.

Shuy, E.B. (1995). *"Approximate wall shear equation for unsteady laminar pipe flows"*, J. Hydr. Res., Vol. (33) 4, pp. 457 – 469.

Thurston, G B. (1952). *"Periodic fluid flow through circulate tubes"*, J. of the Acoustical Soc. of American, Vol. 24, No. 6, pp. 653 – 656.

Trikha, A.K. (1975). *"An efficient method for simulating frequency-dependent friction in transient liquid flow"*, J. Fluids Eng., Trans. ASME, March, pp. 97 - 105.

von Kármán, T. (1939). *"The analogy between fluid friction and heat transfer"*, Trans. ASME, Vol. 61(8), pp. 705.

Vardy, A.E., and Hwang, K.L. (1991). *"A characteristics model of transient friction in pipes"*, J. of Hydr. Res., IAHR, Vol. 29(5), pp. 669 – 684.

Vardy, A.E. (1992). *"Approximating unsteady friction at high Reynolds numbers"*, Pro., Int. Conf. On Unsteady Flow and Fluid Transients, Durham, England, pp. 21 – 29.

Vardy, A.E., Hwang, K.L., and Brown, J.M.B. (1993). *"A weighting function model of transient turbulent pipe flow"*, J. Hydr. Res., IAHR, Vol. 31(4), pp. 533 – 548.

Vardy, A.E. and Brown, J.M.B. (1995). *"Transient, turbulent, smooth pipe flow"*, J. Hydr. Res., IAHR, Vol. 33(4), pp. 435 - 456.

Vardy, A.E. and Brown, J.M.B. (1996). *"On turbulent, unsteady, smooth-pipe flow"*, Pro. Int. Conf. On Pressure Surges and Fluid Transients, BHR Group, Harrogate, England, pp. 289 - 311.

Vardy, A.E. and Brown, J.M.B. (2003). *"Transient turbulent friction in smooth pipe flows"*, J. of Sound and Vibration, Vol. 259(5), pp. 1011 - 1036.

Vardy, A.E. and Brown, J.M.B. (2004). *"Transient turbulent friction in fully rough pipe flows"*, J. of Sound and Vibration, Vol. 270, pp. 233 - 257.
Wood, D.J. and Funk, J.E. (1970). *"A boundary layer theory for transient viscous losses in turbulent flow"*, J. Basic Eng., Trans. ASME, Dec. pp. 865 - 873.

Wylie, E. B., and Streeter, V. L. (1993). *"Fluid transients in systems"*, Prentice-Hall, Englewood Cliffs, N. J.

Zielke, W. (1968), *"Frequency dependent friction in transient pipe flow"*, Trans. ASME, J. Basic Engng, Vol. 90, pp. 109 - 115.

Zhou, R.Q.N., and Chatoorgoon, V. (1994). *"Modelling of acoustic phenomena in reacting piping, Part II: Prediction of Acoustic resonance in tubes"*, AECL Report, ARD-TD-515, COG-94-471.

Zhou, R.Q.N. (1995). *"Modelling of acoustic phenomena in reacting piping, Part IV: Prediction of volumetric drag for turbulent pipe flow"*, AECL Report, ARD-TD-536, COG-94-653.

Appendix A

This appendix summarizes the simplification of pertinent compressible turbulence equations, and the transformation of variables used to solve Eq. (4.27) in Chapter 4. The derivations of cross-sectional velocity averaging procedures are also presented herein.

Summary of simplification of turbulence mean-flow equations

Eqs. (4.6) ~ (4.8) can be simplified by means of comparing turbulence quantity's magnitudes, assume that the turbulence characteristic scales are defined as:

$$\begin{cases} Charateristic\ \ length-scale: & x \sim L,\ r \sim \varepsilon L \ \ where\ \ \varepsilon << 1 \\ Charateristic\ \ velocity-scale: & \bar{u} \sim U,\ \bar{v} \sim \varepsilon U \ \ where\ \ \varepsilon << 1 \ \ and\ \ U << C \\ & \overline{u'^2} \sim V'^2 \ \ and\ \ \overline{u'v'} \sim R_{12}V'^2 \ \ where\ \ R_{12} >> 1 \\ Charateristic\ \ time-scale: & t \sim L/C \end{cases}$$

Where the capital letters denote the turbulence characteristic scales respectively, and ε is the proportional coefficient relates pipe axial length scale to the radial length scale. We know from experience that, in anisotropic shear flows, the intensities of $\overline{u'^2}$ and $\overline{v'^2}$ are roughly of the same magnitude. So we define the same fluctuation velocity-scale for u' *and* v', and R_{12}, the correlation coefficient relates the product of $\overline{u'v'}$ to the square of fluctuation velocity-scale.

Starting from Eq. (4.7), the first two terms of left-hand-side is rewritten after rearrangement from continuity equation. Comparing the magnitudes of parameters using the definition of turbulence characteristic scales, following the rules of $U/C << 1$ for low Mach number flows:

$$
\begin{cases}
\dfrac{\overline{u}}{}\dfrac{\partial\left(\overline{\rho v}\right)}{\partial r} \sim \dfrac{U.\overline{\rho}\varepsilon U}{\varepsilon L} \sim \dfrac{\overline{\rho}U^{2}}{L} << \left\{\dfrac{\overline{}}{\rho}\dfrac{\partial\overline{u}}{\partial t} \sim \dfrac{\overline{\rho}U.C}{L}\right\} \\
\dfrac{\overline{u}}{}\dfrac{\left(\overline{\rho v}\right)}{r} \sim \dfrac{U.\overline{\rho}\varepsilon U}{\varepsilon L} \sim \dfrac{\overline{\rho}U^{2}}{L} << \left\{\dfrac{\overline{}}{\rho}\dfrac{\partial\overline{u}}{\partial t} \sim \dfrac{\overline{\rho}U.C}{L}\right\} \\
\left(\overline{\rho u}\right)\dfrac{\partial\overline{u}}{\partial x} \sim \dfrac{\overline{\rho}U^{2}}{L} << \left\{\dfrac{\overline{}}{\rho}\dfrac{\partial\overline{u}}{\partial t} \sim \dfrac{\overline{\rho}U.C}{L}\right\} \\
\dfrac{\partial\left(\overline{\rho.u\ v}\right)}{\partial r} \sim \dfrac{\overline{\rho}U.\varepsilon U}{\varepsilon L} \sim \dfrac{\overline{\rho}U^{2}}{L} << \left\{\dfrac{\overline{}}{\rho}\dfrac{\partial\overline{u}}{\partial t} \sim \dfrac{\overline{\rho}U.C}{L}\right\} \\
\dfrac{\partial\overline{\left(\rho u'^{2}\right)}}{\partial x} \sim \dfrac{\overline{\rho}V'^{2}}{L} << \left\{\dfrac{\overline{\partial\left(\rho u'v'\right)}}{\partial r} \sim \dfrac{\overline{}}{\rho}\dfrac{R_{12}V'^{2}}{\varepsilon L}\right\} \\
\left(\dfrac{4\mu}{3}\right)\dfrac{\partial^{2}\overline{u}}{\partial x^{2}} \sim \left(\dfrac{4\mu}{3}\right)\dfrac{U}{L^{2}} << \left\{\mu\left(\dfrac{\partial^{2}\overline{u}}{\partial r^{2}}\right) \sim \mu\dfrac{U}{\varepsilon^{2}L^{2}}\right\} \quad or \quad \left\{\mu\left(\dfrac{1}{r}\dfrac{\partial\overline{u}}{\partial r}\right) \sim \mu\dfrac{U}{\varepsilon^{2}L^{2}}\right\} \\
\dfrac{\mu}{3}\dfrac{\partial}{\partial x}\left(\dfrac{\partial\overline{v}}{\partial r}\right) \sim \dfrac{\mu}{3}\dfrac{\varepsilon U}{\varepsilon L^{2}} \sim \dfrac{\mu}{3}\dfrac{U}{L^{2}} << \left\{\mu\left(\dfrac{\partial^{2}\overline{u}}{\partial r^{2}}\right) \sim \mu\dfrac{U}{\varepsilon^{2}L^{2}}\right\} \\
\dfrac{\mu}{3}\dfrac{\partial}{\partial x}\left(\dfrac{\overline{v}}{r}\right) \sim \dfrac{\mu}{3}\dfrac{U}{L^{2}} << \left\{\mu\left(\dfrac{\partial^{2}\overline{u}}{\partial r^{2}}\right) \sim \mu\dfrac{U}{\varepsilon^{2}L^{2}}\right\}
\end{cases}
$$

The longitudinal equation of motion is simplified to the closed approximation:

$$
\frac{-\partial\overline{u}}{\rho\partial t}+\frac{\partial\overline{\rho u'v'}}{\partial r}=-\frac{\partial\overline{p}}{\partial x}+\mu\left(\frac{\partial^{2}\overline{u}}{\partial r^{2}}+\frac{1}{r}\frac{\partial\overline{u}}{\partial r}\right) \qquad (A.1)
$$

Introducing the modified total kinematic viscosity and considering 1-D approximation such as $\overline{\rho}$ is invariant with radius, the simplified turbulence mean-flow equations of conservation can be obtained as Eqs. (4.9) and (4.10).

Summary of the transformation of variables

To acquire an analytical solution of the partial differential equation (Eq. (4.27)), the transformation of variables $z_1(r)$ *and* $z_2(r)$ are defined in Eq. (4.29), as:

$$\begin{cases} z_1(r) = \dfrac{2}{bu_{st}^*}\sqrt{s\,\nu_{T,1}}\ , & 0 \le \dfrac{y}{R} \le 0.175 \\ z_2(r) = r\sqrt{\dfrac{s}{\nu_{T,2}}}\ , & 0.175 \le \dfrac{y}{R} \le 1 \end{cases} \tag{4.29}$$

$$\text{where: } \nu_{T,j} = \begin{cases} \nu_w + b\left(yu_{st}^*\right), & (j=1),\quad 0 \le \dfrac{y}{R} \le 0.175 \\ 0.07\left(Ru_{st}^*\right), & (j=2),\quad 0.175 \le \dfrac{y}{R} \le 1 \end{cases} \tag{4.30}$$

Starting from Eq. (4.27) as $\underbrace{\nu_{T,j}\dfrac{\partial^2 V}{\partial r^2}}_{Term\ I} + \underbrace{\left(\dfrac{d\nu_{T,j}}{dr} + \dfrac{\nu_{T,j}}{r}\right)\dfrac{\partial V}{\partial r}}_{Term\ II} - sV = 0$, the first two terms become after rearranging as:

(1) For sub-region $j=1,\ 0 \le \dfrac{y}{R} \le 0.175$:

$$\frac{\partial V}{\partial r} = \frac{\partial V}{\partial Z_1(r)} \times \frac{\partial Z_1(r)}{\partial r} = \frac{\partial}{\partial r}\left\{\frac{2}{bu_{st}^*}\sqrt{s.\left[\nu_w + bu_{st}^*(R-r)\right]}\right\}.\frac{\partial V}{\partial Z_1(r)}$$

$$\Rightarrow \quad \frac{\partial V}{\partial r} = (-\xi).\frac{\partial V}{\partial Z_1(r)} \tag{A.2}$$

$$where:\ \xi = \frac{1}{\sqrt{\dfrac{1}{s}.\left[\nu_w + bu_{st}^*(R-r)\right]}} \tag{A.3}$$

Differentiating Eq. (*A.2*) with respect to *r*, yields:

$$\frac{\partial^2 V}{\partial r^2} = \frac{\partial}{\partial r}\left(\frac{\partial V}{\partial r}\right) = \frac{\partial}{\partial Z_1(r)}\left(\frac{\partial V}{\partial r}\right) \times \frac{\partial Z_1(r)}{\partial r}$$

$$\therefore \quad \frac{\partial^2 V}{\partial r^2} = (-\xi).\frac{\partial}{\partial Z_1(r)}\left\{(-\xi).\frac{\partial V}{\partial Z_1(r)}\right\} = (-\xi).\frac{\partial^2 V}{\partial Z_1(r)^2} + \frac{\partial V}{\partial Z_1(r)}.\frac{\partial}{\partial Z_1(r)}(-\xi),$$

$$\Rightarrow \quad \frac{\partial^2 V}{\partial r^2} = \xi^2.\frac{\partial^2 V}{\partial Z_1(r)^2} - \frac{bu_{st}^*}{2s}\xi^3.\frac{\partial V}{\partial Z_1(r)} \qquad (A.4)$$

Hence, substituting Eqs. (4.29), (*A.2*), (*A.3*), and (*A.4*) into Eq. (4.27), yields:

$$\left\{s.\frac{1}{\xi^2}\right\}\frac{\partial^2 V}{\partial r^2} + \left(\frac{d}{dr}\left\{s.\frac{1}{\xi^2}\right\} + \frac{\left\{s.\frac{1}{\xi^2}\right\}}{r}\right)\frac{\partial V}{\partial r} - sV = 0$$

$$\therefore \quad \frac{\partial^2 V}{\partial Z_1(r)^2} + \left(\frac{bu_{st}^*}{2s}.\xi + \frac{1}{r\xi}\right)\frac{\partial V}{\partial Z_1(r)} - V = 0$$

$$\Rightarrow \quad \frac{\partial^2 V}{\partial Z_1(r)^2} + \left(1 + \frac{\left(bu_{st}^*\right)^2}{2}\left(\frac{\nu_w}{r.bu_{st}^*} + \frac{R}{r} - 1\right)\right)\frac{1}{Z_1(r)}\frac{\partial V}{\partial Z_1(r)} - V = 0 \qquad (A.5)$$

Tab. A.1 shows the computed values of $\left(1 + \frac{\left(bu_{st}^*\right)^2}{2}\left(\frac{\nu_w}{r.bu_{st}^*} + \frac{R}{r} - 1\right)\right)$ using $R = 0.03\ [m]$ and $b = 0.4 - \frac{\nu_w}{0.175Ru_{st}^*}$ for three different Reynolds numbers, $\mathrm{Re} = 5\times10^4, 8\times10^4$ *and* 1×10^5. The wall effective viscosity ν_w is setting as 100, 150 and 250 times of the kinematic viscosity $\nu = 4.7\times10^{-7}$.

Table A.1: The values of $\left(1+\frac{(bu_{st}^{*})^{2}}{2}\left(\frac{\nu_w}{r.bu_{st}^{*}}+\frac{R}{r}-1\right)\right)$ with increased Reynolds number

Re	5.0×10^4			8.0×10^4			1.0×10^5		
$y/R = 0.061$	$\nu_w = 100.\nu$	$\nu_w = 150.\nu$	$\nu_w = 250.\nu$	$\nu_w = 100.\nu$	$\nu_w = 150.\nu$	$\nu_w = 250.\nu$	$\nu_w = 100.\nu$	$\nu_w = 150.\nu$	$\nu_w = 250.\nu$
	1.000023	1.000029	1.000042	1.000042	1.000052	1.000071	1.000057	1.000069	1.000092
0.0705	1.000025	1.000031	1.000044	1.000046	1.000056	1.000074	1.000063	1.000074	1.000097
0.08	1.000026	1.000033	1.000045	1.00005	1.000059	1.000078	1.000068	1.00008	1.000103
0.0895	1.000028	1.000035	1.000047	1.000053	1.000063	1.000082	1.000074	1.000086	1.000108
0.099	1.00003	1.000036	1.000049	1.000057	1.000067	1.000086	1.00008	1.000092	1.000114
0.1085	1.000031	1.000038	1.000051	1.000061	1.000071	1.00009	1.000086	1.000098	1.00012
0.118	1.000033	1.00004	1.000053	1.000066	1.000075	1.000094	1.000092	1.000104	1.000126
0.1275	1.000035	1.000042	1.000055	1.00007	1.00008	1.000099	1.000098	1.00011	1.000133
0.137	1.000037	1.000044	1.000057	1.000074	1.000084	1.000103	1.000104	1.000116	1.000139
0.1465	1.000039	1.000046	1.000059	1.000078	1.000088	1.000108	1.000111	1.000123	1.000146
0.156	1.000041	1.000048	1.000061	1.000083	1.000093	1.000112	1.000118	1.000129	1.000152
0.1655	1.000043	1.00005	1.000063	1.000088	1.000098	1.000117	1.000124	1.000136	1.000159
0.175	1.000045	1.000052	1.000066	1.000092	1.000102	1.000122	1.000131	1.000143	1.000166

Tab. A.1 indicate that the calculated values of $\left(1+\frac{\left(bu_{st}^{*}\right)^{2}}{2}\left(\frac{\nu_w}{r.bu_{st}^{*}}+\frac{R}{r}-1\right)\right)$ approach their minimum from the near wall to their maximum at the outer layer/core interface (e.g. $y/R=0.175$). All values are nearly equal to unity under all presumed circumstances with the maximum error less than 0.017%. Therefore, an approximation of $\left(1+\frac{\left(bu_{st}^{*}\right)^{2}}{2}\left(\frac{\nu_w}{r.bu_{st}^{*}}+\frac{R}{r}-1\right)\right)\doteq 1$ is valid for high mean Reynolds number, and Eq. (A.5) becomes:

$$\frac{\partial^2 V}{\partial Z_1(r)^2}+\frac{1}{Z_1(r)}\frac{\partial V}{\partial Z_1(r)}-V=0 \qquad (A.6)$$

Vardy *et al.* (1995) made a similar transformed variable as Eq. (4.29), unless their model was described in the Cartesian coordinates. However, this treatment led to the direct solution of Eq. (*A.6*) in the sub-region *j=1* without any approximation.

(2) For sub-region $j=2,\ 0.175\le\frac{y}{R}\le 1$:

$$\frac{\partial V}{\partial r}=\frac{\partial V}{\partial Z_2(r)}\times\frac{\partial Z_2(r)}{\partial r}=\sqrt{\frac{s}{0.07u_{st}^{*}R}}\cdot\frac{\partial V}{\partial Z_2(r)} \qquad (A.7)$$

Differentiating Eq. (*A.7*) with respect to *r*, yields:

$$\frac{\partial^2 V}{\partial r^2}=\frac{\partial}{\partial r}\left(\frac{\partial V}{\partial r}\right)=\frac{\partial}{\partial Z_2(r)}\left(\frac{\partial V}{\partial r}\right)\times\frac{\partial Z_2(r)}{\partial r}=\left(\frac{s}{0.07u_{st}^{*}R}\right)\cdot\frac{\partial^2 V}{\partial Z_2(r)^2} \qquad (A.8)$$

Substituting Eqs. (4.30), (*A.7*), and (*A.8*) into Eq. (4.27), yields:

$$\left\{0.07 u_{st}^{*} R\right\}\frac{\partial^2 V}{\partial r^2}+\left(\frac{d}{dr}\left\{0.07\ u_{st}^{*} R\right\}+\frac{\left\{0.07\ u_{st}^{*} R\right\}}{r}\right)\frac{\partial V}{\partial r}-sV=0$$

$$\therefore\quad s.\frac{\partial^2 V}{\partial Z_2(r)^2}+\frac{\sqrt{s\ 0.07 u_{st}^{*} R}}{r}\frac{\partial V}{\partial Z_2(r)}-sV=0$$

$$\Rightarrow\quad \frac{\partial^2 V}{\partial Z_2(r)^2}+\frac{1}{Z_2(r)}\frac{\partial V}{\partial Z_2(r)}-V=0 \qquad (A.9)$$

Consequently, original equation (4.27) arrives its transform of equation (4.31) in each sub-region.

Summary of cross-sectional averaged velocity distribution

On the assumption of the cross-sectional velocity distribution is always piece-wise continuous, θ^* can be solved by using the recurrence formulas of *modified Bessel Functions*, such as:

$$\begin{cases} \dfrac{d}{dq}\left[q^g I_n(q)\right] = q^n I_{n-1}(q) & (A.10) \\ \dfrac{d}{dq}\left[q^n K_n(q)\right] = -q^n K_{n-1}(q) & (A.11) \end{cases}$$

Where I_ν and K_ν are the modified Bessel functions of first and second kinds of order n respectively, n is any integer or zero, and q is any variable.

Making some transformations before applying integration over each sub-region $j=1,2$, such as:

(a) For sub-region $j=1$, $0.825R<r<R$:

$$\begin{cases} Z_1(r) = \dfrac{2}{bu_{st}^*}\sqrt{S.\nu_{T,1}} \;\; where: \;\; \nu_{T,1} = \left[\nu_w + bu_{st}^*(R-r)\right] & (A.12) \\ \sqrt{\nu_{T,1}} = Z_1(r).\dfrac{bu_{st}^*}{2\sqrt{S}} & (A.13) \\ d\left[Z_1(r)\right] = d\left\{\dfrac{2}{bu_{st}^*}\sqrt{S.\left[\nu_w + bu_{st}^*(R-r)\right]}\right\} = \left(-\sqrt{\dfrac{S}{\nu_{T,1}}}\right)dr & (A.14) \\ dr = d\left[Z_1(r)\right].\left(-\sqrt{\dfrac{\nu_{T,1}}{S}}\right) = \left(-\dfrac{bu_{st}^*}{2S}\right)Z_1(r)d\left[Z_1(r)\right] & (A.15) \end{cases}$$

(b) For sub-region $j=2,\ \ 0<r<0.825R$:

$$\begin{cases} Z_2(r)=r\sqrt{S/\nu_{T,2}} \ \ where:\ \ \nu_{T,2}=\left[0.07.Ru_{st}^{*}\right] & (A.16) \\ d\left[Z_2(r)\right]=d\left\{r\sqrt{S/\nu_{T,2}}\right\}=\left(\sqrt{\dfrac{S}{\nu_{T,2}}}\right)dr \ \ or:\ \ dr=\left(\sqrt{\dfrac{\nu_{T,2}}{S}}\right)d\left[Z_2(r)\right] & (A.17) \end{cases}$$

For sub-region $j=1$, integrating Eq. (4.49) by parts twice, the first integral of $C_1\int_{0.825R}^{R} I_0\left[Z_1(r)\right]rdr$ becomes:

$$C_1\int_{0.825R}^{R} I_0\left[Z_1(r)\right]rdr=\left(-C_1\frac{bu_{st}^{*}}{2S}\right)\left\{\left(r\,Z_1(r)\ I_1\left[Z_1(r)\right]\right)\Big|_{0.825R}^{R}+\left(\frac{bu_{st}^{*}}{2S}\right)\left(Z_1^{\,2}(r)\ I_2\left[Z_1(r)\right]\right)\Big|_{0.825R}^{R}\right\}$$

(A.18)

Similar integral procedure can be done to the second integral of $D_1\int_{0.825R}^{R} K_0\left[Z_1(r)\right]rdr$ in Eq. (4.49), yields:

$$D_1\int_{0.825R}^{R} K_0\left[Z_1(r)\right]rdr=\left(D_1\frac{bu_{st}^{*}}{2S}\right)\left\{\left(r\,Z_1(r)\ K_1\left[Z_1(r)\right]\right)\Big|_{0.825R}^{R}-\left(\frac{bu_{st}^{*}}{2S}\right)\left(Z_1^{\,2}(r)\ K_2\left[Z_1(r)\right]\right)\Big|_{0.825R}^{R}\right\}$$

(A.19)

Where I_2, K_2 are the modified Bessel functions of first and second kinds of order 2 respectively. Thereafter, we define the integral of Eq. (4.49) for sub-region $j=1$ is:

$$\theta_1^{*}=\frac{2}{R^2}\times\left\langle\left(-C_1\frac{bu_{st}^{*}}{2S}\right)\left\{\left(r\,Z_1(r)\ I_1\left[Z_1(r)\right]\right)\Big|_{0.825R}^{R}+\left(\frac{bu_{st}^{*}}{2S}\right)\left(Z_1^{\,2}(r)\ I_2\left[Z_1(r)\right]\right)\Big|_{0.825R}^{R}\right\}\right.$$

$$\left.+\left(D_1\frac{bu_{st}^{*}}{2S}\right)\left\{\left(r\,Z_1(r)\ K_1\left[Z_1(r)\right]\right)\Big|_{0.825R}^{R}-\left(\frac{bu_{st}^{*}}{2S}\right)\left(Z_1^{\,2}(r)\ K_2\left[Z_1(r)\right]\right)\Big|_{0.825R}^{R}\right\}\right\rangle$$

(A.20)

For sub-region $j=2$, the integral procedure is much simple, and arrives the following form:

$$\theta_2^* = \frac{2}{R^2} \times C_2 \int_0^{0.825R} I_0\left[Z_2(r)\right] r dr = \frac{2}{R^2} \times \left\langle \left(C_2 \frac{0.07.Ru_{st}^*}{S} \right) \left(Z_2(r)\ I_1\left[Z_2(r)\right] \right) \Big|_0^{0.825R} \right\rangle \qquad (A.21)$$

The cross-sectional averaged velocity distribution then arrives the form of Eq. (4.50).

Appendix B

Summary of Fortran code

This appendix summarizes the computer programs written in Fortran, which are employed to compute and verify the linear acoustic model.

Main Program

```
      PROGRAM      MAIN
      USE          MSIMSL
C  ++++++++++++++++++++++++++++++++++++++++++++++++++++++++++++++++++++++++++++
CC ----- GENERAL PART DEFINITION ------
      INTEGER      IM, ID
      PARAMETER    (IM =100000 )
      INTEGER      ITER
      PARAMETER    (ITER=201)
      INTEGER N
      PARAMETER (N=1)
      REAL XNU
      PARAMETER (XNU = 2.0)
      REAL R1, R2, CH32_L, VISCO, FREQU(IM), W(IM)
      REAL DEN, KERXI, MQ, PI, TEMP
      COMPLEX S(IM)

C  ++++++ DEFINITION OF SONIC VELOCITY  ++++++++++++++++++++++++++++++++
SS    REAL C1(IM), C2(IM)
      COMPLEX C1(IM), C2(IM)

C  ++++++ LOCAL VARIABLES OF CHANNEL_32 ++++++++++++++++++++++++++++++
      REAL Uf_1, Rou_1, RE_1, AREA_1
      COMPLEX    CH32_GAMAS(IM), CH32_BETA(IM), CH32_ALFA(IM), CH32_ZA(IM)
      REAL CH32_VDRAG(IM)
      COMPLEX    CH32_RP(IM)
```

```
C  ++++++ LOCAL VARIABLES OF CHANNEL_29 ++++++++++++++++++++++++++++++++
      REAL Uf_2, Rou_2, RE_2, AREA_2
      COMPLEX   CH29_GAMAS(IM), CH29_BETA(IM), CH29_ALFA(IM), CH29_ZA(IM)
      COMPLEX     U1(IM), U2(IM), U3(IM), U4(IM), CA29_ZA(IM)
      REAL   CH29_VDRAG(IM)
      COMPLEX   CH29_RP(IM)

C  ++++++ LOCAL VARIABLES OF CHANNEL_30 & CHANNEL_31 ++++++++++++++++++++
      COMPLEX   CHAN_GAMAS(IM), CHAN_BETA(IM), CHAN_ALFA(IM), CHAN_ZA(IM)
      REAL   CHAN_VDRAG(IM)
      COMPLEX   CHAN_RP(IM)
      COMPLEX   U5(IM), U6(IM), U7(IM), U8(IM), CHANNEL_ZA(IM)

C  ++++++++++++++++++++++++++++++++++++++++++++++++++++++++++++++++++++++++
      COMPLEX CH29_AMPLIT(IM), AMPLIT(IM), CHAN_AMPLIT(IM)
      REAL AMPLITM(IM)

C  ++++++ DEFINITIONS OF ZHOU'S VOLUMETRIC DRAG ++++++++++++++++++++++++
      REAL ZH1_VDRAG(IM), ZH2_VDRAG(IM), ZH3_VDRAG(IM)

CC  ----- ZHOU'S MODEL DEFINITION -----
      COMPLEX ZH1_GAMAS(IM), ZH1_BETA(IM), ZH1_ALFA(IM)
      COMPLEX ZH1_RP(IM), ZH1_ZA(IM)
      COMPLEX ZH2_GAMAS(IM), ZH2_BETA(IM), ZH2_ALFA(IM)
      COMPLEX ZH2_RP(IM), ZH2_ZA(IM)
      COMPLEX ZH3_GAMAS(IM), ZH3_BETA(IM), ZH3_ALFA(IM)
      COMPLEX ZH3_RP(IM), ZH3_ZA(IM)

A  --------   DEFINITIONS OF USER SPECIFIED DERIVATIVE --------
      EXTERNAL DERIVES, DERIVES_B, DERIVES_C
      COMPLEX YY(IM), YYB(IM), YYC(IM)
      REAL MA, PH, NIK

Ba  -- DEFINITIONS OF BROWN'S QUASI-STEADY EDDY VISCOSITY MODEL "A" --
      REAL NIKU, NIKU2
      COMPLEX BRA1_GAMAS(IM), BRA1_BETA(IM), BRA1_ALFA(IM)
      COMPLEX   BRA1_RP(IM), DUDR1_A(IM), BRA1_ZA(IM)
      COMPLEX BRA2_GAMAS(IM), BRA2_BETA(IM), BRA2_ALFA(IM)
      COMPLEX   BRA2_RP(IM), DUDR2_A(IM), BRA2_ZA(IM)
      COMPLEX BRA3_GAMAS(IM), BRA3_BETA(IM), BRA3_ALFA(IM)
      COMPLEX   BRA3_RP(IM), DUDR3_A(IM), BRA3_ZA(IM)
```

```
      REAL BRA1_VDRAG(IM), BRA2_VDRAG(IM), BRA3_VDRAG(IM)

A     -------- DEFINITIONS OF "A" RUNGER-KUTTA ALGORITHM --------
      EXTERNAL RK4_1A, RK4_2A, RK4_3A

Bz    -- DEFINITIONS OF BROWN'S ZERO PERTURBATION EDDY VISCOSITY MODEL "B" --
      COMPLEX BRB1_GAMAS(IM), BRB1_BETA(IM), BRB1_ALFA(IM)
      COMPLEX    BRB1_RP(IM), DUDR1_B(IM), BRB1_ZA(IM)
      COMPLEX BRB2_GAMAS(IM), BRB2_BETA(IM), BRB2_ALFA(IM)
      COMPLEX    BRB2_RP(IM), DUDR2_B(IM), BRB2_ZA(IM)
      COMPLEX BRB3_GAMAS(IM), BRB3_BETA(IM), BRB3_ALFA(IM)
      COMPLEX    BRB3_RP(IM), DUDR3_B(IM), BRB3_ZA(IM)
      REAL BRB1_VDRAG(IM), BRB2_VDRAG(IM), BRB3_VDRAG(IM)

B     -------- DEFINITIONS OF "B" RUNGER-KUTTA ALGORITHM --------
      EXTERNAL RK4_1B, RK4_2B, RK4_3B

Bd    -- DEFINITIONS OF BROWN'S DYNAMIC EDDY VISCOSITY MODEL "C" --
      REAL MAG, MAG2, PHA, PHA2
      COMPLEX BRC1_GAMAS(IM), BRC1_BETA(IM), BRC1_ALFA(IM)
      COMPLEX    BRC1_RP(IM), DUDR1_C(IM), BRC1_ZA(IM)
      COMPLEX BRC2_GAMAS(IM), BRC2_BETA(IM), BRC2_ALFA(IM)
      COMPLEX    BRC2_RP(IM), DUDR2_C(IM), BRC2_ZA(IM)
      COMPLEX BRC3_GAMAS(IM), BRC3_BETA(IM), BRC3_ALFA(IM)
      COMPLEX    BRC3_RP(IM), DUDR3_C(IM), BRC3_ZA(IM)
      REAL BRC1_VDRAG(IM), BRC2_VDRAG(IM), BRC3_VDRAG(IM)

A     -------- DEFINITIONS OF "C" RUNGER-KUTTA ALGORITHM --------
      EXTERNAL RK4_1C, RK4_2C, RK4_3C

C     ++ DEFINITIONS OF PRESENT VOLUMETRIC DRAG ++
      REAL RW32_VDRAG(IM), RW29_VDRAG(IM), RWCH_VDRAG(IM)

CC    ----- PRESENT MODEL DEFINITION -----
      COMPLEX RW32_GAMAS(IM), RW32_BETA(IM), RW32_ALFA(IM)
      COMPLEX RW32_RP(IM), RW32_ZA(IM)
      COMPLEX RW29_GAMAS(IM), RW29_BETA(IM), RW29_ALFA(IM)
      COMPLEX RW29_RP(IM), RW29_ZA(IM)
      COMPLEX RWCH_GAMAS(IM), RWCH_BETA(IM), RWCH_ALFA(IM)
      COMPLEX RWCH_RP(IM), RWCH_ZA(IM)
```

```
CC
      DATA PI/3.1415926/, MQ/28.0/

CC    ----- PARAMETER DEFINITION OF COLD EXPERIMENT -----
      DATA TEMP/60.6/, Den/983.0/, VISCO/4.6897E-07/

AC    ----- PARAMETER DEFINITION OF BROWN'S "C" MODELS -----
      DATA NIKU/18.7/, NIKU2/18.7/
      DATA MAG/1.0/, MAG2/1.0/, KERXI/6.0/, PHA/0.08/, PHA2/0.08/

CC    ----- PARAMETER DEFINITION OF CH32 -----
      DATA CH32_L/4.51/, R1/0.0295/

CC    ----- PARAMETER DEFINITION OF CH29 -----
      DATA CH29_L/1.48/, R2/0.03683/

CC    ----- PARAMETER DEFINITION OF CH30 & CH31 -----
C30 DATA CHAN_L/3.04/
      DATA CHAN_L/5.56/

C     ------ PARAMETERS CALCULATION ------
      ID = IM
      DO 55 I = 1, ITER
         FREQU(I) = 50.0
55    CONTINUE

        DO 100 I = 2, ITER
C     ----- INPUR PARAPETERS ------
         FREQU(I) = FREQU(I-1) + 1.0
           W(I) = 2*PI*FREQU(I)
         S(I) = CMPLX(0.0,W(I))

C     ------OHMI'S MODEL CALLING ------
O     CALL CHANNEL32( R1, CH32_L, VISCO, W, DEN, C1, ID, I,
O        K                S, Uf_1, Rou_1, CH32_GAMAS, CH32_BETA,
O        K                N, XNU, MQ, RE_1, AREA_1, PI, TEMP, KERXI,
O        K                CH32_ALFA, CH32_VDRAG, CH32_RP, CH32_ZA )

CC
O     CALL CHANNEL29( R2, CH29_L, VISCO, W, DEN, C2, ID, I,
O        K                S, Uf_2, Rou_2, CH29_GAMAS, CH29_BETA,
```

```
O      K                N, XNU, MQ, RE_2, AREA_2, PI, TEMP, KERXI,
O      K                CH29_ALFA, CH29_VDRAG, CH29_RP, CH29_ZA )

O    CALL CHANNEL( R2, CHAN_L, VISCO, W, DEN, C2, ID, I,
O      K              S, Uf_2, Rou_2, CHAN_GAMAS, CHAN_BETA,
O      K              N, XNU, MQ, RE_2, AREA_2, PI, TEMP, KERXI,
O      K              CHAN_ALFA, CHAN_VDRAG, CHAN_RP, CHAN_ZA )
EF   ++++++++++++++++++++++++++++++++++++++++++++++++++++++++++++++++++++++++++

A3   ------ZHOU'S MODEL ON CALLING ------
Z    CALL ZHVD1( R1, CH32_L, VISCO, W, DEN, C1, ID, I,
Z      K              S, Uf_1, Rou_1, ZH1_GAMAS, ZH1_BETA,
Z      K              N, XNU, MQ, RE_1, AREA_1, PI, TEMP, KERXI,
Z      K              ZH1_ALFA, ZH1_VDRAG, ZH1_RP, ZH1_ZA )

Z    CH32_GAMAS(I) = ZH1_GAMAS(I)
Z    CH32_BETA(I) = ZH1_BETA(I)

C    ------ EXPERIMENTAL BOUNDARY CONDITIONS ------
Z    CH32_RP(I) = ZH1_RP(I)
Z    CH32_ZA(I) = ZH1_ZA(I)
Z    CH32_VDRAG(I) = ZH1_VDRAG(I)
FF   ++++++++++++++++++++++++++++++++++++++++++++++++++++++++++++++++++++++++++
Z    CALL ZHVD2( R2, CH29_L, VISCO, W, DEN, C2, ID, I,
Z      K              S, Uf_2, Rou_2, ZH2_GAMAS, ZH2_BETA,
Z      K              N, XNU, MQ, RE_2, AREA_2, PI, TEMP, KERXI,
Z      K              ZH2_ALFA, ZH2_VDRAG, ZH2_RP, ZH2_ZA )

Z    CH29_GAMAS(I) = ZH2_GAMAS(I)
Z    CH29_BETA(I) = ZH2_BETA(I)
Z    CH29_VDRAG(I) = ZH2_VDRAG(I)
Z    CH29_RP(I) = ZH2_RP(I)
Z    CH29_ZA(I) = ZH2_ZA(I)
FF   ++++++++++++++++++++++++++++++++++++++++++++++++++++++++++++++++++++++++++
Z    CALL ZHVD3( R2, CHAN_L, VISCO, W, DEN, C2, ID, I,
Z      K              S, Uf_2, Rou_2, ZH3_GAMAS, ZH3_BETA,
Z      K              N, XNU, MQ, RE_2, AREA_2, PI, TEMP, KERXI,
Z      K              ZH3_ALFA, ZH3_VDRAG, ZH3_RP, ZH3_ZA )

Z    CHAN_GAMAS(I) = ZH3_GAMAS(I)
```

```
Z    CHAN_BETA(I) = ZH3_BETA(I)
Z    CHAN_VDRAG(I) = ZH3_VDRAG(I)
Z    CHAN_RP(I) = ZH3_RP(I)
Z    CHAN_ZA(I) = ZH3_ZA(I)

BA   ================================================================
A    -- BROWN'S QUASI-STEADY EDDY VISCOSITY MODEL "A" CALLING --
A    CALL BRVD1_A(R1, CH32_L, VISCO, W, DEN, C1, ID, I, NIKU,
A       K             S, Rou_1, BRA1_GAMAS, BRA1_BETA, DUDR1_A,
A       K             MQ, RE_1, AREA_1, PI, TEMP, KERXI,  BRA1_ALFA,
A       K             BRA1_VDRAG, BRA1_RP, BRA1_ZA, RK4_1A )

A    CH32_GAMAS(I) = BRA1_GAMAS(I)
A    CH32_BETA(I) = BRA1_BETA(I)

C    ------ EXPERIMENTAL BOUNDARY CONDITIONS ------
A    CH32_RP(I) = (BRA1_RP(I))
A    CH32_ZA(I) = BRA1_ZA(I)
A    CH32_VDRAG(I) = BRA1_VDRAG(I)
FF   ++++++++++++++++++++++++++++++++++++++++++++++++++++++++++++++++++++++++
A    CALL BRVD2_A(R2, CH29_L, VISCO, W, DEN, C2, ID, I, NIKU,
A       K             S, Rou_2, BRA2_GAMAS, BRA2_BETA, DUDR2_A,
A       K             MQ, RE_2, AREA_2, PI, TEMP, KERXI, BRA2_ALFA,
A       K             BRA2_VDRAG, BRA2_RP, BRA2_ZA, RK4_2A )

A    CH29_GAMAS(I) = BRA2_GAMAS(I)
A    CH29_BETA(I) = BRA2_BETA(I)
A    CH29_VDRAG(I) = BRA2_VDRAG(I)
A    CH29_RP(I) = (BRA2_RP(I))
DD   ================================================================
A    CALL BRVD3_A(R2, CHAN_L, VISCO, W, DEN, C2, ID, I, NIKU,
A       K             S, Rou_2, BRA3_GAMAS, BRA3_BETA, DUDR3_A,
A       K             MQ, RE_2, AREA_2, PI, TEMP, KERXI, BRA3_ALFA,
A       K             BRA3_VDRAG, BRA3_RP, BRA3_ZA, RK4_3A )

A    CHAN_GAMAS(I) = BRA3_GAMAS(I)
A    CHAN_BETA(I) = BRA3_BETA(I)
A    CHAN_VDRAG(I) = BRA3_VDRAG(I)
A    CHAN_RP(I) = (BRA3_RP(I))
```

```
BB    -- BROWN'S ZERO PERTURBATION EDDY VISCOSITY MODEL "B" CALLING --
B    CALL BRVD1_B(R1, CH32_L, VISCO, W, DEN, C1, ID, I, NIKU,
B      K          S, Rou_1, BRB1_GAMAS, BRB1_BETA, DUDR1_B,
B      K          MQ, RE_1, AREA_1, PI, TEMP, KERXI,  BRB1_ALFA,
B      K          BRB1_VDRAG, BRB1_RP, BRB1_ZA, RK4_1B )

B    CH32_GAMAS(I) = BRB1_GAMAS(I)
B    CH32_BETA(I) = BRB1_BETA(I)

C    ------ EXPERIMENTAL BOUNDARY CONDITIONS ------
B    CH32_RP(I) = BRB1_RP(I)
B    CH32_ZA(I) = BRB1_ZA(I)
B    CH32_VDRAG(I) = BRB1_VDRAG(I)

BB   ++++++++++++++++++++++++++++++++++++++++++++++++++++++++++++++++++++++
B    CALL BRVD2_B(R2, CH29_L, VISCO, W, DEN, C2, ID, I, NIKU,
B      K          S, Rou_2, BRB2_GAMAS, BRB2_BETA, DUDR2_B,
B      K          MQ, RE_2, AREA_2, PI, TEMP, KERXI, BRB2_ALFA,
B      K          BRB2_VDRAG, BRB2_RP, BRB2_ZA, RK4_2B )

B    CH29_GAMAS(I) = BRB2_GAMAS(I)
B    CH29_BETA(I) = BRB2_BETA(I)
B    CH29_VDRAG(I) = BRB2_VDRAG(I)
B    CH29_RP(I) = BRB2_RP(I)
B    CH29_ZA(I) = BRB2_ZA(I)

BB   ++++++++++++++++++++++++++++++++++++++++++++++++++++++++++++++++++++++
B    CALL BRVD3_B(R2, CHAN_L, VISCO, W, DEN, C2, ID, I, NIKU,
B      K          S, Rou_2, BRB3_GAMAS, BRB3_BETA,  DUDR3_B,
B      K          MQ, RE_2, AREA_2, PI, TEMP, KERXI, BRB3_ALFA,
B      K          BRB3_VDRAG, BRB3_RP, BRB3_ZA, RK4_3B )

B    CHAN_GAMAS(I) = BRB3_GAMAS(I)
B    CHAN_BETA(I) = BRB3_BETA(I)
B    CHAN_VDRAG(I) = BRB3_VDRAG(I)
B    CHAN_RP(I) = BRB3_RP(I)
B    CHAN_ZA(I) = BRB2_ZA(I)

BC   **********************************************************************
BB    -- BROWN'S DYNAMIC EDDY VISCOSITY MODEL "C" CALLING --
     CALL BRVD1_C(R1, CH32_L, VISCO, W, DEN, C1, ID, I, NIKU,
```

```
      K              S, Rou_1, BRC1_GAMAS, BRC1_BETA,  DUDR1_C,
      K              MQ, RE_1, AREA_1, PI, TEMP, KERXI, BRC1_ALFA,
      K              BRC1_VDRAG, BRC1_RP, BRC1_ZA, RK4_1C, MAG, PHA)

      CH32_GAMAS(I) = BRC1_GAMAS(I)
      CH32_BETA(I) = BRC1_BETA(I)

C     ------ EXPERIMENTAL BOUNDARY CONDITIONS ------
      CH32_RP(I) = BRC1_RP(I)
      CH32_ZA(I) = BRC1_ZA(I)
      CH32_VDRAG(I) = BRC1_VDRAG(I)

BC    ++++++++++++++++++++++++++++++++++++++++++++++++++++++++++++++++++++++++++
      CALL BRVD2_C(R2, CH29_L, VISCO, W, DEN, C2, ID, I, NIKU2,
      K              S, Rou_2, BRC2_GAMAS, BRC2_BETA,  DUDR2_C,
      K              MQ, RE_2, AREA_2, PI, TEMP, KERXI, BRC2_ALFA,
      K              BRC2_VDRAG, BRC2_RP, BRC2_ZA, RK4_2A, MAG2, PHA2)

      CH29_GAMAS(I) = BRC2_GAMAS(I)
      CH29_BETA(I) = BRC2_BETA(I)
      CH29_VDRAG(I) = BRC2_VDRAG(I)
      CH29_RP(I) = BRC2_RP(I)
      CH29_ZA(I) = BRC2_ZA(I)
BC    ==========================================================================
      CALL   BRVD3_C(R2, CHAN_L, VISCO, W, DEN, C2, ID, I, NIKU2,
      K              S, Rou_2, BRC3_GAMAS, BRC3_BETA,      DUDR3_C,
      K              MQ, RE_2, AREA_2, PI, TEMP, KERXI, BRC3_ALFA,
      K              BRC3_VDRAG, BRC3_RP, BRC3_ZA, RK4_3C, MAG2, PHA2)

      CHAN_GAMAS(I) = BRC3_GAMAS(I)
      CHAN_BETA(I) = BRC3_BETA(I)
      CHAN_VDRAG(I) = BRC3_VDRAG(I)
      CHAN_RP(I) = BRC3_RP(I)
      CHAN_ZA(I) = BRC3_ZA(I)

PP    ++++++++++++++++++++++++++++++++++++++++++++++++++++++++++++++++++++++++++
C     ------      PRSENT MODEL CALLING      ------
R     CALL RWCHAN32( R1, CH32_L, VISCO, W, DEN, C1, ID, I,
R       K              S, Uf_1, Rou_1, RW32_GAMAS, RW32_BETA,
R       K              N, XNU, MQ, RE_1, AREA_1, PI, TEMP, KERXI,
R       K              RW32_ALFA, RW32_VDRAG, RW32_RP, RW32_ZA )
```

```
R    CH32_GAMAS(I) = RW32_GAMAS(I)
R    CH32_BETA(I) = RW32_BETA(I)

C    ------ EXPERIMENTAL BOUNDARY CONDITIONS ------
R    CH32_RP(I) = RW32_RP(I)
R    CH32_ZA(I) = RW32_ZA(I)
R    CH32_VDRAG(I) = RW32_VDRAG(I)

PP   ++++++++++++++++++++++++++++++++++++++++++++++++++++++++++++++++++++++++
R    CALL RWCHAN29( R2, CH29_L, VISCO, W, DEN, C2, ID, I,
R      K              S, Uf_2, Rou_2, RW29_GAMAS, RW29_BETA,
R      K              N, XNU, MQ, RE_2, AREA_2, PI, TEMP, KERXI,
R      K              RW29_ALFA, RW29_VDRAG, RW29_RP, RW29_ZA )

R    CH29_GAMAS(I) = RW29_GAMAS(I)
R    CH29_BETA(I) = RW29_BETA(I)
R    CH29_VDRAG(I) = RW29_VDRAG(I)
R    CH29_RP(I) = RW29_RP(I)
R    CH29_ZA(I) = RW29_ZA(I)

PP   ++++++++++++++++++++++++++++++++++++++++++++++++++++++++++++++++++++++++
R    CALL RWCHAN( R2, CHAN_L, VISCO, W, DEN, C2, ID, I,
R      K            S, Uf_2, Rou_2, RWCH_GAMAS, RWCH_BETA,
R      K            N, XNU, MQ, RE_2, AREA_2, PI, TEMP, KERXI,
R      K            RWCH_ALFA, RWCH_VDRAG, RWCH_RP, RWCH_ZA )

R    CHAN_GAMAS(I) = RWCH_GAMAS(I)
R    CHAN_BETA(I) = RWCH_BETA(I)
R    CHAN_VDRAG(I) = RWCH_VDRAG(I)
R    CHAN_RP(I) = RWCH_RP(I)
R    CHAN_ZA(I) = RWCH_ZA(I)

PP   ++++++++++++++++++++++++++++++++++++++++++++++++++++++++++++++++++++++++
C    ------ FIELD MATRIX ELEMENTS OF SERIES CONNECTION ------
     U1(I) = (AREA_2/AREA_1)*CCOSH(CH32_GAMAS(I)*CH32_L)
      K          *CCOSH(CH29_GAMAS(I)*CH29_L) +
      K          (CH29_BETA(I)/CH32_BETA(I))*CSINH(CH32_GAMAS(I)*CH32_L)
      K          *CSINH(CH29_GAMAS(I)*CH29_L)
A
     U2(I) = (AREA_2/AREA_1)*CCOSH(CH32_GAMAS(I)*CH32_L)
```

```
      K        * (-1.0/CH29_BETA(I))*CSINH(CH29_GAMAS(I)*CH29_L)
      K        + (-1.0/CH32_BETA(I))*CSINH(CH32_GAMAS(I)*CH32_L)
      K        *CCOSH(CH29_GAMAS(I)*CH29_L)
CC
      U3(I) = (-CH32_BETA(I))*CSINH(CH32_GAMAS(I)*CH32_L)
      K        *CCOSH(CH29_GAMAS(I)*CH29_L)*(AREA_2/AREA_1)
      k       -(CH29_BETA(I))*CCOSH(CH32_GAMAS(I)*CH32_L)
      k        *CSINH(CH29_GAMAS(I)*CH29_L)

      U4(I) = (CH32_BETA(I)/CH29_BETA(I))*CSINH(CH32_GAMAS(I)*CH32_L)
      K        *CSINH(CH29_GAMAS(I)*CH29_L)*(AREA_2/AREA_1)
      k       +CCOSH(CH32_GAMAS(I)*CH32_L)*CCOSH(CH29_GAMAS(I)*CH29_L)

RR    ================================================================
      U5(I) = (AREA_2/AREA_1)*CCOSH(CH32_GAMAS(I)*CH32_L)
      K        *CCOSH(CHAN_GAMAS(I)*CHAN_L) +
      K        (CHAN_BETA(I)/CH32_BETA(I))*CSINH(CH32_GAMAS(I)*CH32_L)
      K        *CSINH(CHAN_GAMAS(I)*CHAN_L)

      U6(I) = (AREA_2/AREA_1)*CCOSH(CH32_GAMAS(I)*CH32_L)
      K        * (-1.0/CHAN_BETA(I))*CSINH(CHAN_GAMAS(I)*CHAN_L)
      K        + (-1.0/CH32_BETA(I))*CSINH(CH32_GAMAS(I)*CH32_L)
      K        *CCOSH(CHAN_GAMAS(I)*CHAN_L)
CC
      U7(I) = (-CH32_BETA(I))*CSINH(CH32_GAMAS(I)*CH32_L)
      K        *CCOSH(CHAN_GAMAS(I)*CHAN_L)*(AREA_2/AREA_1)
      k       -(CHAN_BETA(I))*CCOSH(CH32_GAMAS(I)*CH32_L)
      k        *CSINH(CHAN_GAMAS(I)*CHAN_L)

      U8(I) = (CH32_BETA(I)/CHAN_BETA(I))*CSINH(CH32_GAMAS(I)*CH32_L)
      K        *CSINH(CHAN_GAMAS(I)*CHAN_L)*(AREA_2/AREA_1)
      k       +CCOSH(CH32_GAMAS(I)*CH32_L)*CCOSH(CHAN_GAMAS(I)*CHAN_L)

C     ------ SPECFIC ACOUSTIC IMPEDANCE OF SERIES CONNECTION ------

      CA29_ZA(I)= ( (CH32_RP(I)*AREA_2/AREA_1*1.0)
      K                -CH29_BETA(I)*CTANH(CH29_GAMAS(I)*CH29_L) )/
      K           ( 1.0-(CH32_RP(I)*AREA_2/AREA_1*1.0
      K                /CH29_BETA(I))*(CTANH(CH29_GAMAS(I)*CH29_L)) )

RR
```

```
      CHANNEL_ZA(I)=      ( (CH32_RP(I)*AREA_2/AREA_1*1.0)
     K                   -CHAN_BETA(I)*CTANH(CHAN_GAMAS(I)*CHAN_L) )/
     K              ( 1.0-(CH32_RP(I)*AREA_2/AREA_1*1.0
     K                   /CHAN_BETA(I))*CTANH(CHAN_GAMAS(I)*CHAN_L) )

DD  ========== CHANNEL29 & CHANNEL31 CALCULATION ==========
      CH29_AMPLIT(I)= 1.0/(U4(I)+U3(I)/CA29_ZA(I))

      CHAN_AMPLIT(I)=1.0/(U8(I)+U7(I)/CHANNEL_ZA(I))
DD  ++++++++++++++++++++++++++++++++++++++++++++++++++++++++++++++++++++++++++
EE  ========== NOMALIZED PRESSURE TO CH29 CALCULATION ==========
      AMPLIT(I) = CHAN_AMPLIT(I)/CH29_AMPLIT(I)

      AMPLITM(I) = CABS(AMPLIT(I))

FF  ++++++++++++++++++++++++++++++++++++++++++++++++++++++++++++++++++++++++++++++
C *** Print the results ***
        WRITE(IOFLE, 200) I
200   FORMAT(1X/1X,'< PRINT OUT RESULTS >', I10/ )
100    CONTINUE
C
        OPEN(UNIT=300, FILE='FINBR31p_OUT.dat')

      WRITE(300,'(1X, "<Frequency>", 4X, "<Amplitude>",
      K             6X, "<CH32_VD>", 6X, "<CH29_VD>", 6X, "<CHAN_VD>",
      K             15X, "<CH32_RP>" 20X, "<CH29_RP>"    / )' )

      DO 301 I= 1 , ITER
        WRITE(300,'(1X,1PE12.6,3X,1PE12.6,3x,1PE14.6,3X,1PE14.6,
      K          3X,1PE14.6,3X,1PE14.6,1PE14.6,3X,1PE14.6,1PE14.6 )')
      K          FREQU(I), AMPLITM(I), CH32_VDRAG(I), CH29_VDRAG(I),
      K       CHAN_VDRAG(I), CH32_RP(I), CH29_RP(I)


301         CONTINUE

     CLOSE(UNIT = 300)
     END
```

```
C-----------------------------------------------------------------------+
      SUBROUTINE BRVD1_C(R1, CH32_L, VISCO, W, DEN, C1, ID, I, NIKU,
     K                   S, Rou_1, BRC1_GAMAS, BRC1_BETA,    DUDR1_C,
     K                   MQ, RE_1, AREA_1, PI, TEMP, KERXI, BRC1_ALFA,
     K                   BRC1_VDRAG, BRC1_RP, BRC1_ZA, RK4_1C, MAG, PHA)
C-----------------------------------------------------------------------+
      USE MSIMSL
      EXTERNAL RK4_1C, DERIVES_C

CC ----- CALLING PRAMETERS DEFINITION --------
      REAL MAG, PHA
      INTEGER ID, I
      REAL R1, CH32_L, VISCO, W(ID), NIKU, RG1
      REAL DEN, KERXI
      COMPLEX S(ID), DUDR1_C(ID), C1(ID)
      COMPLEX BRC1_GAMAS(ID), BRC1_BETA(ID), BRC1_ALFA(ID)
      REAL    BRC1_VDRAG(ID)
CC ^^^^^^^^^^^^^^^^^^^^^^^^^^^^^^^^^^^^^^^^^^^^^^^^^^^^^^^^^^^^^^^^^^^^^^^^
F     BROWN'S UNIFORM DYNAMIC EDDY-VISCOSITY MODEL "C" ON CALLING,
F     WHICH RETURNS THE VOLUMETRIC DRAG TO THE STANDARD TRANSFER
F     FUNCTION TO SIMULATE THE PRESSURE FACTOR.
F     ^^^^^^^^^^^^^^^^^^^^^^^^^^^^^^^^^^^^^^^^^^^^^^^^^^^^^^^^^^^^^^^^^^^^^^^^
CC    ----- BOUNDARY CONDITION DEFINITION -----
      REAL MQ, RE_1, AREA_1, PI, SqF_1, DR1
      REAL TEMP
      COMPLEX BRC1_ZA(ID), BRC1_RP(ID)
C     ++++++ LOCAL VARAIBLE DEFINITION ++++++++++
      REAL PrL1_C0, DPrL1_C0, H1_C0, DH1_C0
      REAL G1_C0, DG1_C0, EDD1_C0, DEDD1_C0
      REAL P1_C0, DP1_C0, Q1_C0, DQ1_C0
      COMPLEX K1_C0, DK1_C0, A01_C0, B01_C0
      COMPLEX Y1_C0(ID), DUDR1_C0(ID), JC

C     ------ PARAMETERS CALCULATION ------
AA    ------ FOR ANY GIVEN VOLUME FLOW RATE ----------
      AREA_1 = PI*R1**2
D     AREA_1 = 0.002734
      ROU_1 = 0.00085*2.0*R1
      RE_1 = 2.0*R1*(MQ/DEN/AREA_1)/VISCO
      SqF_1 = (1.0/(-1.8*log10(6.9/Re_1+(Rou_1/3.7/2.0/R1)**1.11)))
```

```
C     ------ ACOUSTIC SOUND SPEED -----
      C1(I) = CMPLX(1495.0,0.0)
      JC = CMPLX(0.0, 1.0)
AA    ================================================================
      RG1 = 0.996*R1
      DR1 = R1 - RG1
AA    %% PARAMETERS IN CALCULATION   %%
      PrL1_C0 = 0.14*R1-0.075*RG1**2/R1-0.065*RG1**4/(R1**3)
      DPrL1_C0 = -0.15*RG1/R1-0.26*(RG1**3)/(R1**3)
CC    ------CALCUALTION OF STEADY EDDY VISCOSITY   ---------
      H1_C0 = (Re_1/4.0/NIKU/R1)*DR1*SQRT(RG1/2.0/R1)*SqF_1
      DH1_C0 = (Re_1/4.0/NIKU/R1)*((R1-3.0*RG1)/2.0/RG1)*
     K                 SQRT(RG1/2.0/R1)*SqF_1

      G1_C0 = (SqF_1**2)*(Re_1**2)/32.0/(R1**3)*RG1*(PrL1_C0**2)
C
      DG1_C0 = (SqF_1**2*Re_1**2/32.0/(R1**3))*(PrL1_C0**2)
     K                 *(1.0+2.0*RG1/PrL1_C0*DPrL1_C0)

      EDD1_C0 = 0.5+SQRT(0.25+G1_C0*(1.0-EXP(-H1_C0))**2)

      DEDD1_C0 = 0.5/SQRT( 0.25+G1_C0*(1.0-EXP(-H1_C0))**2 )
     K          * ( G1_C0*2.0*(1.0-EXP(-H1_C0))*EXP(-H1_C0)*DH1_C0
     K          +DG1_C0*(1.0-EXP(-H1_C0))**2 )

CC    ------CALCUALTION OF QUASI-STEADY EDDY VISCOSITY     -----
      P1_C0 = -1.0*(PrL1_C0**2)/Visco*(1.0-EXP(-H1_C0))*
     K       (1.0-EXP(-H1_C0)+H1_C0*EXP(-H1_C0))

      DP1_C0 = (1.0-EXP(-H1_C0))*(1.0-EXP(-H1_C0)+H1_C0*EXP(-H1_C0))
     K           *(-2.0*PrL1_C0/Visco*DPrL1_C0)
     K       - (PrL1_C0**2/Visco)*
     K             (EXP(-H1_C0)*DH1_C0)*( 3.0-H1_C0-3.0*EXP(-H1_C0)
     K               +2.0*H1_C0*EXP(-H1_C0) )

      Q1_C0 = 1.0+(PrL1_C0**2)/Visco*(1.0-EXP(-H1_C0))*H1_C0*EXP(-H1_C0)
     K       *( (-(SqF_1*Re_1)**2*Visco/32.0/(R1**3)) *RG1/EDD1_C0 )

      DQ1_C0 = (PrL1_C0**2/Visco)*
     K          (     -(SqF_1*Re_1)**2*Visco/32.0/(R1**3) *RG1/EDD1_C0
```

```
   K   *( H1_C0*EXP(-2.0*H1_C0)*DH1_C0+EXP(-H1_C0)*DH1_C0*(1.0-H1_C0) )
   K      + ( -(SqF_1*Re_1)**2*Visco/32.0/(R1**3)
   K           *(1.0/EDD1_C0-RG1/(EDD1_C0**2)*DEDD1_C0) )
   K              *(1.0-EXP(-H1_C0))*H1_C0*EXP(-H1_C0)     )
   K       + (1.0-EXP(-H1_C0))*H1_C0*EXP(-H1_C0) *
   K        (-SqF_1*Re_1)**2*Visco/32.0/(R1**3) *RG1/EDD1_C0
   K           *2.0*PrL1_C0/Visco*DPrL1_C0
D
      K1_C0 = MAG*CEXP(PHA*JC)*P1_C0/Q1_C0
      DK1_C0 = MAG*CEXP(PHA*JC)*DP1_C0/Q1_C0 -P1_C0*DQ1_C0/(Q1_C0**2)

EE  ~~~~~~~~~~ TRANSFORMED VARIABLES A0 & B0  ~~~~~~~~~~
      A01_C0 = (Visco*EDD1_C0)+ (Visco*K1_C0)*
   K           (-(SqF_1*Re_1)**2*Visco/32.0/(R1**3))
   K                *(1.0/EDD1_C0-RG1/(EDD1_C0**2)*DEDD1_C0)

      B01_C0 = (Visco*EDD1_C0/RG1+Visco*DEDD1_C0)+
   K           (-(SqF_1*Re_1)**2*Visco/32.0/(R1**3))
   K                *(1.0/EDD1_C0-RG1/(EDD1_C0**2)*DEDD1_C0)
   K       *( Visco*K1_C0+Visco*K1_C0/RG1+DK1_C0 )

FF  ~~~~~~~~~~ INITIAL VALUES AT GUESSED POINT  ~~~~~~~~~~
      Y1_C0(I) = (S(I)/A01_C0)/(2.0/ 25.0 /DR1-S(I)/A01_C0*DR1
   K                          + B01_C0/A01_C0)

      DUDR1_C0(I)=Y1_C0(I)*(S(I)/A01_C0*DR1-B01_C0/A01_C0)+S(I)/A01_C0

F   ---------- FOURTH-ORDER RUNGE-KUTTA ALGORITHM ---------
        CALL RK4_1C(Y1_C0, DUDR1_C0, ID, I, VISCO, NIKU, S, RE_1,
       K            SqF_1, R1, RG1, DR1, DUDR1_C, DERIVES_C,
       K            MAG, PHA )

EE  == AXIAL VELOCITY DISTRIBUTION CALCULATION ==
      BRC1_ALFA(I) = (2.0*Visco/R1/S(I)*DUDR1_C(I) -1.0 )*1.0

EF  == VOLUMETRIC DRAG CALCULATION USING BROWN'S MODEL "C" ==

      BRC1_VDRAG(I) = -W(I)*DEN*AIMAG(BRC1_ALFA(I))/
   K                          (CABS(BRC1_ALFA(I))**2)
   K     +1.0/( (-1.8*log10(6.9/Re_1+(Rou_1/3.7/2.0/R1)**1.11))**2 )
   K              *Re_1*VISCO*DEN/4.0/(R1**2)
```

```
A2 ------      BROWN'S MODEL "C" APPLIED TO TRANSFER FUNCTION     ------
      BRC1_GAMAS(I)=S(I)/C1(I)*CSQRT(1.0+1.0*BRC1_VDRAG(I)/S(I)/DEN)
      BRC1_BETA(I)=( (-1.0)*DEN*C1(I)**2/S(I) )*BRC1_GAMAS(I)

C     ------ EXPERIMENTAL BOUNDARY CONDITIONS ------
      BRC1_RP(I) =   ( -KERXI* (DEN*S(I)/ BRC1_ALFA(I) ) )

      BRC1_ZA(I)=(BRC1_RP(I)-BRC1_BETA(I)*CTANH(BRC1_GAMAS(I)*CH32_L) )
     K      /( 1.0-BRC1_RP(I)/BRC1_BETA(I)*CTANH(BRC1_GAMAS(I)*CH32_L) )

      RETURN
      END
```

SUB2

```
C-----------------------------------------------------------------------+
      SUBROUTINE RWCHAN32( R1, CH32_L, VISCO, W, DEN, C1, ID, I,
       K                        S, Uf_1, Rou_1, RW32_GAMAS, RW32_BETA,
       K                        N, XNU, MQ, RE_1, AREA_1, PI, TEMP,
       K                        RW32_ALFA, RW32_VDRAG, RW32_RP, RW3

C-----------------------------------------------------------------------+
      USE MSIMSL
CC ----- CALLING PRAMETERS DEFINITION ------
      INTEGER ID, I
      REAL R1, CH32_L, VISCO, W(ID)
      REAL DEN, KERXI
      COMPLEX S(ID)

C   ++++++ LOCAL VARAIBLE DEFINITION ++++++++++++++++++++++++++++++++++++
CC    ----- TURBULENCE PART DEFINITION -----
      REAL Uf_1, Rou_1,    RW32_b
      REAL RW32_Vedd1(ID), RW32_Vedd2(ID)
      REAL RW32_QR(ID),RW32_Q1(ID),RW32_Q2(ID)
      COMPLEX RW32_DELTA(ID),RW32_DELT1(ID),RW32_DELT2(ID)
      COMPLEX RW32_IR0(ID),RW32_IR1(ID),RW32_IQ01(ID)
      COMPLEX RW32_IQ02(ID),RW32_IQ1(ID),RW32_IQ2(ID)
      COMPLEX RW32_KR0(ID),RW32_KR1(ID),RW32_KQ01(ID)
      COMPLEX RW32_KQ1(ID),RW32_KQ2(ID),RW32_C1(ID)
      COMPLEX RW32_D1(ID), JS
```

```
      COMPLEX RW32_GAMAS(ID), RW32_BETA(ID), RW32_FS(ID)

C  ++++++++++++++++++++++++++++++++++++++++++++++++++++++++++++++++++++++++++++
CC   ----- TURBULENCE VOLUMETRIC DRAG DEFINITION -----
      INTEGER N
      REAL XNU
      COMPLEX RW32_CBS1(ID),RW32_CBS2(ID),RW32_Z1(ID),
     K       RW32_Z2(ID)
      COMPLEX RW32_CBS3(ID),RW32_CBS4(ID),RW32_Z3(ID),
     K       RW32_Z4(ID)
C
      COMPLEX RW32_I2Q1(ID), RW32_I2QR(ID)
      COMPLEX RW32_K2Q1(ID), RW32_K2QR(ID)
      COMPLEX RW32_C2(ID), RW32_PART1(ID), RW32_PART2(ID)
      COMPLEX RW32_ALFA(ID), RW32_ALFA1(ID), RW32_ALFA2(ID)
      REAL RW32_VDRAG(ID)
C  ++++++++++++++++++++++++++++++++++++++++++++++++++++++++++++++++++++++++++++
CC   ----- BOUNDARY CONDITION DEFINITION -----
      REAL MQ, RE_1, AREA_1, PI
      REAL TEMP
      COMPLEX RW32_ZA(ID)
      COMPLEX    RW32_RP(ID)
CC  ------ COMPLEX SONIC VELOCITY DEFINTION -----
      COMPLEX C1(ID)
      REAL PJ_32(ID)
      REAL RCON_32(ID), RW32_CHK(ID), Ks_1
C  ++++++++++++++++++++++++++++++++++++++++++++++++++++++++++++++++++++++++++++
C   ------ PARAMETERS CALCULATION ------
AA  ------ FOR ANY GIVEN VOLUME FLOW RATE ----------
      AREA_1 = PI*R1**2
DD  AREA_1 = 0.002734

      ROU_1 = 0.00085*2.0*R1
      RE_1 = 2.0*R1*(MQ/DEN/AREA_1)/VISCO
      Uf_1 = (Re_1*Visco/2.0/R1)/
     K        ((-1.8*log10(6.9/Re_1+(Rou_1/3.7/2.0/R1)**1.11)))/SQRT(8.0)

      Ks_1 = Rou_1*Uf_1/VISCO
      RCON_32(I) = 250.0
      RW32_b = 0.4-( RCON_32(I)*VISCO/0.175/R1/Uf_1 )
```

```
      RW32_Vedd1(I) = RCON_32(I)*VISCO*
     K                (1.0+ RW32_b*0.175*R1*Uf_1/RCON_32(I)/VISCO
      RW32_Vedd2(I) = 0.07*Uf_1*R1
C
      JS = CMPLX(0.0,1.0)

      PJ_32(I) = RW32_Vedd2(I)/rcon_32(i)/visco
AA    ================================================================
C     ------ ACOUSTIC SOUND SPEED -----
        C1(I) = CMPLX(1495, 0.0)
BB    ++++++++++++++++++++++++++++++++++++++++++++++++++++++++++++++++
C     ----- WALL-SHEAR CONSTANTS CALCULATION ------
        RW32_QR(I) = (2.0/RW32_b/Uf_1)*SQRT(W(I)*RCON_32(I)*VISCO)
        RW32_Q1(I) = (2.0/RW32_b/Uf_1)*SQRT(W(I)*RW32_Vedd1(I))
        RW32_Q2(I) = (0.825*R1)*SQRT(W(I)/RW32_Vedd2(I))
C     ------ MODIFIED {I} BESSEL FUNC. ------
        RW32_IR0(I) = BER0(RW32_QR(I))+JS*BEI0(RW32_QR(I))
        RW32_IR1(I) = BER1(RW32_QR(I))+JS*BEI1(RW32_QR(I))
        RW32_IQ01(I) = BER0(RW32_Q1(I))+JS*BEI0(RW32_Q1(I))
        RW32_IQ02(I) = BER0(RW32_Q2(I))+JS*BEI0(RW32_Q2(I))
        RW32_IQ1(I) = BER1(RW32_Q1(I))+JS*BEI1(RW32_Q1(I))
        RW32_IQ2(I) = BER1(RW32_Q2(I))+JS*BEI1(RW32_Q2(I))
C     ------ MODIFIED {K} BESSEL FUNC. ------
        RW32_KR0(I) = AKER0(RW32_QR(I))+JS*AKEI0(RW32_QR(I))
        RW32_KR1(I) = AKER1(RW32_QR(I))+JS*AKEI1(RW32_QR(I))
        RW32_KQ01(I) = AKER0(RW32_Q1(I))+JS*AKEI0(RW32_Q1(I))
        RW32_KQ1(I) = AKER1(RW32_Q1(I))+JS*AKEI1(RW32_Q1(I))
        RW32_KQ2(I) = AKER1(RW32_Q2(I))+JS*AKEI1(RW32_Q2(I))
C     ------ ACOUSTIC WAVE PROPAGATION CONSTANTS ------
         RW32_DELT1(I) = SQRT(RW32_Vedd1(I)/RW32_Vedd2(I))
       K                      *(RW32_IQ1(I)/RW32_IQ2(I))
       K                       + (RW32_IQ01(I)/RW32_IQ02(I))

        RW32_DELT2(I) = SQRT(RW32_Vedd1(I)/RW32_Vedd2(I))
       K                      *(RW32_KQ1(I)/RW32_IQ2(I))
       K                       - (RW32_KQ01(I)/RW32_IQ02(I))
C
        RW32_DELTA(I) = RW32_DELT1(I)/RW32_DELT2(I)
        RW32_C1(I) =1.0/(RW32_IR0(I)+RW32_DELTA(I)*RW32_KR0(I))
        RW32_D1(I) = RW32_C1(I)*RW32_DELTA(I)
```

```
C      ------ TURBULENCE VOLUMETRIC DRAG CALCULATION ------
EA          ------ SUB-REGION 2 INTEGRATION CONSTANT ------
      RW32_C2(I) = RW32_C1(I)*(RW32_IQ01(I)/RW32_IQ02(I))
     K                  +RW32_D1(I)*(RW32_KQ01(I)/RW32_IQ02(I))

EB          ------ BESSEL FUNCTION OF I2(Z) CALCULATION ------
C                 ------ I2(Z) at (r=R) / PIPE WALL ------
      RW32_Z1(I) = CSQRT(JS)*RW32_QR(I)
        CALL CBIS (XNU, RW32_Z1(I), N, RW32_CBS1(I))
          RW32_I2QR(I) = RW32_CBS1(I)
C                 ------ I2(Z) at (r=0.825R) ------
      RW32_Z2(I) = CSQRT(JS)*RW32_Q1(I)
        CALL CBIS (XNU, RW32_Z2(I), N, RW32_CBS2(I))
          RW32_I2Q1(I) = RW32_CBS2(I)

EC          ------ BESSEL FUNCTION OF K2(Z) CALCULATION ------
C                 ------ K2(Z) at (r=R) / PIPE WALL ------
      RW32_Z3(I) = CSQRT(JS)*RW32_QR(I)
        CALL CBKS (XNU, RW32_Z3(I), N, RW32_CBS3(I))
          RW32_K2QR(I) = RW32_CBS3(I)
C                 ------ K2(Z) at (r=0.825R) ------
      RW32_Z4(I) = CSQRT(JS)*RW32_Q1(I)
        CALL CBKS (XNU, RW32_Z4(I), N, RW32_CBS4(I))
          RW32_K2Q1(I) = RW32_CBS4(I)

ED  ======= RADIAL VELOCITY DISTRIBUTION INTEGRATION PROCEDURE =====
C                 ------ SUBREGION #1 (0.825R <= r <= R) ------
        RW32_PART1(I) =    -1.0*RW32_C1(I)*RW32_b*Uf_1/2.0/S(I)
       K  *( (RW32_Z1(I)*RW32_IR1(I)*R1-RW32_Z2(I)
       K                    *RW32_IQ1(I)*0.825*R1)
       K          +(RW32_b*Uf_1/2.0/S(I))*((RW32_Z1(I)**2)
       K                    *RW32_I2QR(I)
       K               -(RW32_Z2(I)**2)*RW32_I2Q1(I)) )

      RW32_PART2(I) =    -1.0*RW32_D1(I)*RW32_b*Uf_1/2.0/S(I)
       K         *( (-RW32_Z3(I)*RW32_KR1(I)*R1 +
       K    RW32_Z4(I)*RW32_KQ1(I)*0.825*R1) +(RW32_b*Uf_1/2.0/S(I))*
       k    ((RW32_Z3(I)**2)*RW32_K2QR(I) -
       K               (RW32_Z4(I)**2)*RW32_K2Q1(I)) )
```

```
      RW32_ALFA1(I) = RW32_PART1(I) + RW32_PART2(I)

C               ------ SUBREGION #2 (0 <= r <= 0.825R) ------
      RW32_ALFA2(I) = (RW32_C2(I)*RW32_Vedd2(I)/S(I))
     K                      *(CSQRT(JS)*RW32_Q2(I)*RW32_IQ2(I))

EE  $$$$$$ AXIAL VELOCITY DISTRIBUTION CALCULATION $$$$$$
      RW32_ALFA(I) = 2.0/(R1**2)*(
     k      (-RW32_C1(I)*RW32_b*Uf_1/2.0/S(I))
     K             *( RW32_Z1(I)*RW32_IR1(I)*R1
     k         +(RW32_b*Uf_1/2.0/S(I))*RW32_Z1(I)**2*RW32_I2QR(I) ) +
     k   (-RW32_D1(I)*RW32_b*Uf_1/2.0/S(I))*
     K             ( -RW32_Z3(I)*RW32_KR1(I)*R1
     k    + (RW32_b*Uf_1/2.0/S(I))*(RW32_Z3(I)**2)*RW32_K2QR(I) )
     k             - (R1**2)/2.0 )*1.0

EF  @@@@@@ VOLUMETRIC DRAG CALCULATION @@@@@@

      RW32_VDRAG(I)= -W(I)*DEN*AIMAG(RW32_ALFA(I))/
     k                      (CABS(RW32_ALFA(I))**2)
     K         +1.0/( (-1.8*log10(6.9/Re_1+(Rou_1/3.7/2/R1)**1.11))**2 )
     K              *Re_1*VISCO*DEN/4.0/(R1**2)

BB  ++++++++++++++++++++++++++++++++++++++++++++++++++++++++++++++++++++++++++++++
A2  ------PRESENT MODEL ON CALLING      ------

      RW32_GAMAS(I)=(S(I)/C1(I))*CSQRT(1.0+1.0*RW32_VDRAG(I)/S(I)/DEN)

      RW32_BETA(I)=( (-1.0)*DEN*C1(I)**2/S(I) )*RW32_GAMAS(I)

EE    ***************************************************************.
C   ------ EXPERIMENTAL BOUNDARY CONDITIONS ------
      RW32_RP(I) =    ( -KERXI* (DEN*S(I)/ (RW32_ALFA(I)-0.0) ) )

      RW32_ZA(I)=(RW32_RP(I)-RW32_BETA(I)*CTANH(RW32_GAMAS(I)*CH32_L) )
    K      /( 1.0-RW32_RP(I)/RW32_BETA(I)*CTANH(RW32_GAMAS(I)*CH32_L) )

      RETURN
C
      END
```